NASA Technical Memorandum 100690

Global Atmospheric Circulation Statistics—Four Year Averages

M.F. Wu, M.A. Geller,
E.R. Nash, and M.E. Gelman
Goddard Space Flight Center
Greenbelt, Maryland

National Aeronautics
and Space Administration

**Scientific and Technical
Information Branch**

1987

Table of Contents

1. Introduction

This report is the second in a series dealing with the general circulation statistics for the stratosphere. Its main purpose is to provide a reference source for those who want to use the statistics to validate numerical models. The first volume published about three years ago (Wu et al., 1984) utilized Northern Hemispheric data only. The present one extends the data coverage to the Southern Hemisphere. Similar statistics are compiled with vertical and meridional velocities also included. In the previous publication, we described the annual cycle of the basic fields and the diagnostic quantities. Here we intend to point out some of the major differences between the Northern and the Southern Hemispheric statistics. Some possibly biased results inherited from poor data quality will be examined and discussed.

2. Data and Analysis Procedures

2.1 Data

We used the global temperature data for the period December 1978 through November 1982 at 18 pressure levels (1000-0.4 mb) that were provided by NOAA/NMC. The temperatures at 5, 2, 1 and 0.4 mb were retrieved from the satellite sounding systems of the Vertical Temperature Profiler Radiometer (VTPR) on NOAA-5 and the Stratospheric Sounding Unit (SSU) on Tiros-N. These temperatures were adjusted based on the rocket statistics according to the suggestion of Gelman et al. (1982, 1986). At and below 10 mb conventional rawinsonde data were used. More details on data sources and quality are given in appendix A.

2.2 Analysis Procedures

The analysis procedures adopted in this report are the same as before. Therefore, only a short summary of the computation technique is given below.

We first transferred the basic data from the NMC 65 x 65 polar stereographic map onto a 2.5° latitude by 5° longitude grid and then built the geopotential height fields at and above 850 mb by hydrostatically integrating the temperature fields using 1000 mb heights as the lower boundary condition. The zonal and meridional components of the geostrophic wind were calculated at each grid point between 10°N (or S) and 85°N (or S). The vertical velocity on the same grid was deduced using the thermodynamic equation which includes the diabatic heating term. Since no observed winds are available at the levels being analyzed, we decided to use geostrophic winds to evaluate the horizontal temperature advection term in the calculation of the vertical velocity, as was done by Dopplick (1971) and Hartmann (1976). The SBUV ozone profiles are used in calculating the heating rate. The computation was not carried out in the equatorial region (between 10°S and 10°N) where the geostrophic approximation becomes untrustworthy. We then solved the zonally averaged thermodynamic and continuity equations simultaneously for the zonal mean meridional and vertical motions with the meridional wind speed set to zero at the pole and the vertical wind speed set to zero at the surface. These total wind fields are presented in Tables 3-6. Since the satellite temperatures over the NH were adjusted based on the rocket statistics (Gelman et al., 1982, 1986) and no similar rocket data were available over the SH, we decided to use the NH rocket information to adjust the SH satellite temperature as well to remove

the obvious bias between the two hemispheric statistics. Effects due to this data treatment are found to be slight.

3. Results

Before presenting the results, we will first remark on the vertical scale used in the diagrams. To each figure we indicate both pressure (p) and the pressure scale heights defined as $z = \ln (p_0/p)$, where p_0=1000 mb. Figure 1 shows how z values correspond to altitudes in pressure and approximately in height units. The geometric altitude variation with pressure has been taken from the 1976 U.S. Standard Atmosphere (NOAA, 1976). In this report, about 400 cross sections have been selected for illustrating the most important features. In addition, numerical values of certain quantities are tabulated in appendix B.

3.1 Zonally Averaged Temperatures

3.1.1 Latitude-Altitude Section

Fig. 2 shows the four year mean values of the zonally averaged temperature $[\overline{T}]$ for the twelve calendar months. The major points with regard to the interhemispheric difference are noted below.

(a) The temperatures in the polar upper stratospheric regions are higher in the Southern Hemisphere (SH) summer than in the Northern Hemisphere (NH) summer. A similar feature was reported by Fritz and Soules (1970) and Barnett (1974) who suggest that the shorter distance between the Sun and Earth in January is the cause.

(b) During the SH winter the zonal mean temperature at the high latitude upper stratosphere increases toward the South Pole (SP). As a result, the winter SP is warmer than the southern midlatitudes. A similar feature is seen in the NH winter, but the poleward increase in $[\overline{T}]$ is comparatively less. Barnett (1974) also reported this phenomenon when he examined the SCR data for the period November 1970 to November 1971. The warmer winter SP is believed to be created dynamically by mean subsidence (Mechoso et al., 1985).

(c) The polar winter lower stratosphere $[\overline{T}]$ is colder in the SH than in the NH.

3.1.2 Time-Latitude and Altitude Sections

Fig. 3 presents a time-latitude section of the zonally averaged monthly mean temperature at 0.4 mb, 1 mb, 2 mb and 5 mb. The most interesting features are: the temperature in the high latitudes is higher in the SH than in the NH during summer due to more radiative energy available, and the seasonal variation in monthly mean temperature is larger in the SH than in the NH.

Fig. 4 shows a time-altitude section of the zonally averaged monthly mean temperature at 60°N and 60°S latitudes. We see that during the winter season the minimum temperature in the lower stratosphere is generally lower in the SH by as much as 8 K, but the summer maximum temperature in the upper stratosphere is about 5 K higher in the SH. The difference varies with location and season.

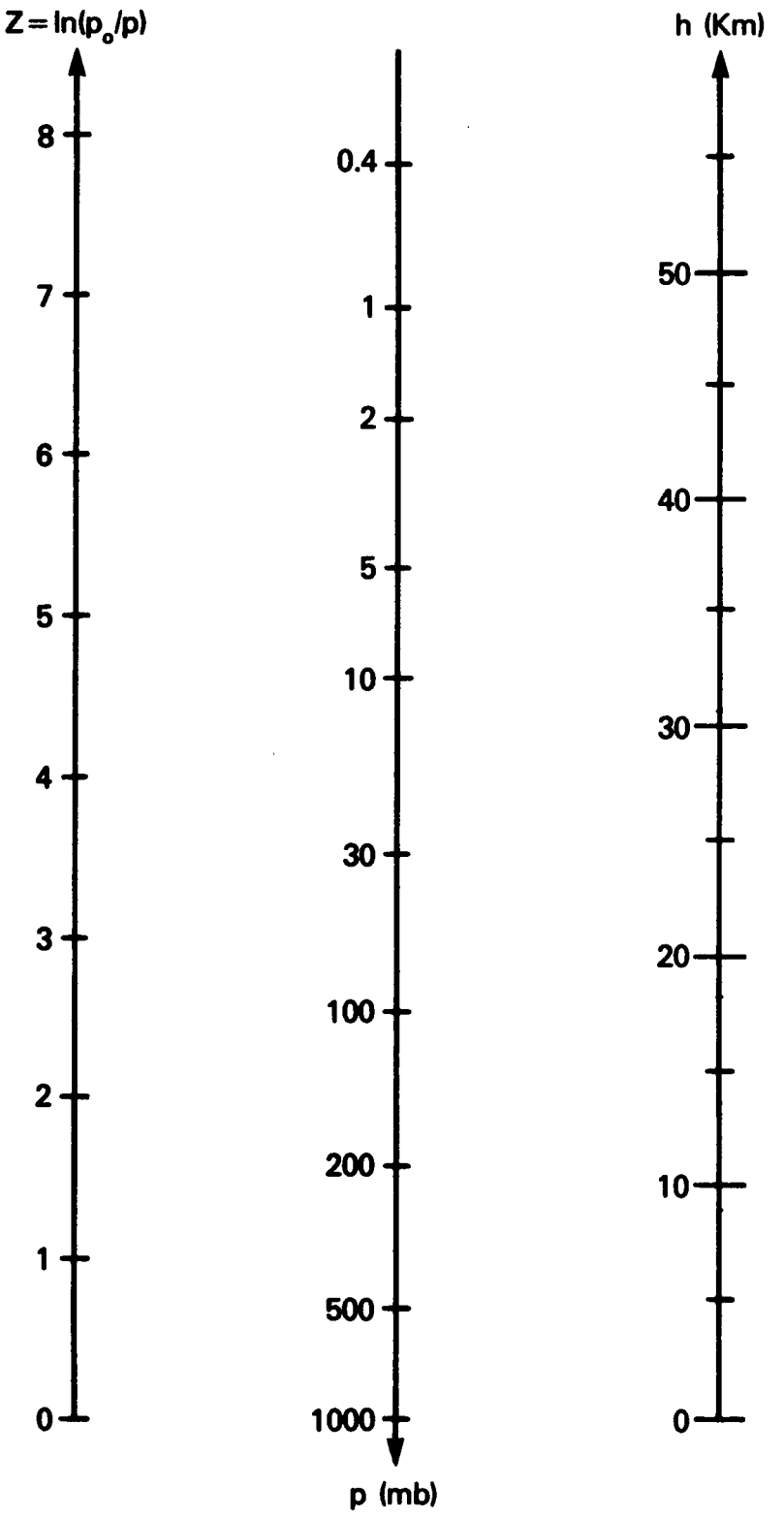

Figure 1. Relationship among $z = \ell n\ (p_o/p)$, pressure and geometric altitude scales.

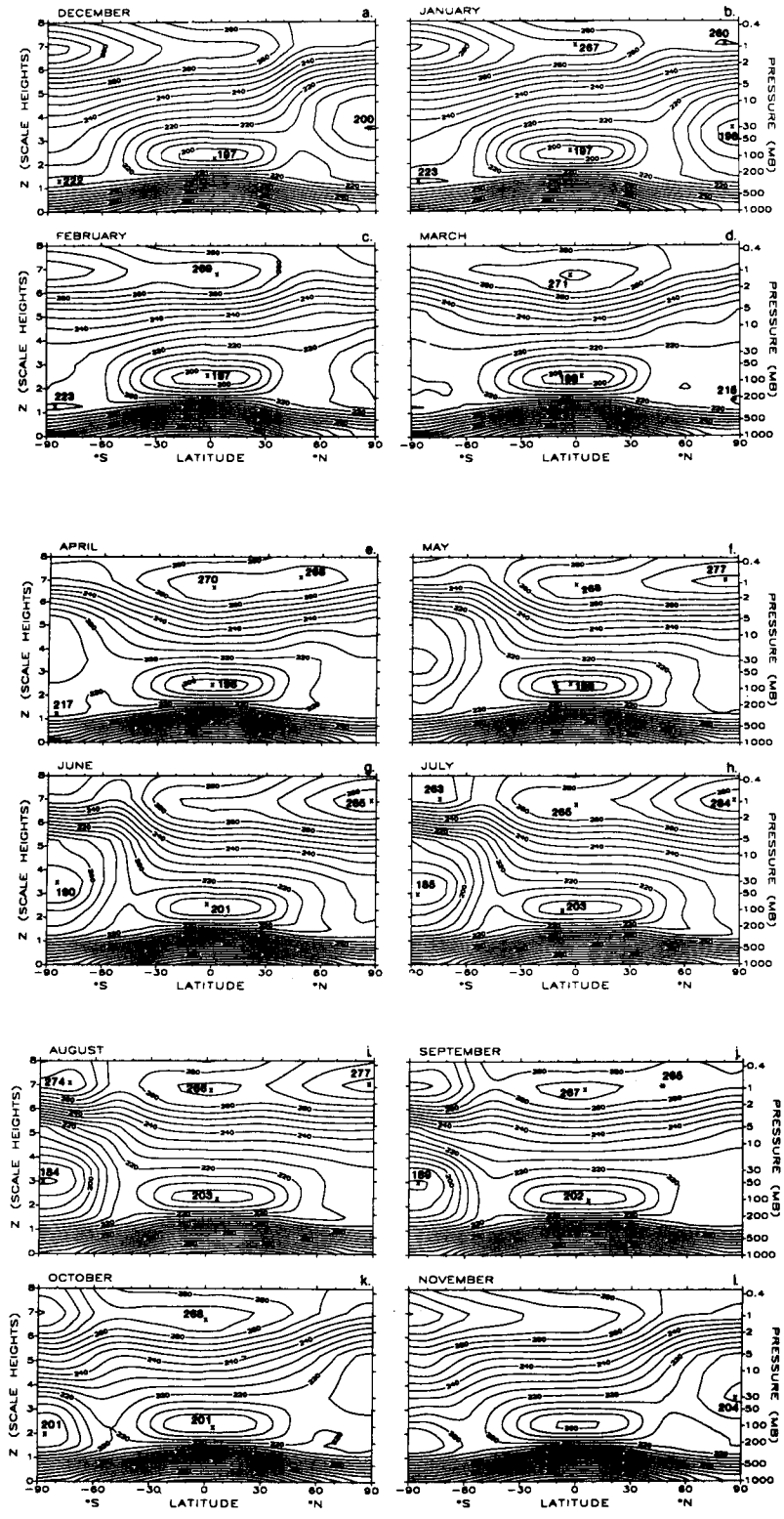

Figure 2. Four year mean zonally averaged temperatures [T] (K) for the 12 months.

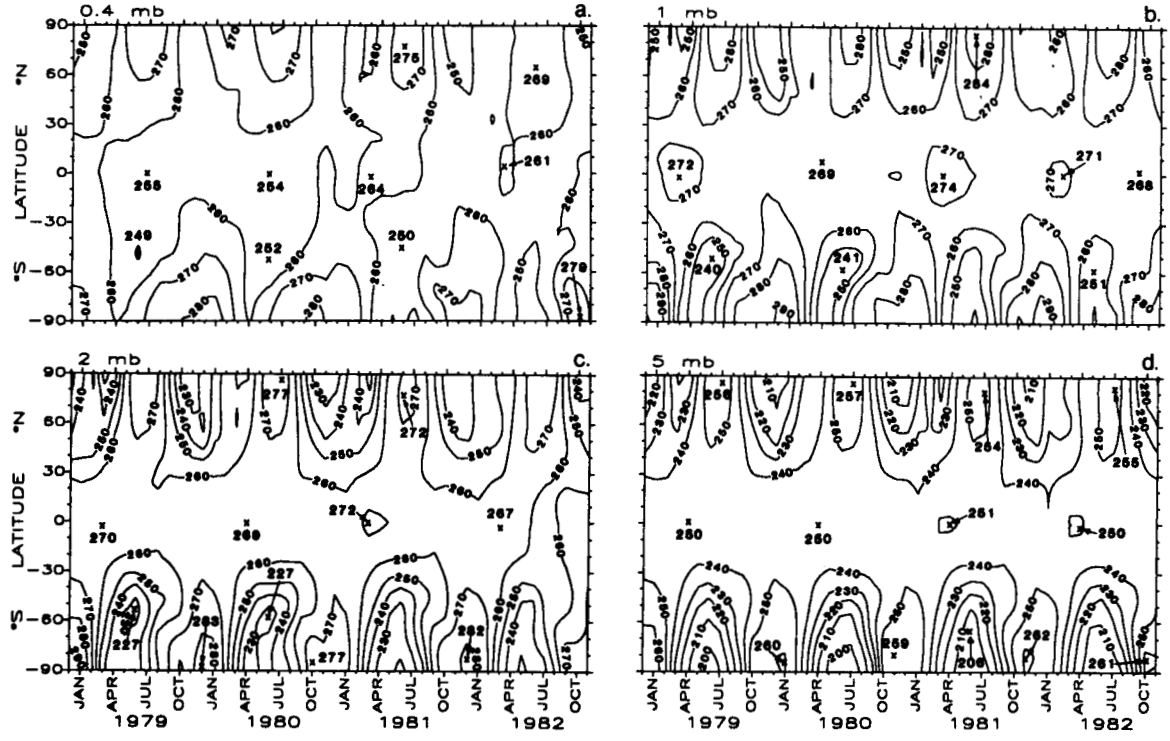

Figure 3. Time-latitude section of the zonally averaged monthly mean temperature $\overline{[T]}$ (K) at 0.4 mb, 1 mb, 2 mb and 5 mb.

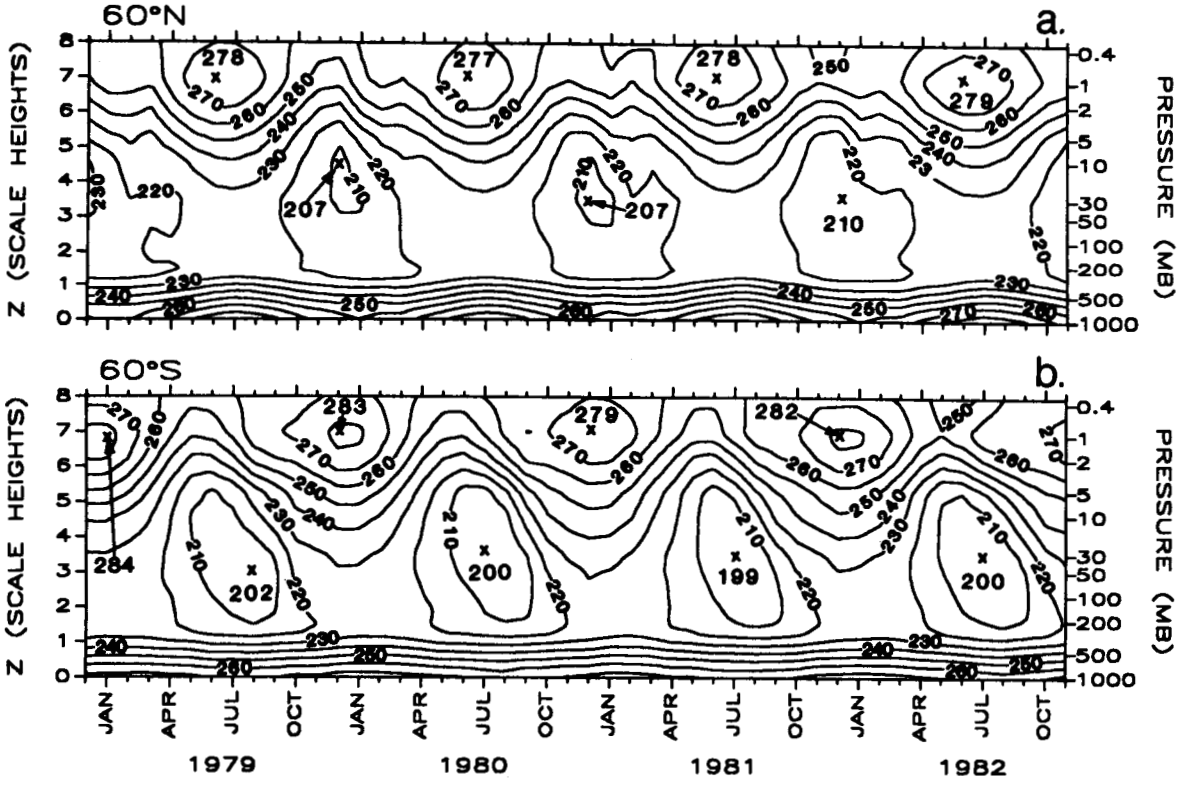

Figure 4. Time-altitude section of the zonally averaged monthly mean temperature (K), (a) at 60°N, (b) at 60°S.

3.2 Zonally Averaged Zonal Winds

3.2.1 Latitude-Altitude Section

Fig. 5 shows four year averages of the monthly mean zonally averaged zonal wind $[\bar{u}]$ for January through December for the regions between the latitudes 10° and 85° in both hemispheres. Areas of easterlies are shaded. The major differences between the two hemispheres are:

(a) The winter stratospheric westerlies are stronger in the SH than in the NH (Hartmann, 1976; Hirota et al., 1983).

(b) The center of the stratospheric westerly jet in the NH is always above the stratopause (~50 km) and often splits in late winter, whereas the jet in the SH stratosphere moves poleward and downward during winter and is closed below the stratopause in August in response to the poleward increase of the zonal mean temperature (Hartmann, 1976; Mechoso et al., 1985).

(c) The maximum speed of the tropospheric jet is higher in the NH than in the SH.

(d) In the NH the tropospheric jet increases its maximum speed from 37 m/sec in December to 45 m/sec in February, while the stratospheric jet at 55 km altitude decreases its wind speed from about 100 to about 50 m/sec during the same period. In the SH the situation appears differently. The stratospheric jet reduces its strength from about 130 m/sec in June to 97 m/sec in August, while the tropospheric maximum wind remains almost unchanged at about 39 m/sec.

(e) The maximum speed of the summer easterlies is less in the NH than in the SH.

3.2.2 Time-Latitude and Altitude Sections

The time-latitude display of the monthly mean zonally averaged zonal wind at the 0.4 mb, 1 mb, 2 mb and 5 mb pressure level and the time-altitude diagrams of the same parameter at 40°N and 40°S latitudes are presented in Figs. 6 and 7, respectively. Regions of easterlies are shaded. The following points are worth noting:

(a) The winter stratospheric jet has a much higher speed in the SH than in the NH.

(b) The maximum speed of the summer easterly winds is also larger in the SH. However, the position of the maximum easterly wind is farther away from the equator in the NH compared with that in the SH, opposite to the case of the winter westerlies.

3.3 Zonally Averaged Meridional and Vertical Velocities

The Eulerian mean meridional circulation was calculated by solving the thermodynamic and continuity equations using temperature, geostrophic winds and SBUV ozone profiles as inputs. The radiative heating calculations were carried out using the methods described in Rosenfield et al. (1987). The values from 30 mb to 0.4 mb are given in Tables 3 through 6 and plotted in Figs. 8 and 9. No similar calculation is done below 30 mb due to unavailability of SBUV ozone data. In the figures, regions of negative values (i.e. southward or downward flow) are shaded. The major features are noted below.

(a) During NH winter one sees a nearly vertical zero-line in the zonally averaged meridional wind ($[\bar{v}]$) field at about 45°N latitude between about 20 to 0.5 mb (Fig. 8a, b, c). South of this latitude the wind blows northward

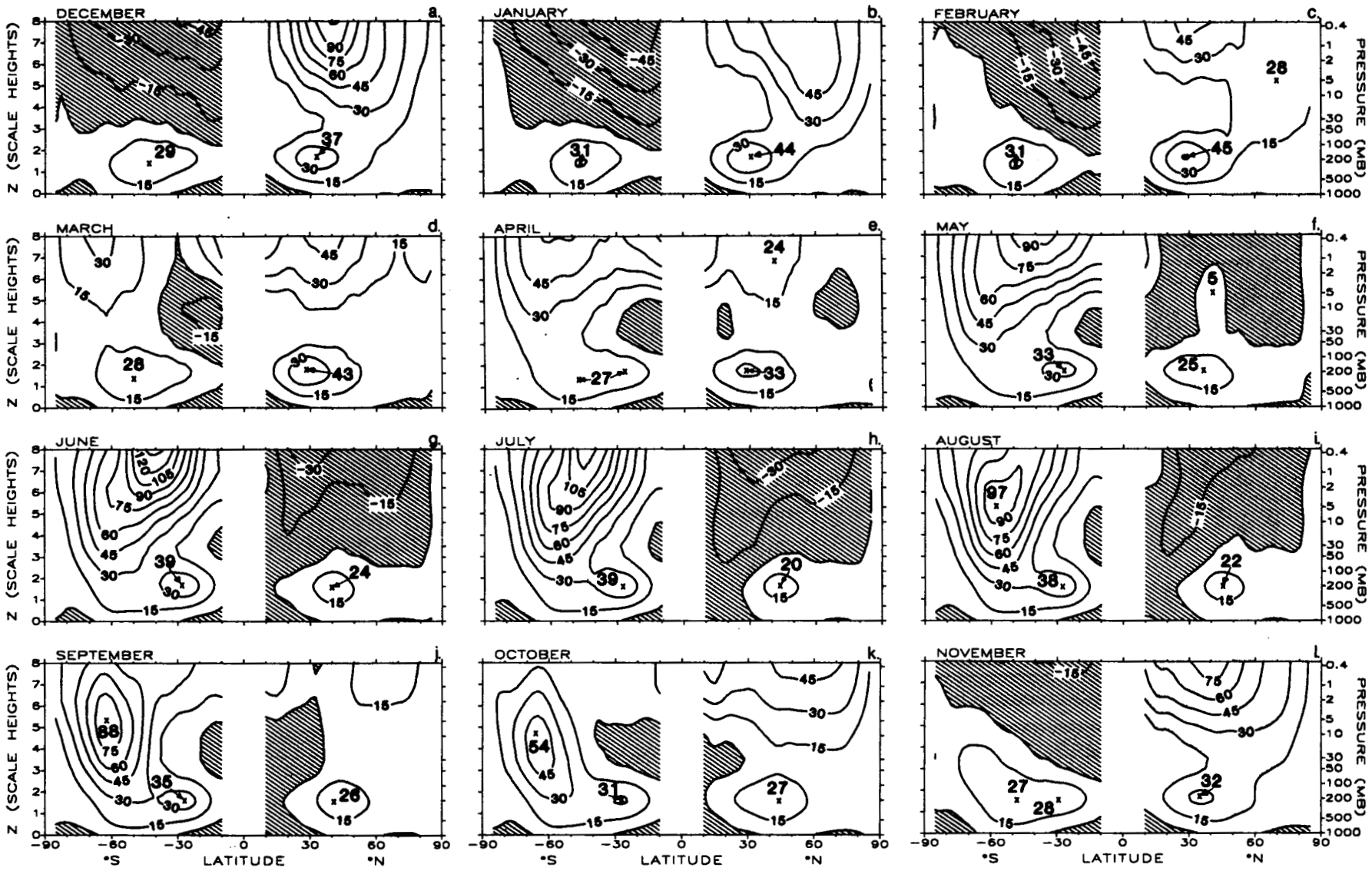

Figure 5. Four year mean zonally averaged zonal winds $[\bar{u}]$ (m/sec) for the 12 months.

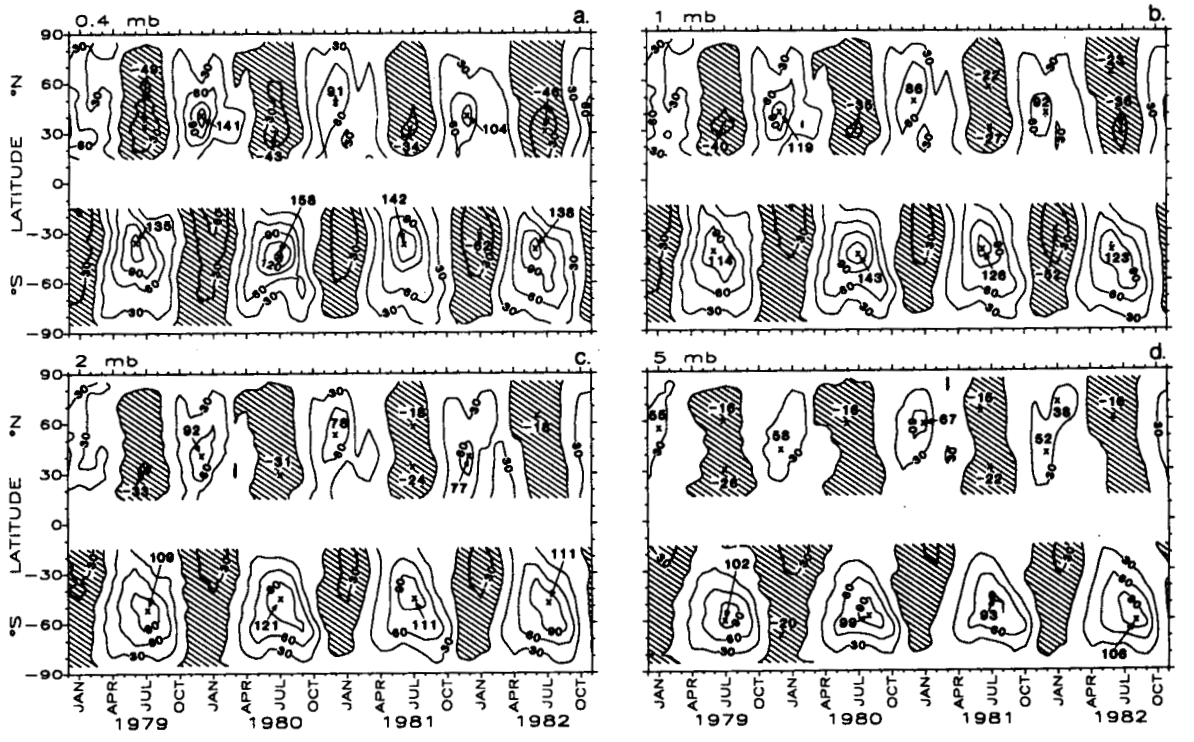

Figure 6. Time-latitude section of the zonally averaged monthly mean zonal wind $[\bar{u}]$ (m/sec) at 0.4 mb, 1 mb, 2 mb and 5 mb.

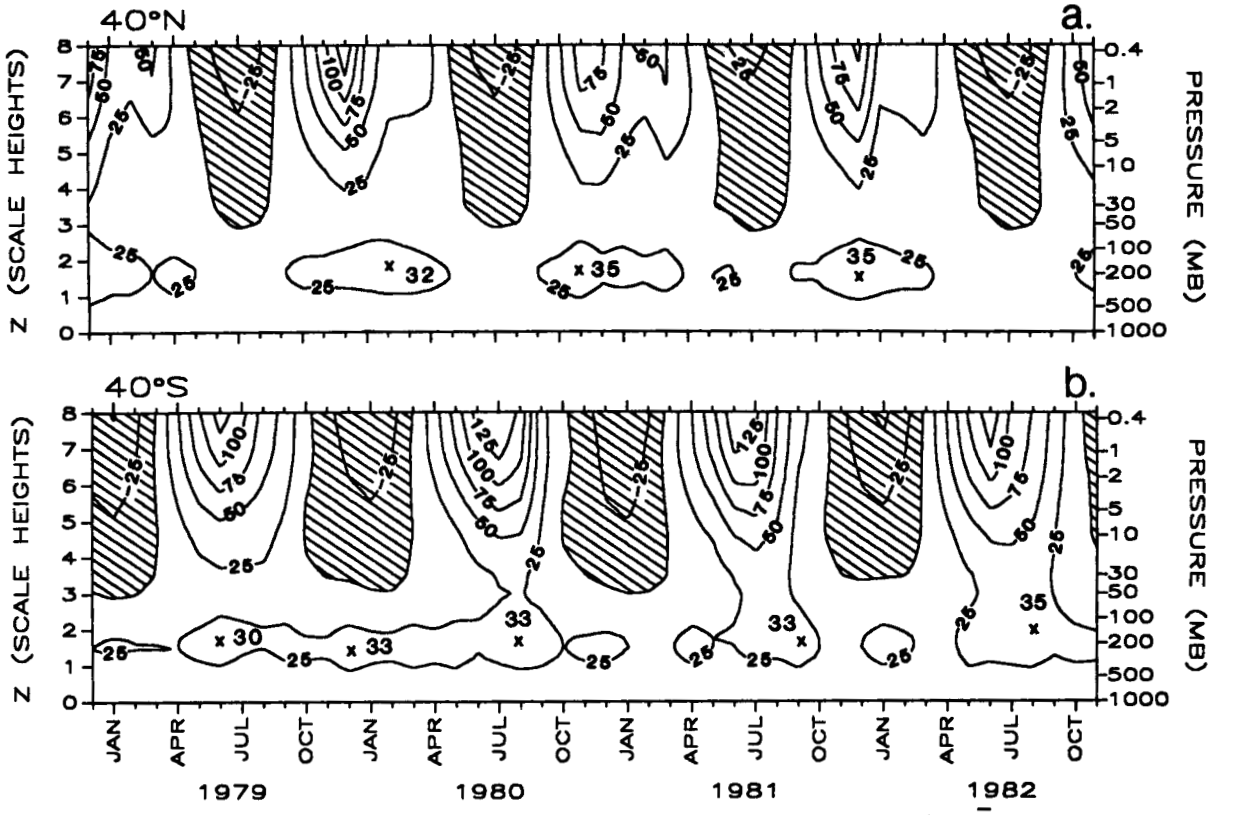

Figure 7. Time-latitude section of the zonally averaged monthly mean zonal wind $[\bar{u}]$ (m/sec), (a) at 40°N, (b) at 40°S.

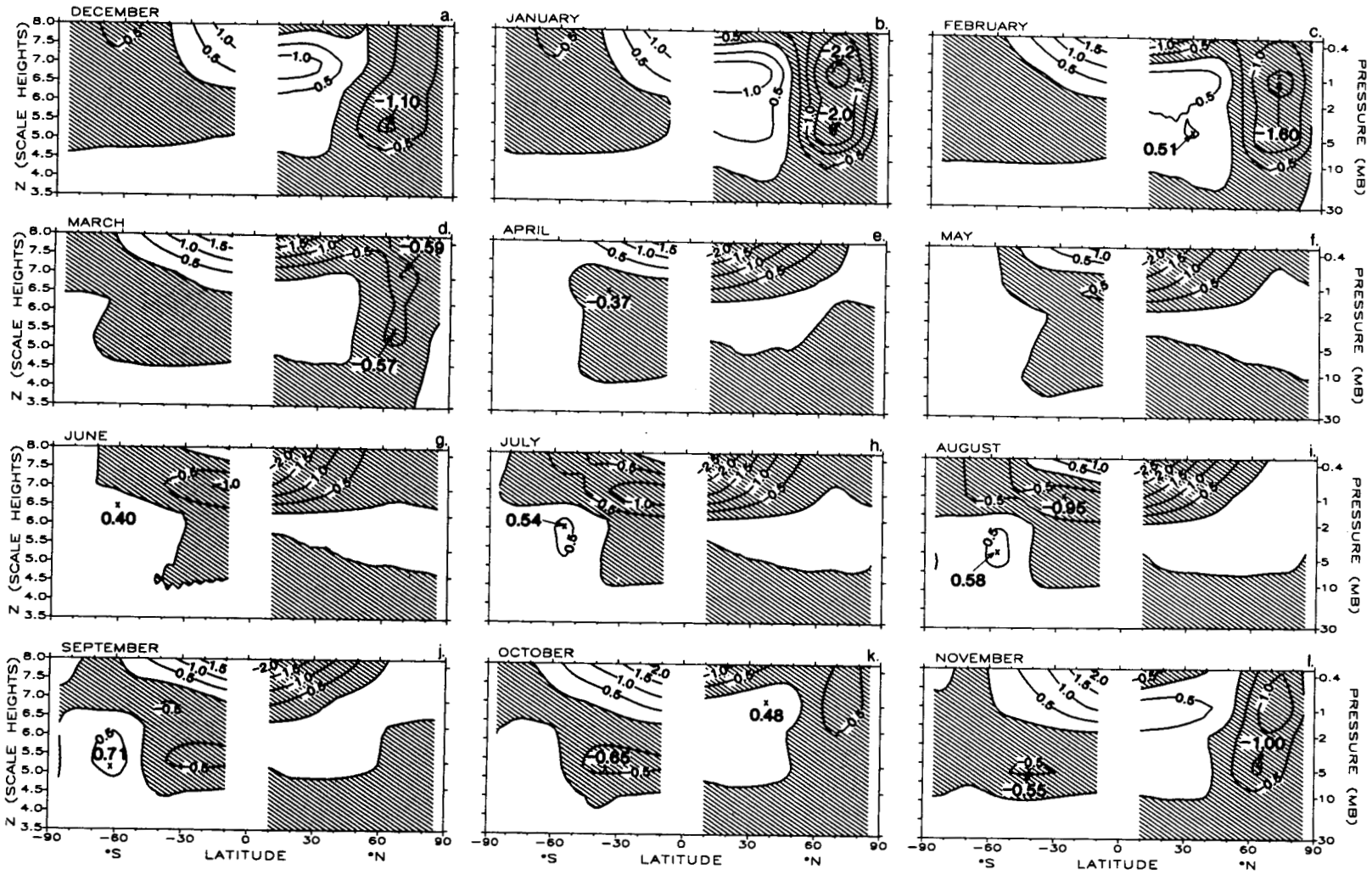

Figure 8. Four year mean zonally averaged meridional velocities derived from the heat balance and continuity equations, $[\bar{v}]$ (m/sec).

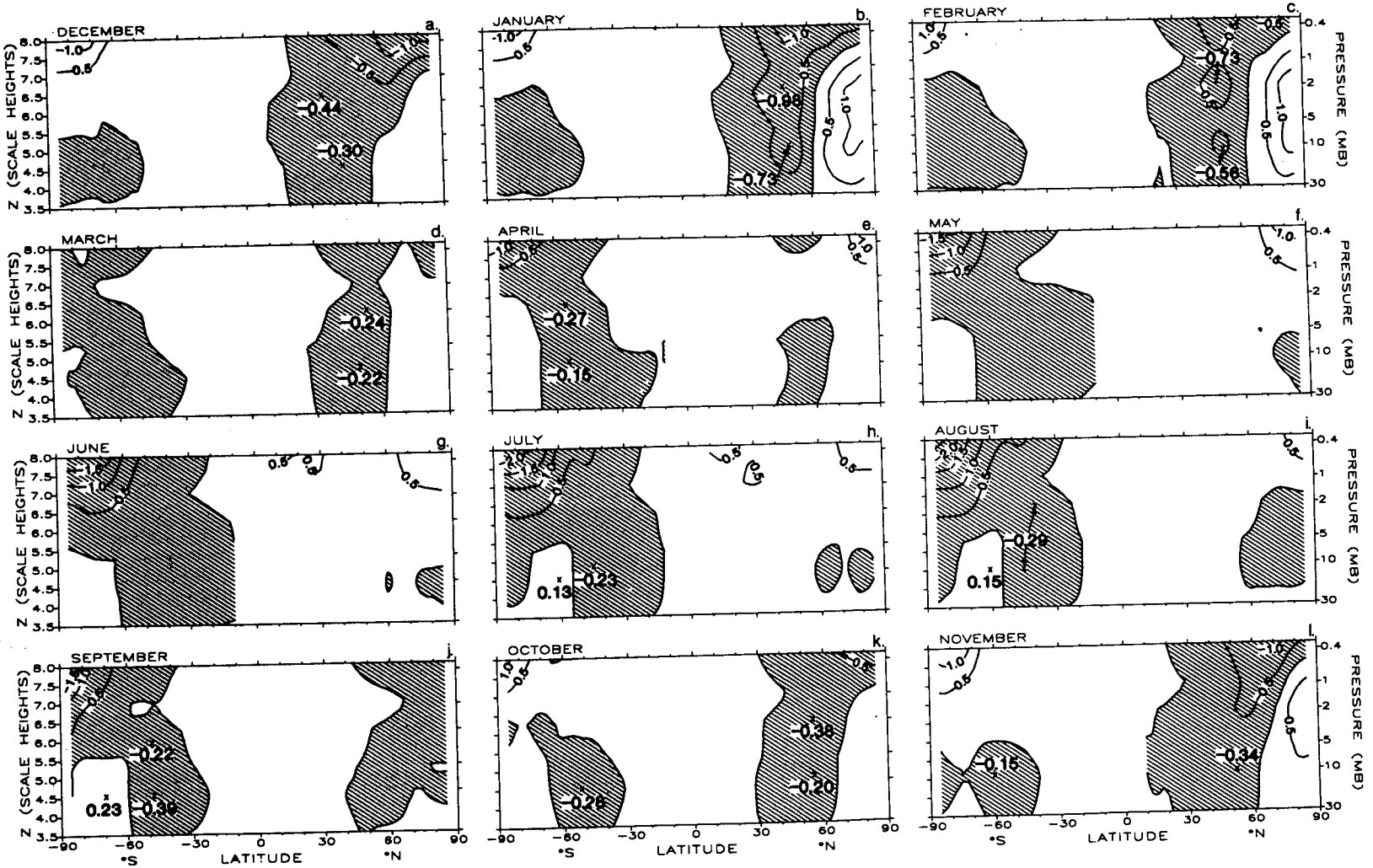

Figure 9. As in Figure 8, but for vertical velocities $[\overline{w}]$ (10^{-2} m/sec).

with a maximum value of more than 1 m/sec, and north of 45°N the wind blows towards the Equator with a maximum value of about 2 m/sec. The zonally averaged vertical velocity ([w]) field (Fig. 9a, b, c) shows upward motion over low and high latitudes with downward motion in between. The largest value of the upward velocity is about 1 cm/sec and occurs in polar regions, whereas the largest downward velocity is a bit less than 1 cm/sec at about 50°N.

(b) The pattern of the [v]-field in the SH winter (Fig. 8g, h, i) looks similar to that in the NH. The difference is that the maximum value of the equatorward wind speed in the SH is reduced to about 0.5 m/sec. The vertical motion during SH winter (Fig. 9g, h, i) is downward in middle latitudes and upward in the tropical region, similar to that in the NH counterpart. However, in the polar upper stratosphere, downward motion with a maximum speed of about 2 cm/sec occurs in the SH, whereas in the NH the downward motion is confined to middle latitudes and is of lesser speed. This calculated large downward motion near the SH winter pole is a result of the relatively high observed temperatures that were used in the calculations. The reality of the high SH winter temperatures over the polar upper stratosphere is open to question. It should be pointed out, however, that warm upper stratosphere temperatures have been noted by previous authors (Barnett, 1974; Barnett and Corney, 1985).

(c) The meridional wind in the NH summer (Fig. 8g, h, i) is northward in the middle stratosphere north of about 20°N latitude, but southward everywhere else. A large interhemispheric difference occurs in the polar upper stratosphere in summer where the mean meridional wind is poleward in the SH summer instead of equatorward as seen in the NH summer. In our computations, this difference is due to the differences in the temperature fields between the two hemispheres. The NOAA/NMC temperature data indicate that the four year mean zonally averaged temperature is about 9 K higher in the SH than in the NH polar region at 1 mb during middle summer. While this may be due to a data problem, it is pointed out that higher temperatures in SH summer than in NH summer have been reported earlier by Fritz and Soules (1970) and Barnett (1974) as mentioned in Section 3.1.1a.

(d) Generally speaking, the meridional wind in the NH spring blows towards the equator below about 35 km and above about 48 km with poleward flow in between (Fig. 8d, e, f) while the vertical wind is upward over the greater portion of the middle and upper stratosphere (Fig. 9d, e, f). The meridional wind pattern during the SH spring (Fig. 8j, k, l) is similar to that of its NH counterpart. The vertical wind, however, shows a larger area of downward flow in middle latitudes during the SH spring (Fig. 9j, k, l). The magnitudes of the wind speeds are comparable between the two hemispheres.

(e) There is a lot of similarity in the pattern of the meridional and vertical winds during fall between the two hemispheres (Fig. 8d, e, f and Fig. 9d, e, f for SH; Fig.8j, k, l and Fig. 9 j, k, l for NH).

In the transitional months, April and October, the net diabatic heating is the highest over the equatorial upper stratosphere, while the largest net cooling occurs in the polar regions. In the low latitudes the eddy heat transfer is small, therefore balance is approximately maintained there between the meridional circulation and the diabatic heating. One would expect that an upward motion with equatorward flow from north and south should appear. These circulation patterns are indeed present as shown in Fig. 16 e and k. However, the detailed structure of the circulation can not be delineated based on the present data using geostrophic winds.

3.4 Planetary Waves

3.4.1 Latitude-Altitude Section

Fig. 10 shows latitude-altitude plots of the amplitude structure of the stationary planetary waves in the geopotential height field for zonal wavenumber one for the months January to December. Somewhat similar diagrams have been shown by Hirota (1976) and Hirota et al. (1983). The major differences between the NH and SH are:

(a) In the NH stratosphere the seasonal cycle of the planetary wave 1 is pronounced with an amplitude of about 1010 m occurring in middle winter at about 65°N; the minimum occurs in summer. The seasonal cycle is less pronounced in the SH with a maximum value of about 700 m appearing in middle spring (not in winter) at about 60°S. Again, the minimum occurs in summer.

(b) The waves usually start building their strength in middle or late fall in both hemispheres, reaching their peak in winter or spring and then decaying. The differences between the two hemispheres are: (i) the waves in the NH become weak after early spring, whereas in the SH the waves maintain their vigorous activity until middle or even late spring; (ii) although the maximum amplitude of the wave in the NH is larger than that in the SH during winter, the reverse is true during spring.

Fig. 11 shows the structures of wavenumber two amplitudes. The average magnitude of the wave 2 maximum is less than half of that of wave 1 in both hemispheres. The difference is that in the NH the location of the wave 2 maximum is at least 10 km lower than that of the wave 1 maximum, while in the SH the wave 2 maximum is about the same height as the wave 1 maximum. In the SH, the wavenumber 2 amplitude is smaller in winter than in spring.

The wavenumber 3 structures are shown in Fig. 12. In the NH winter and spring one sees two maxima, one in the troposphere the other in the stratosphere, whereas in the SH only a tropospheric maximum appears. The value of the tropospheric wave maximum is larger in the NH than in the SH during winter and spring. The seasonal cycle is more pronounced in the NH than in the SH. The largest maximum amplitude occurs in middle winter in both hemispheres in contrast to the wave 1 case in which a time lag of about 2 months is seen in the SH.

3.4.2 Time-Altitude Sections

Figs. 13-15 show the time-altitude section of the monthly mean planetary wave amplitudes for wavenumber 1, 2, and 3 at 60° N and 60° S. The major features are described below.

(a) The amplitudes of the waves are smaller in the SH than in the NH.

(b) The interannual variation of the maximum monthly wave 1 amplitude at 60° N ranges from 900 m occurring in year one to 1038 m occurring in year 3 in the NH, while in the SH the limits are from about 600 m to 800 m. These figures along with other plots in different sectors show that in the period December 1978 through November 1982 the interannual variability is larger in the NH than in the SH.

(c) From time-latitude sections (not shown) one may see that the interannual variability of the wave 1 amplitude in the SH is less in winter than in spring.

(d) The amplitude of the planetary wave 2 appears to be anti-correlated with wave 1 in the NH; there is no clear correlation in the SH.

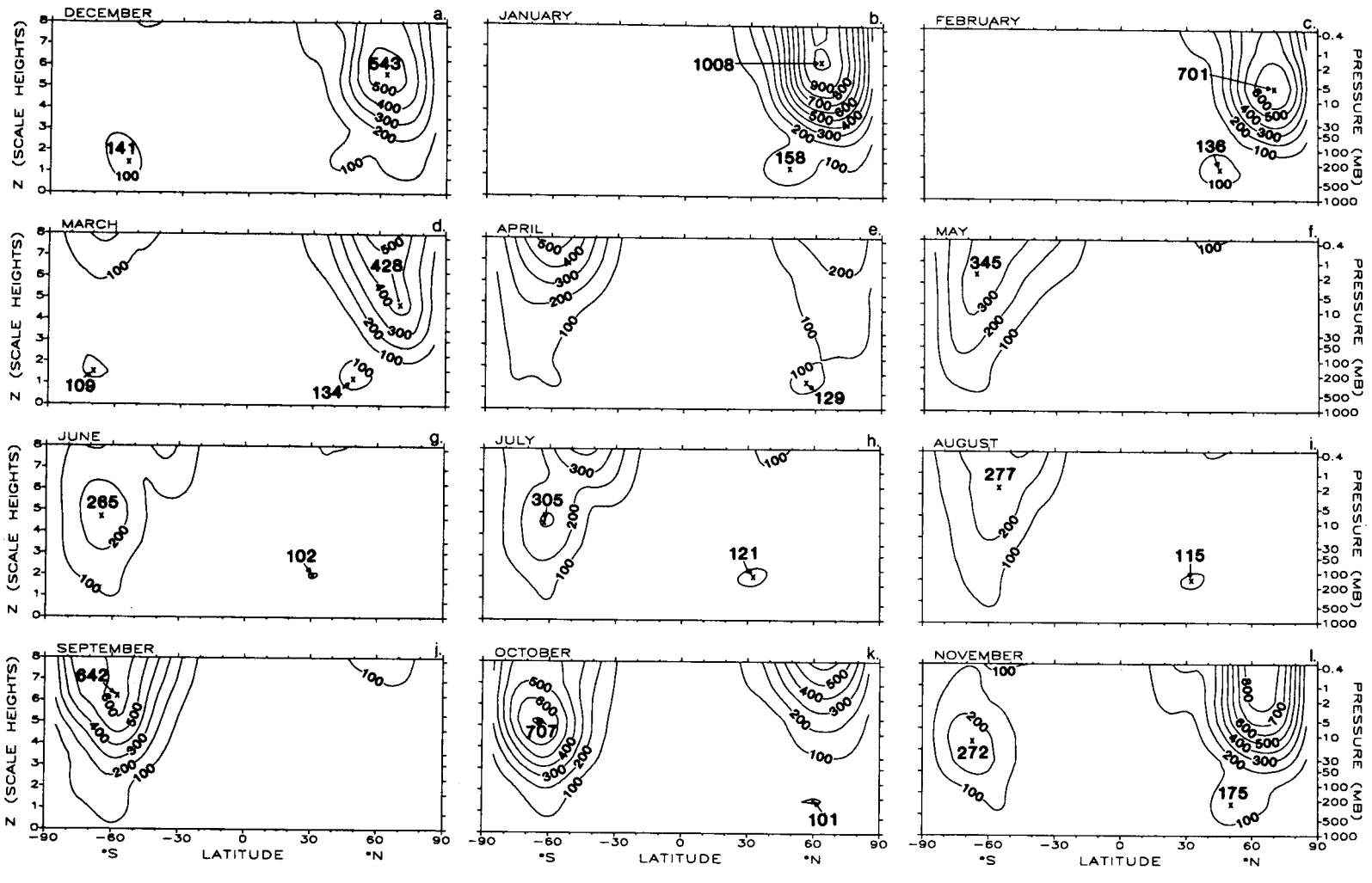

Figure 10. Four year mean geopotential height amplitudes (m) of zonal wavenumber one for the 12 months.

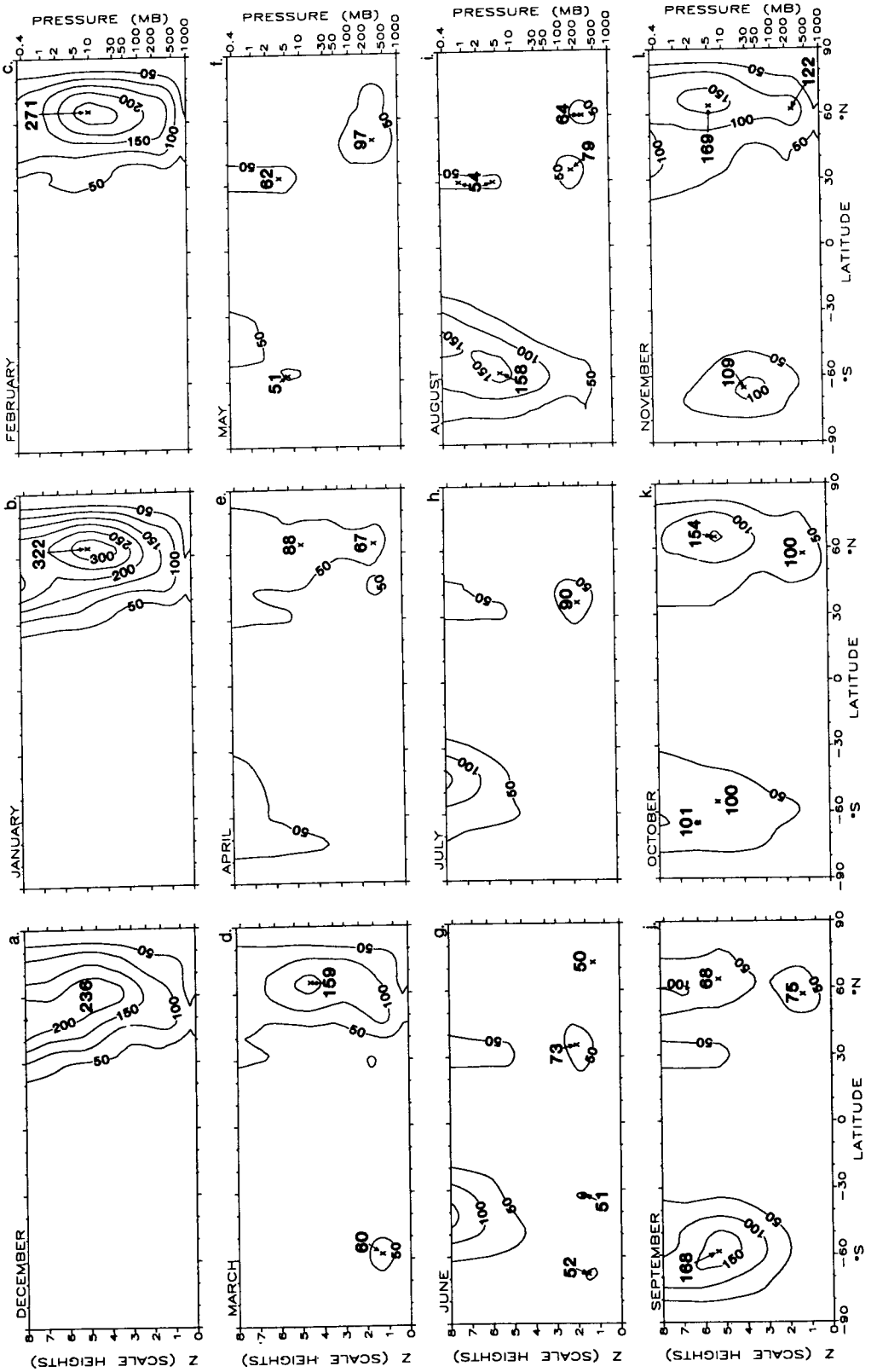

Figure 11. As in Figure 10, but for wavenumber two.

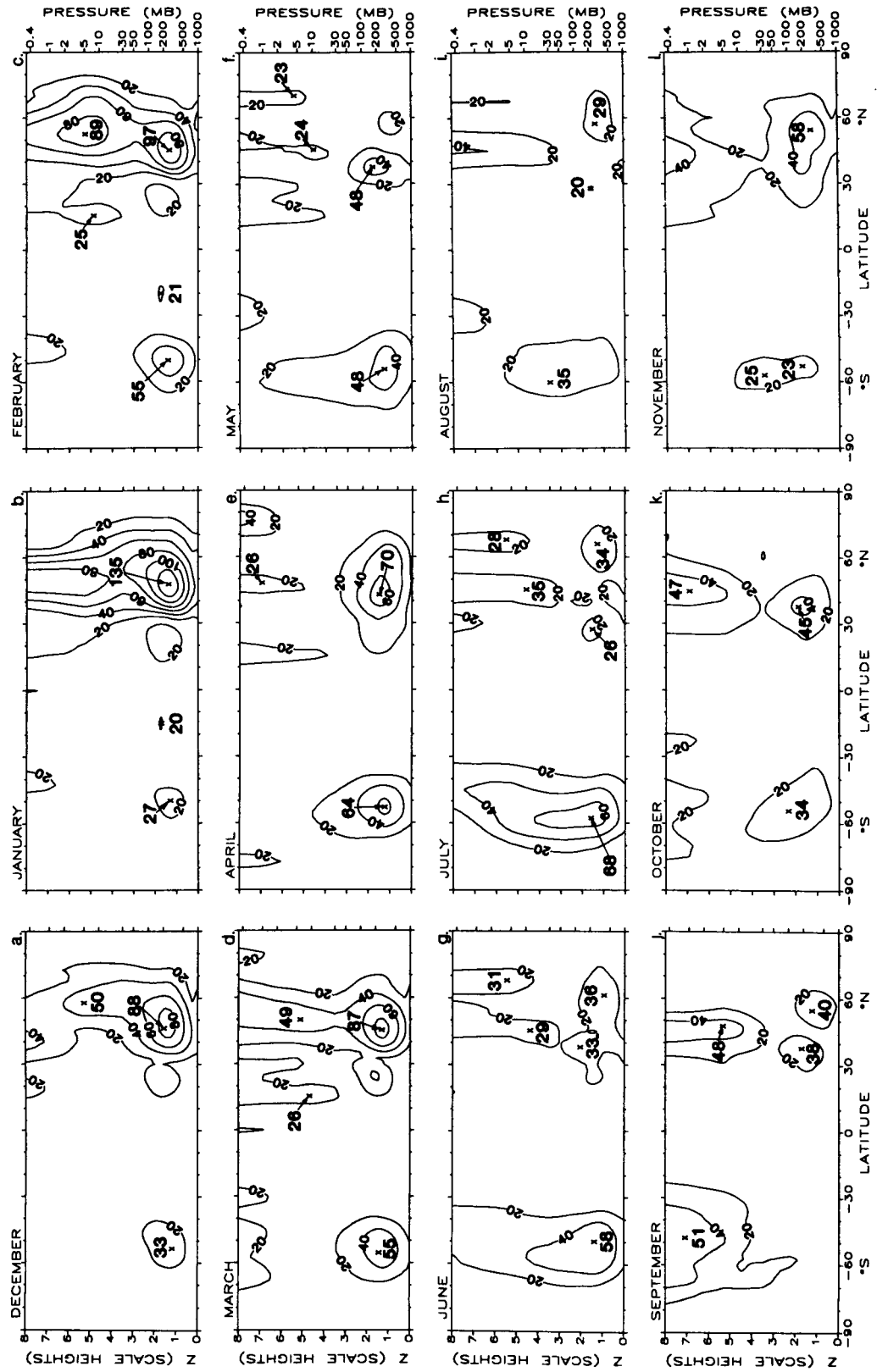

Figure 12. As in Figure 10, but for wavenumber three.

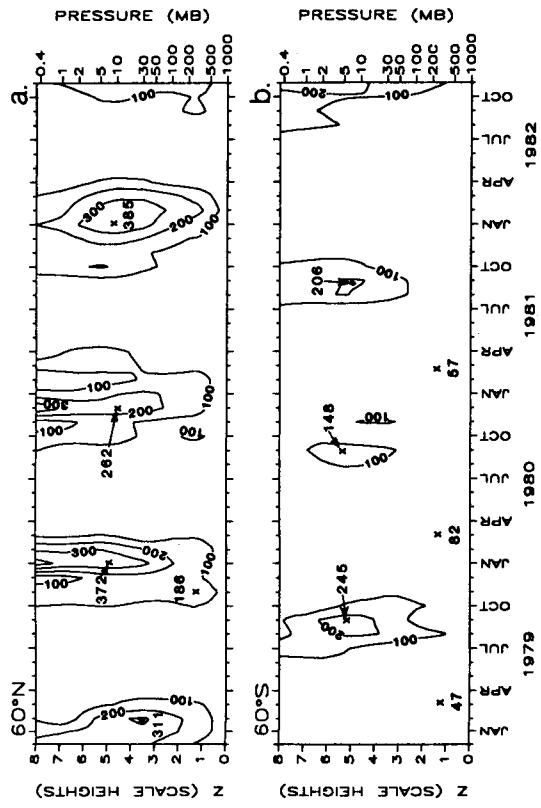

Figure 13. Time-altitude section of monthly mean geopotential height amplitude (m) of zonal wavenumber one (a) at 60°N, (b) at 60°S.

Figure 14. As in Figure 13, but for wavenumber two.

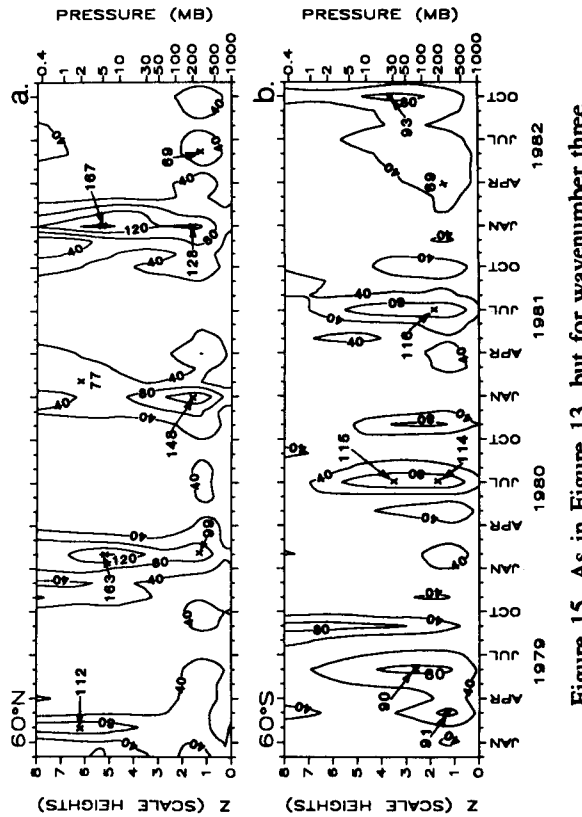

Figure 15. As in Figure 13, but for wavenumber three.

(e) The large wave amplitude shown in the SH fall in wavenumber one does not appear in wavenumbers 2 and 3.

3.5 Heat Fluxes
3.5.1 Due to Standing Eddies
3.5.1.1 Latitude-Altitude Section

Fig. 16 shows latitude-altitude cross sections of the northward heat fluxes averaged over the four years due to standing eddies $[\overline{v^*T^*}]$. Regions of negative values are shaded. With regard to the interhemispheric differences the following points may be noted:

(a) In the NH the annual variation of the heat flux is pronounced with a strong maximum of about 153 K m/sec in middle winter, whereas in the SH the seasonal cycle is weak with a maximum poleward flux of about -55 K m/sec in middle spring.

(b) On the average the winter poleward heat flux is more than five times greater in the NH than in the SH, but the spring poleward flux is about a factor of 3 larger in the SH than in the NH.

(c) The heat fluxes by the wave components are shown in Figs. 17 to 19. The features described in (a) and (b) are clearly associated with planetary wave activity and the planetary waves 1 and 2 account for most of the variance of the total standing eddy heat fluxes. Although wavenumber one dominates the heat flux in both hemispheres, notable differences exist. First, in the NH although wavenumber one plays a leading role in the heat flux, wavenumber two also contributes a substantial portion of the total standing eddy flux especially in winter, whereas in the SH wavenumber one possesses overwhelming power over the other components. Secondly, in spring the heat flux in the NH begins to decrease rapidly after March following the sharp decline in wavenumber one activity, while in the SH the heat flux remains strong until middle spring.

3.5.1.2 Time-Latitude and Altitude Sections

Fig. 20 shows the time-latitude section of the sensible heat fluxes due to standing eddies at 0.4 mb, 1 mb, 2 mb and 5 mb. The distributions and variations in the $[\overline{v^*T^*}]$-field are determined by the planetary wave activity.

(a) Poleward heat flux during winter is more than two times larger in the NH than in the SH at the 1 mb level. However, the size of the area of the poleward heat flux is larger in the SH on an annual basis for all 4 sample years.

(b) There is a steady poleward heat flux in the SH during spring year after year, but no similar flux is seen in the NH spring.

(c) Planetary wavenumber one dominates the interannual variations both in the NH and SH (not shown).

Time-altitude sections of the northward heat fluxes at the 60°N and 60°S latitudes are depicted in Fig. 21. These figures provide another view of the global heat fluxes at particular locations (60° in the present case). The diagrams shown in Fig. 21 reconfirm the findings reported previously.

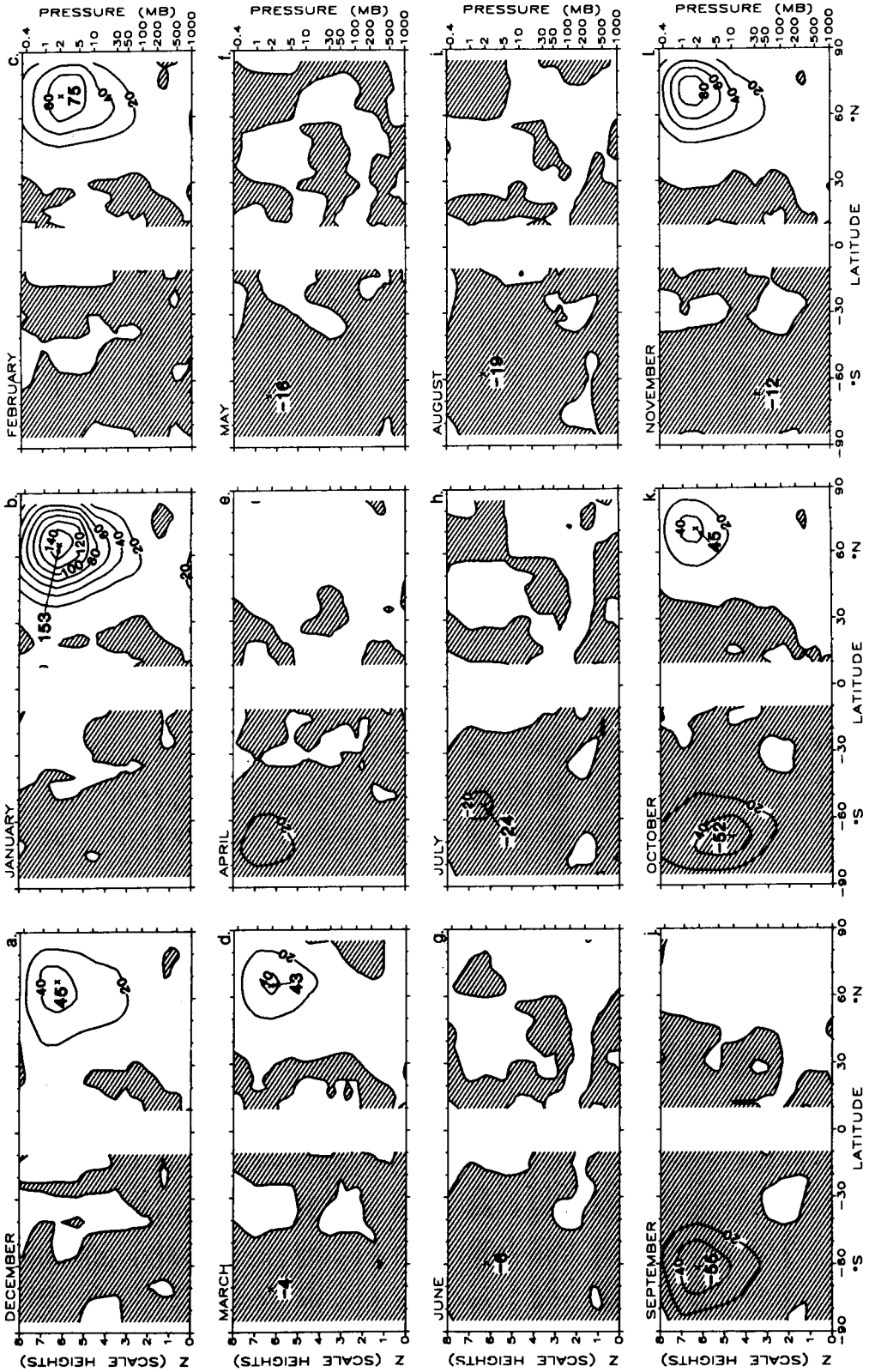

Figure 16. Monthly four year mean northward flux of sensible heat by the standing eddies $[\bar{v}^*\bar{T}^*]$ (K m/sec).

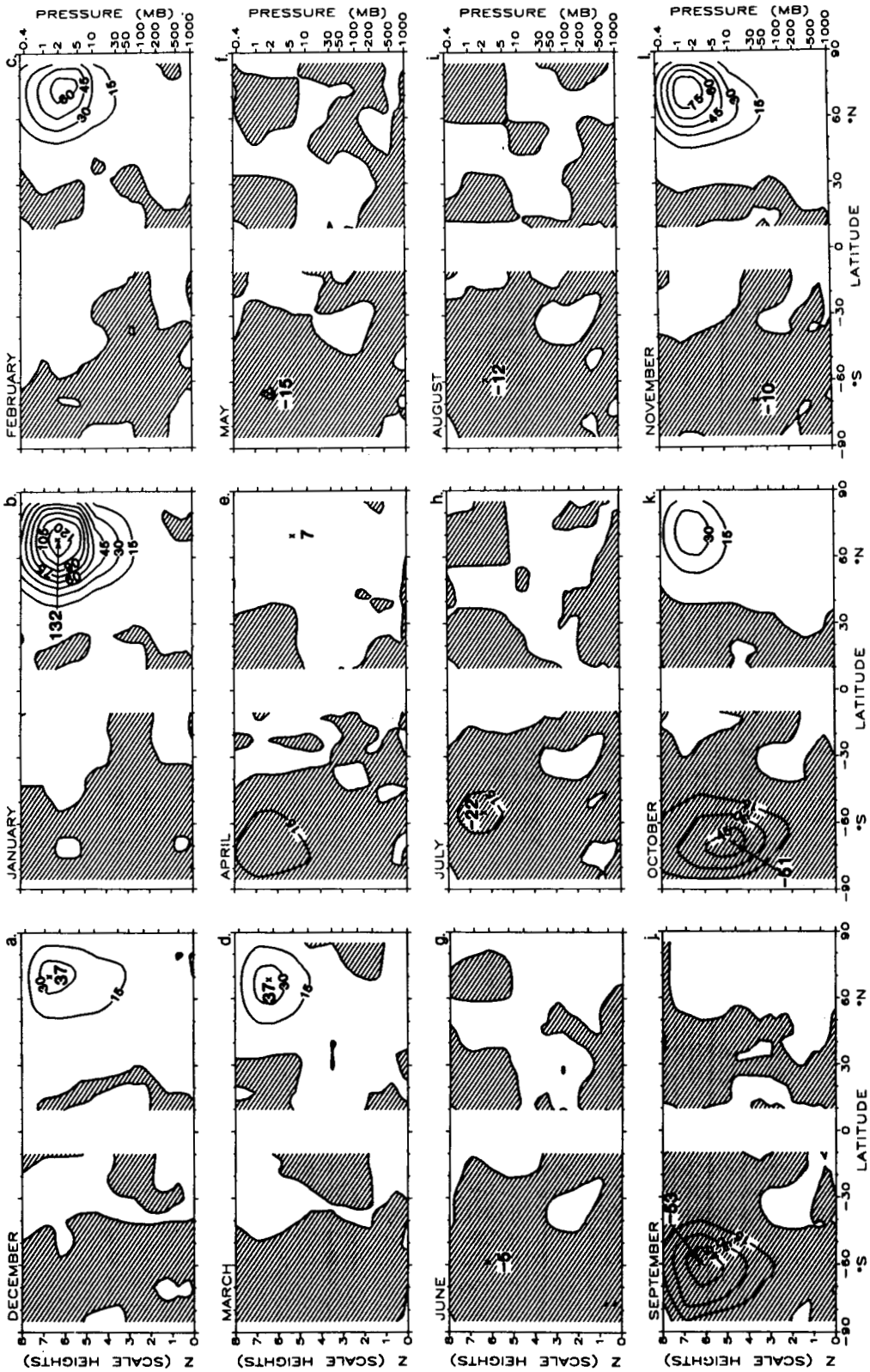

Figure 17. Northward flux of heat by stationary eddy zonal wavenumber one $[\bar{v}^*\bar{T}^*]_{m=1}$ (K m/sec).

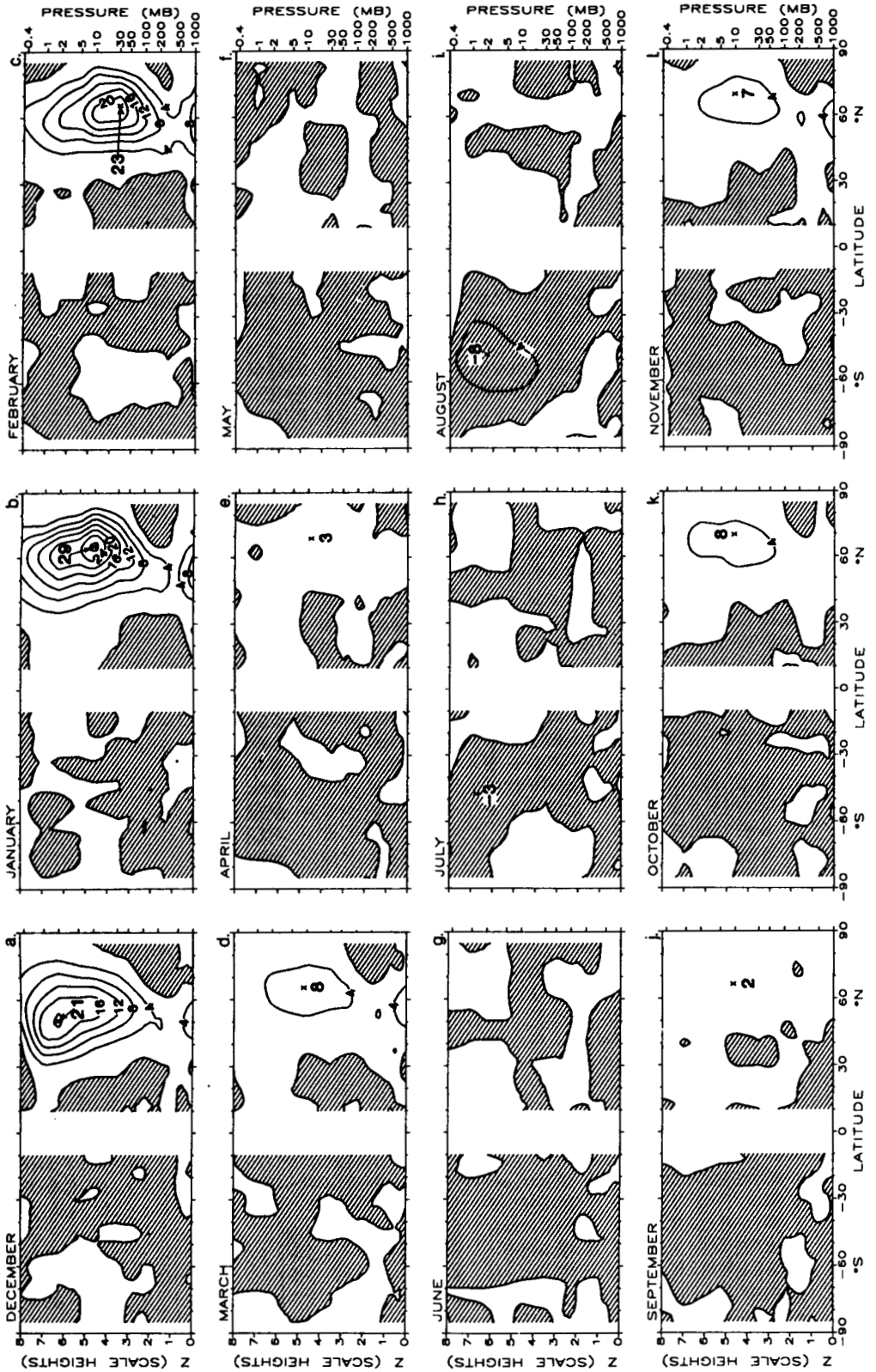

Figure 18. As in Figure 17, but for wavenumber two.

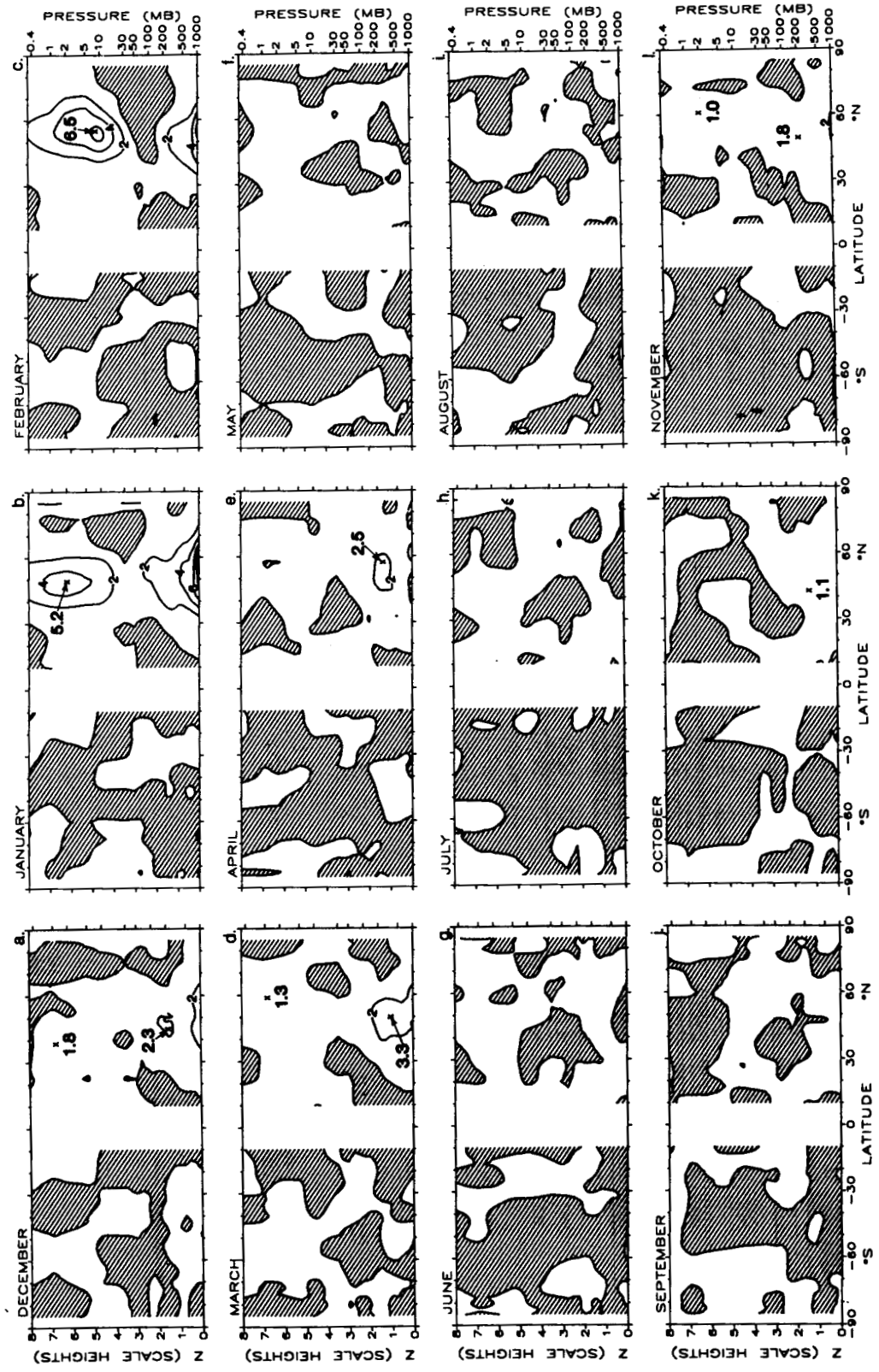

Figure 19. As in Figure 17, but for wavenumber three.

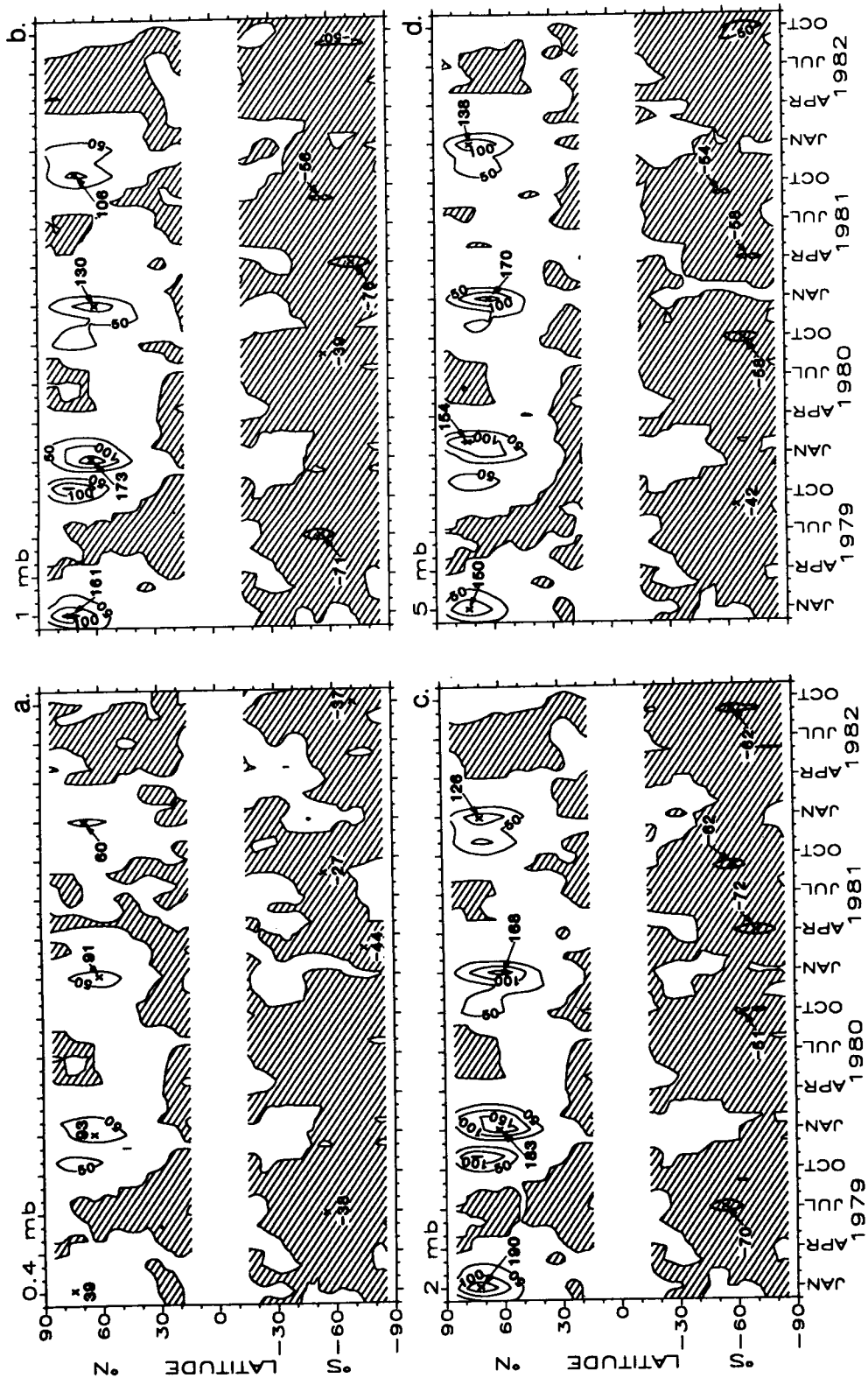

Figure 20. Time-latitude section of northward flux of sensible heat by the standing eddies at 0.4 mb, 1 mb, 2 mb and 5 mb.

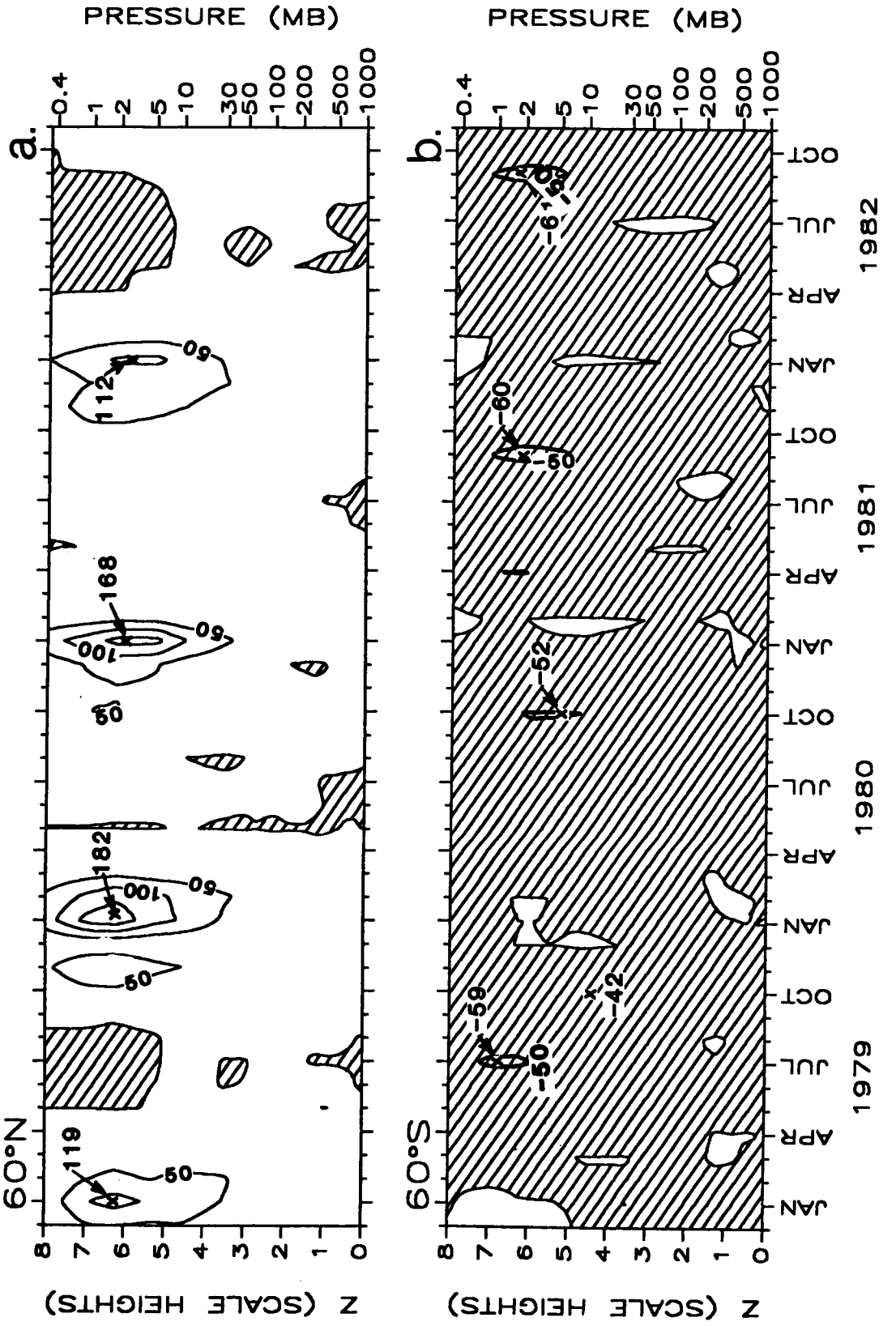

Figure 21. Time-altitude section of northward flux of sensible heat by the standing eddies, (a) at 60°N, (b) 60°S.

3.5.2 Due to Transient Eddies

3.5.2.1 Latitude-Altitude Section

Fig. 22 shows latitude-altitude cross sections of the northward fluxes of sensible heat by the transient eddies $[\overline{v'T'}]$. Regions of negative values are shaded. The main highlights are:

(a) In the annual variation, the largest poleward heat flux due to the transient eddies occurs in the late winter in both hemispheres (i.e. in February and August). This aspect is different from what happens in the standing eddy heat fluxes which maximize their values in middle winter in the NH (or in January), and in middle spring in the SH (or in October).

(b) Generally speaking, in the SH the overall contribution to the poleward heat fluxes is more from the transient eddies than from the standing eddies during winter, but less during spring. The magnitude of the transient eddy heat fluxes during NH winter are about half of that of the standing eddies.

(c) In the NH, the transient eddy fluxes begin to build their strength in October, subsequently, there is a short setback in November after which they increase steadily throughout the entire winter. The fluxes reach their annual peak in late winter and then decline sharply in March. In middle spring the fluxes are very weak and remain so throughout the rest of the year. The behavior of the annual march of the transient eddy fluxes in the SH acts in a similar manner to its NH counterpart. This aspect is different from what we have seen in the standing eddy case.

As for the contributions from wave components, we find the following interesting points (see Figs. 23-25):

(d) During NH winter and early spring, although the wavenumber one flux is relatively larger than the wavenumber two flux, wavenumber one no longer plays a dominant role as it does in the standing eddy flux case.

(e) During SH winter and early spring wavenumber 2 contributes more than wavenumber 1 to the transient eddy poleward flow of heat.

(f) Generally speaking, during the NH fall, wavenumber one is comparatively more effective than wavenumber two in providing heat to the polar region.

3.5.2.2 Time-Latitude and Altitude Sections

Fig. 26 shows the time-latitude section of the monthly mean northward heat fluxes due to transient eddies at 0.4 mb, 1 mb, 2 mb and 5 mb. The time-altitude sections of $[\overline{v'T'}]$ at 60°N and 60°S latitudes are presented in Fig. 27. Regions of southward fluxes are shaded. The following points are noted.

(a) The interannual variations in the magnitude and time of occurrence of the annual peak flux differ from one hemisphere to the other. For example, in the present sample, it is found that the largest maximum transient heat flux appears in year 4 and the smallest maximum occurs in year 3 in the NH, whereas in the SH the corresponding events are seen in years 1 and 3 (Fig. 26).

It should be noted that the annual maximum occurs in different seasons in each hemisphere. In the NH, three out of four cases happen in February (or late winter in years 2, 3, 4) and one case in January (or middle winter in year 1), whereas in the SH, the most cases appears in August (or late winter in years 1, 3, 4) with one case in September (or early spring in year 2).

(b) In the NH, both waves 1 and 2 contribute about equally to the heat flux during winter. In the SH, wave 2 appears to contribute more than wave 1 (see Figs. 23 & 24).

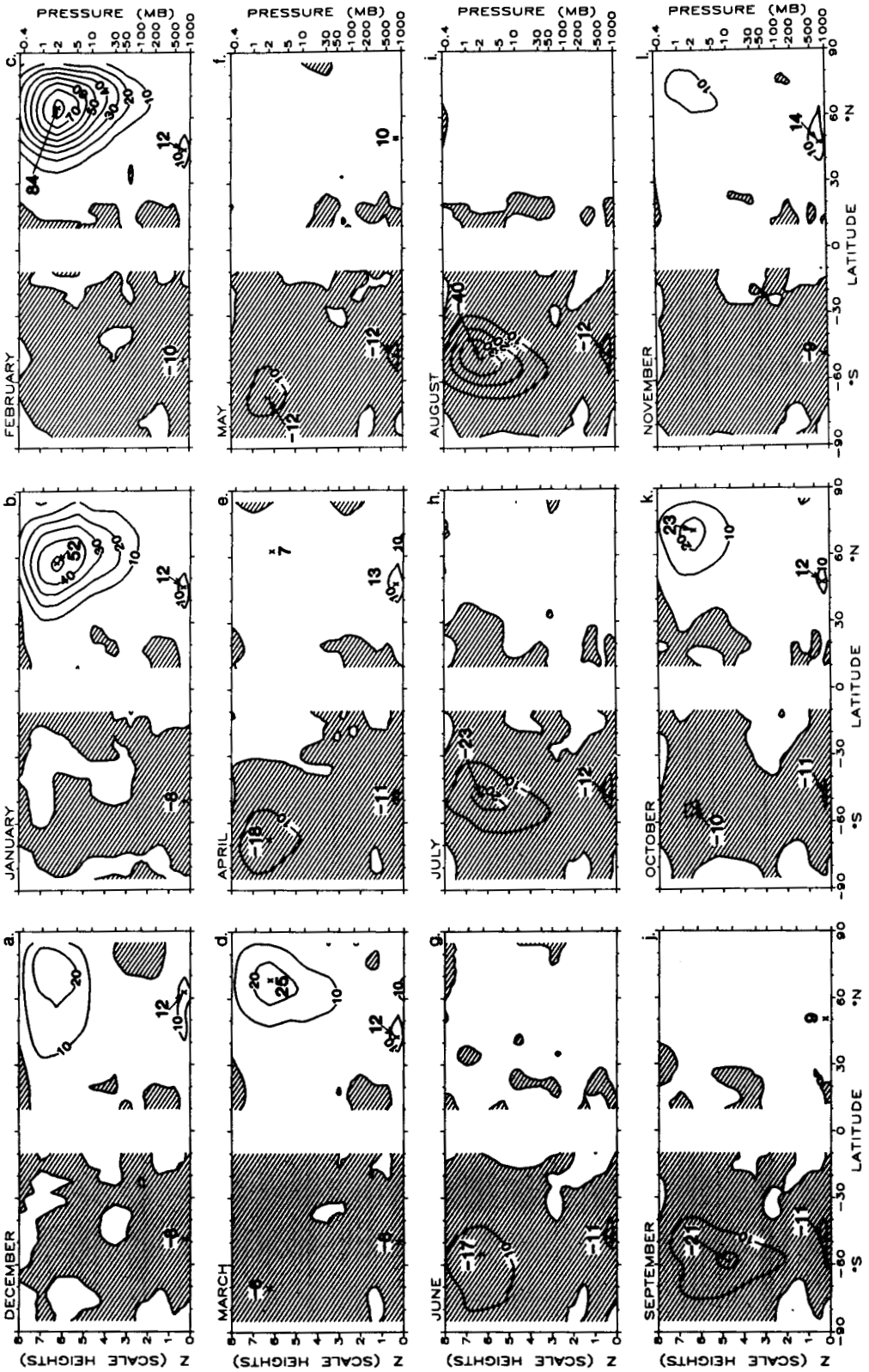

Figure 22. As in Figue 16, but for the northward flux of heat by transient eddies $[\overline{v'T'}]$ (K m/sec).

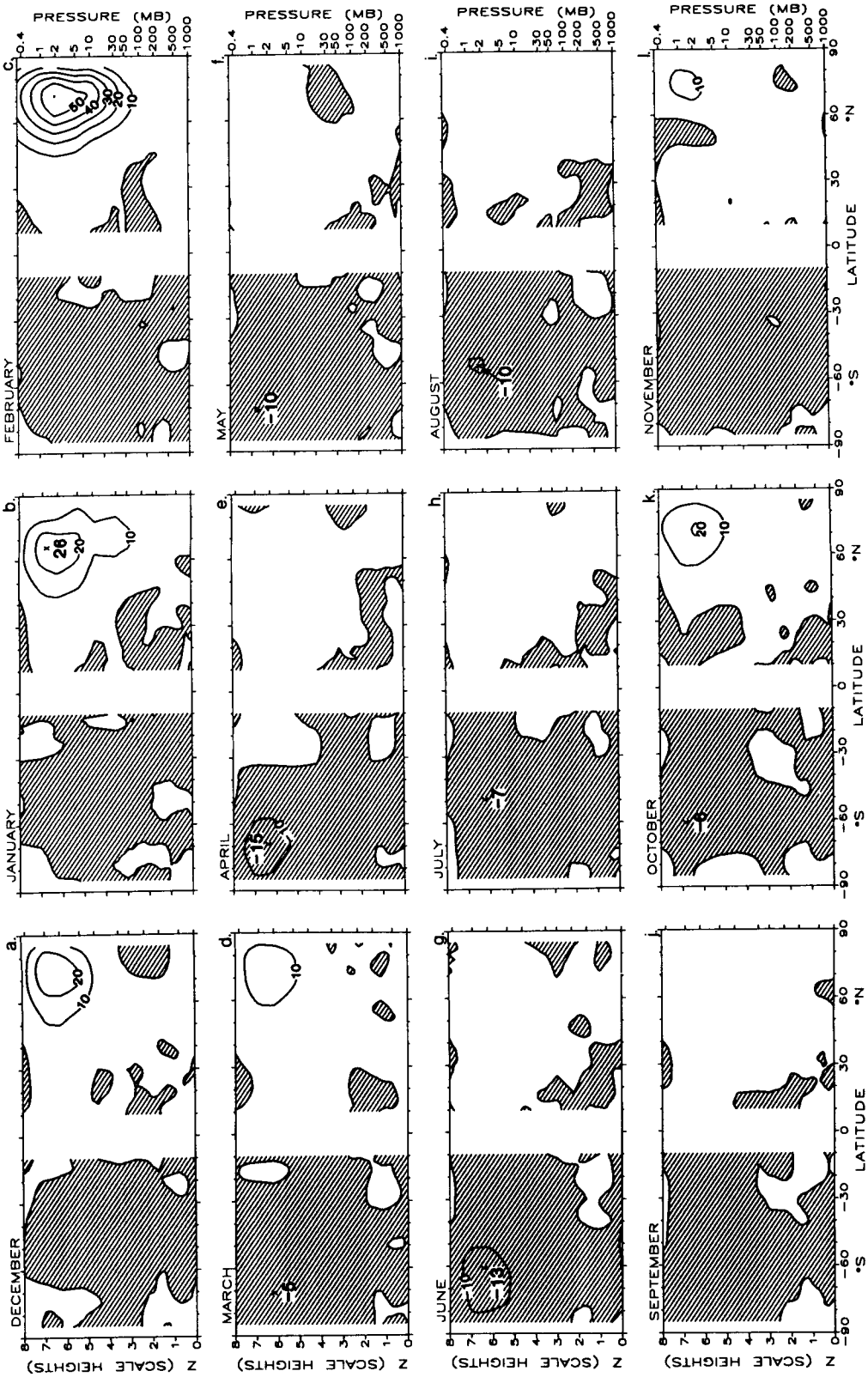

Figure 23. Northward flux of heat by the transient eddy zonal wave number one $[\overline{v'T'}]_{m=1}$ (K m/sec).

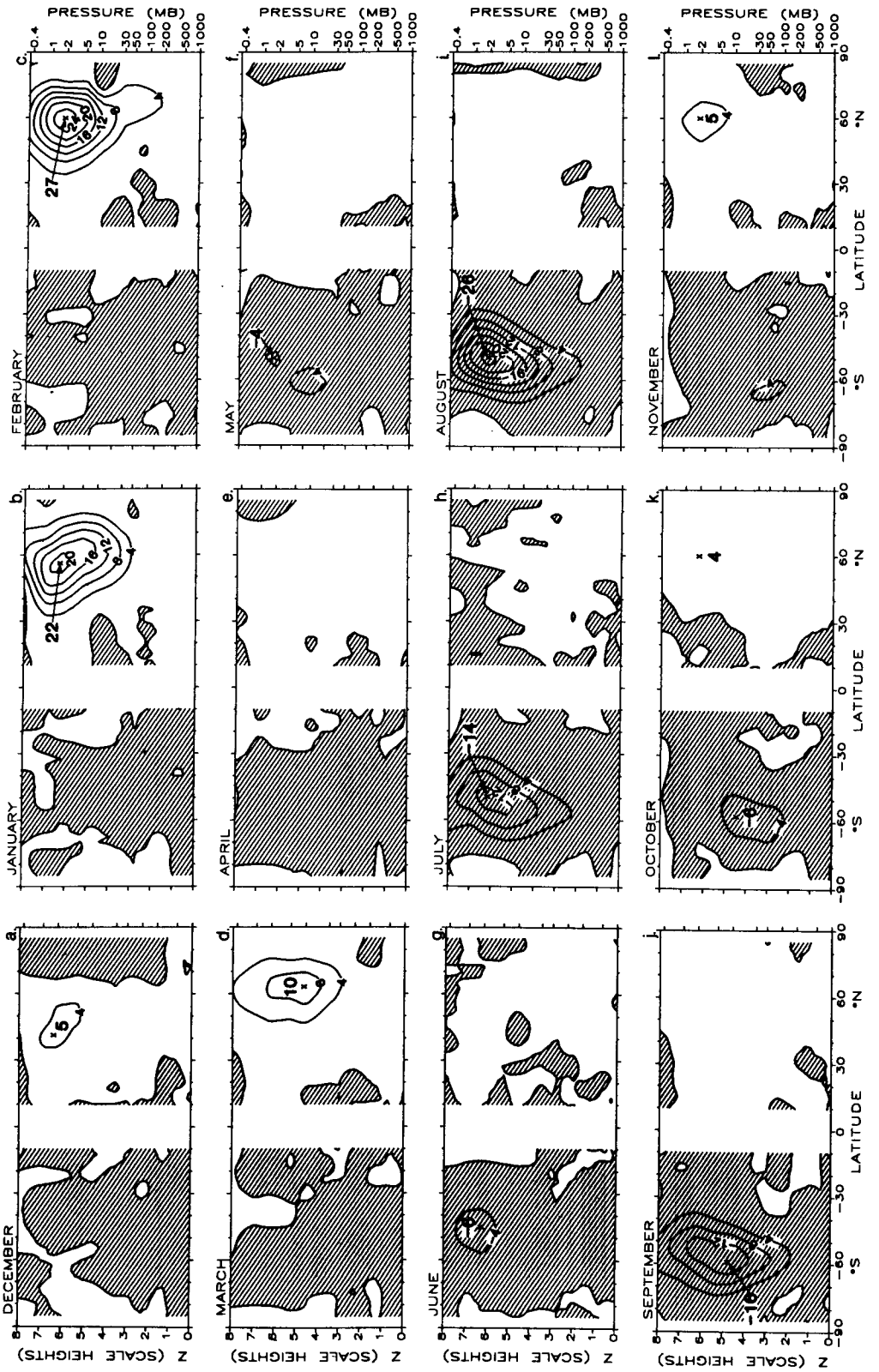

Figure 24. As in Figure 23, but for zonal wavenumber two.

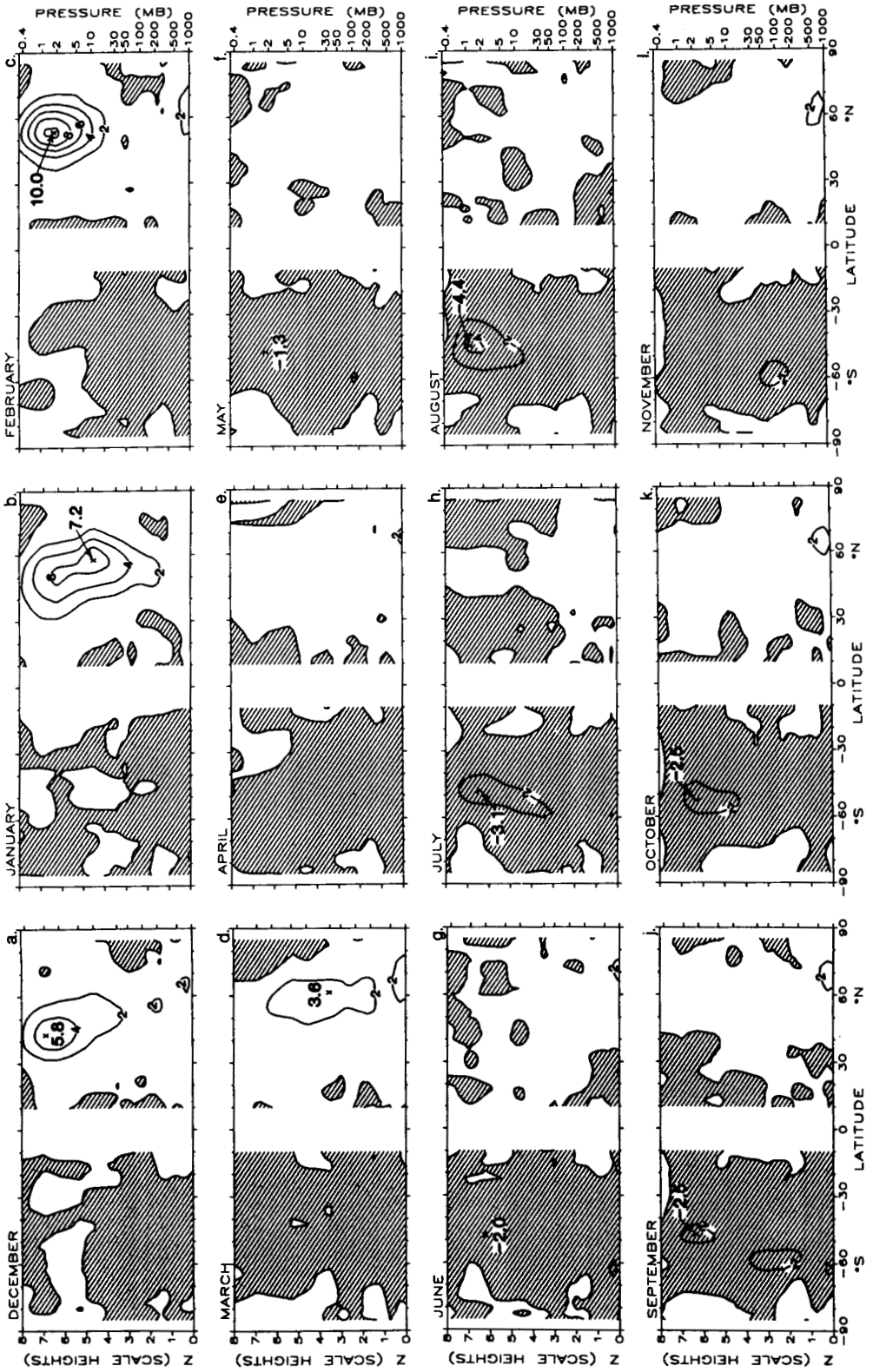

Figure 25. As in Figure 23, but for zonal wavenumber three.

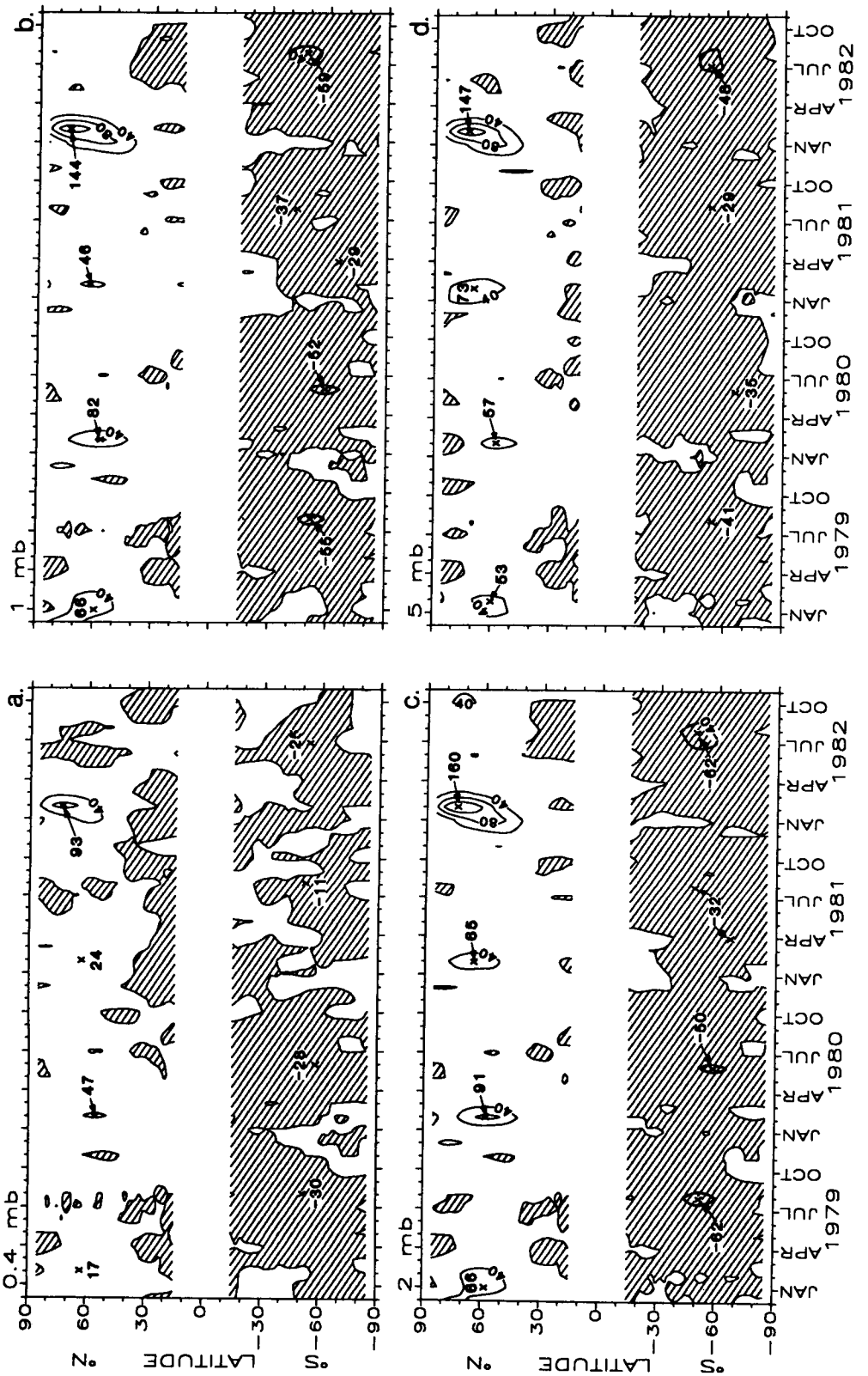

Figure 26. Time-latitude section of northward flux of sensible heat by the transient eddies at 0.4 mb, 1 mb, 2 mb and 5 mb.

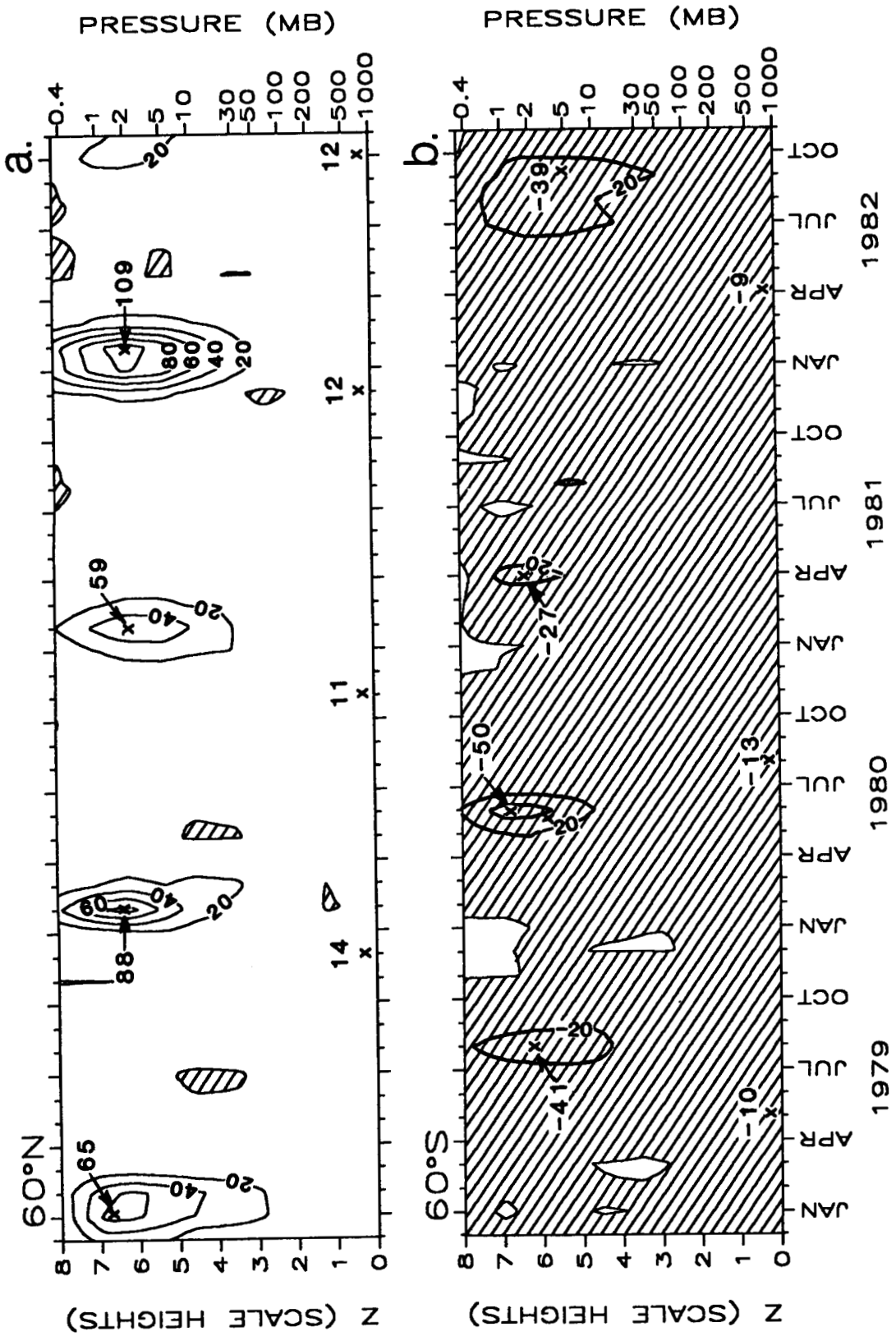

Figure 27. Time-altitude section of northward flux of sensible heat by the transient eddies, (a) at 60°N, (b) at 60°S.

3.6 Momentum Fluxes

3.6.1 Due to Standing Eddies

3.6.1.1 Latitude-Altitude Section

Fig. 28 shows latitude-altitude plots of the northward fluxes of westerly momentum due to standing eddies $[\bar{u}^*\bar{v}^*]$. Regions of negative values are shaded. The differences between the NH and SH in the standing eddy momentum fluxes are in many aspects similar to those appearing in the standing eddy heat fluxes. The main points are:

(a) The seasonal cycle is more pronounced in the NH than in the SH.

(b) The largest value of the $[\bar{u}^*\bar{v}^*]$ is about 300 m^2/sec^2 in the NH against -96 m^2/sec^2 in the SH. The maximum occurs in middle winter in the NH but in early spring in the SH.

(c) On the average the highest seasonal poleward flux of momentum is in winter in the NH, but in spring in the SH.

(d) In the annual march the NH westerly momentum flux steadily increases beginning in middle fall until reaching its peak in January and then decaying, whereas in the SH the flux also begins to increase in middle fall but in a quasi-oscillatory manner.

(e) In the stratospheric middle and high latitudes:

In the SH wave 1 dominates the standing eddy momentum flux field, but in the NH wave 2 contributes as much as one third of the total flux. Wave 3 can also have noticeable effects especially in the NH (Figs. 29-31).

(f) In the tropospheric low latitude:

In the NH there is a secondary westerly momentum maximum situated in the upper troposphere and centered around 30°N. This maximum appears almost year-round with the largest annual value occurring in late fall or early spring. It is created by the waves with wavenumbers higher than 3. In the SH, no similar secondary maximum is seen (Figs. 29-31).

3.6.1.2 Time-Latitude and Altitude Sections

The monthly mean flux of westerly momentum by the standing eddies at 0.4 mb, 1 mb, 2 mb and 5 mb is shown in Fig. 32. The time-altitude views at 60°N and 60°S latitudes for the 4 year period are presented in Fig. 33.

(a) The year-to-year changes in the annual maximum momentum flux are different in the two hemispheres. The magnitude of the NH maximum is more than twice as large as that in the SH. The location of the maximum shifts in a different manner in the two hemispheres. At 1 mb the annual largest flux in the NH is about 250 m^2/sec^2 increasing to 359 m^2/sec^2 in year 2, and then decreasing to 270 and 213 m^2/sec^2 in the last 2 years. The location of the maximum is at about 48°N and above 55 km altitude in the first two years but at about 65° N and below 42 km in the last two years. In the SH at 1 mb, the maximum value is about 150 m^2/sec^2 in July in year 1 and decreases to about 100 m^2/sec^2 in the rest of the years with the location being at about 45°S, 57°S, 65°S and 55°S in years 1 to 4. All these changes are found to be associated with the changes in geopotential height waves.

(b) Planetary wavenumber 1 provides the largest portion of the total standing eddy momentum fluxes both in the NH and SH with wavenumber 2 acting as a secondary contributor. Wavenumber 3 contributes a sizable amount in the NH, but not in the SH (see Figs. 29-31).

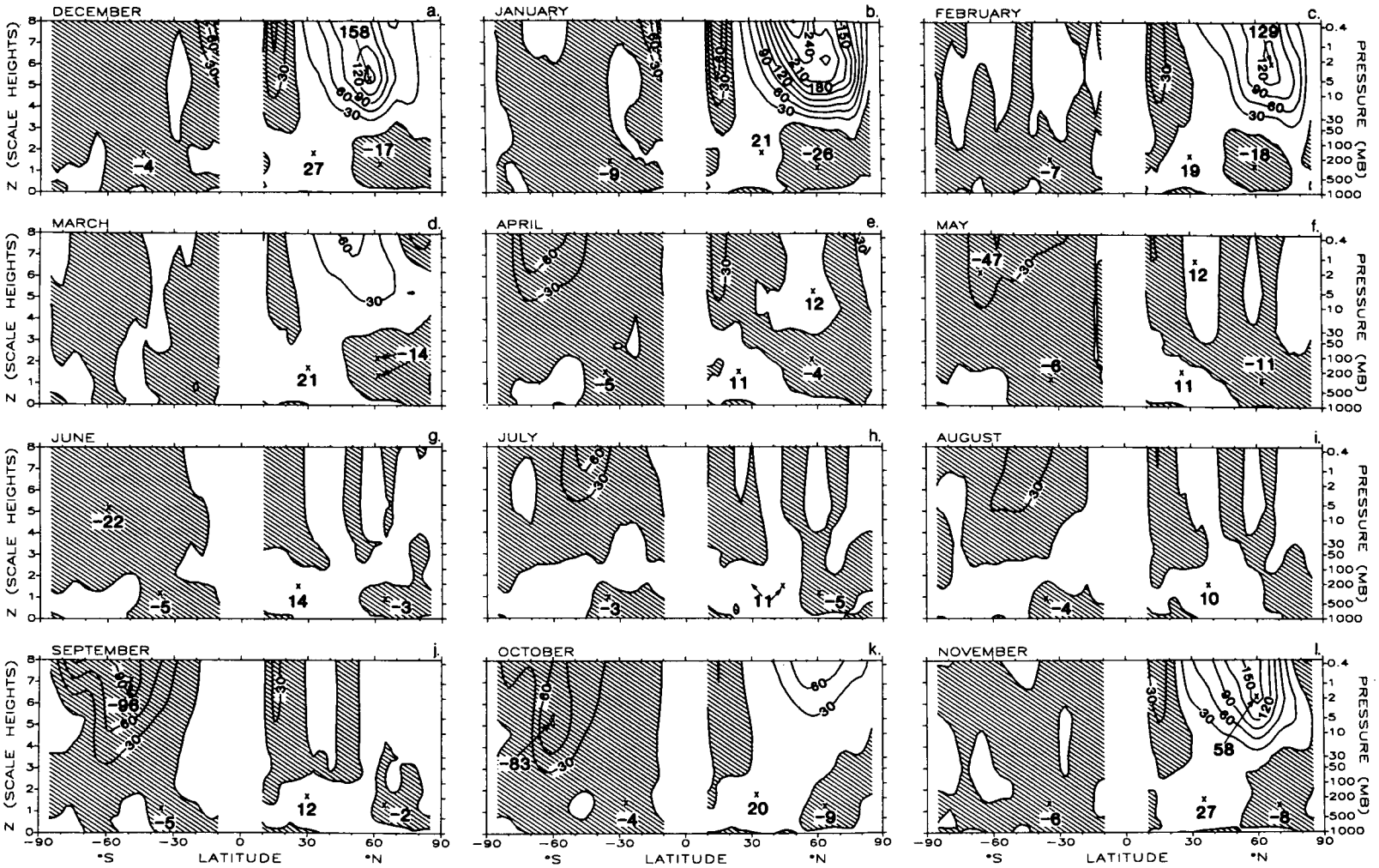

Figure 28. Monthly four year mean northward flux of eastward momentum by the standing eddies $[\bar{u}^*\bar{v}^*]$ (m^2/sec^2).

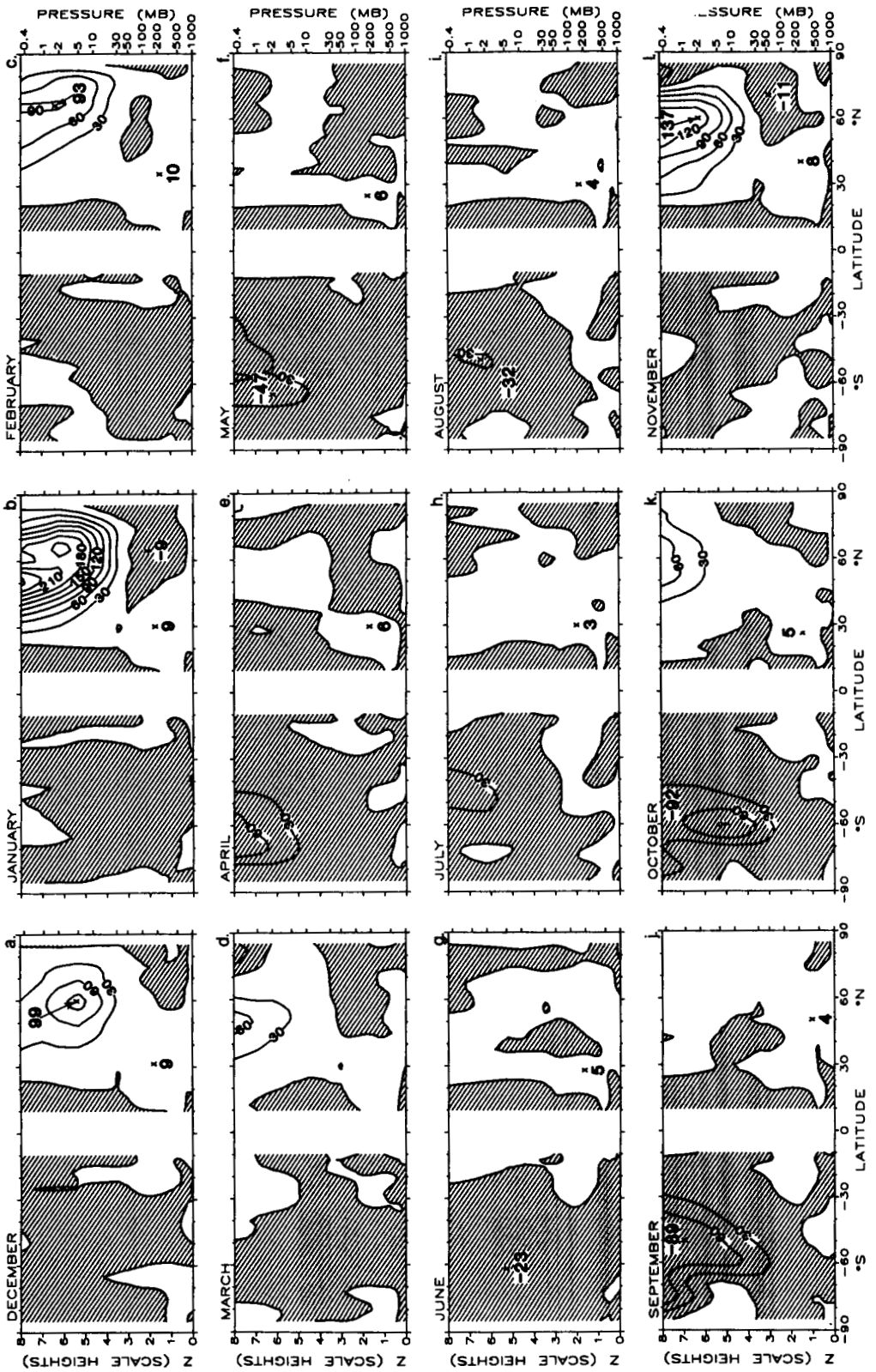

Figure 29. Northward flux of eastward momentum by the stationary eddy zonal wavenumber one $[\bar{u}^*\bar{v}^*]m=1$ (m^2/sec^2).

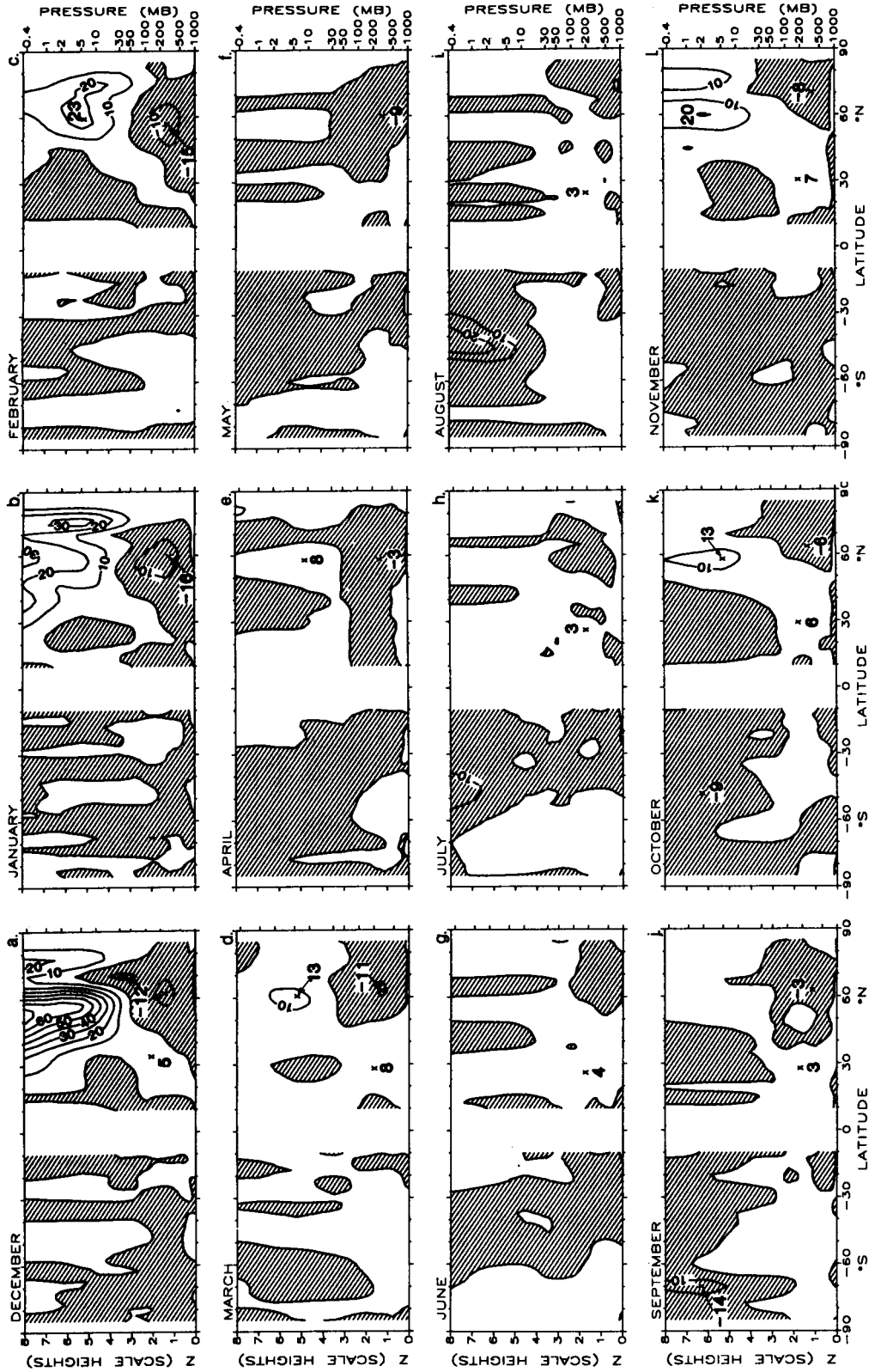

Figure 30. As in Figure 29, but for wavenumber two.

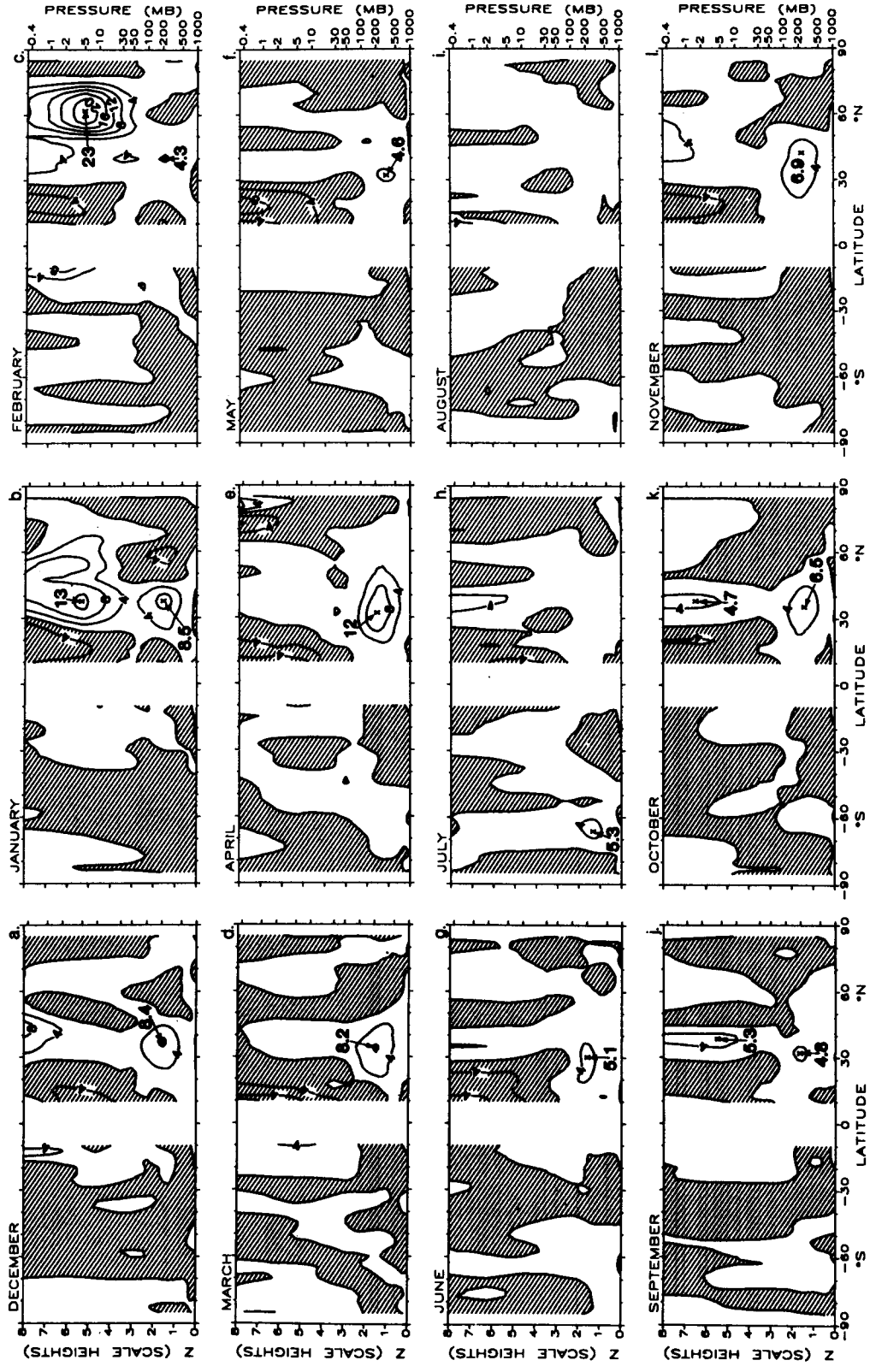

Figure 31. As in Figure 29, but for wavenumber three.

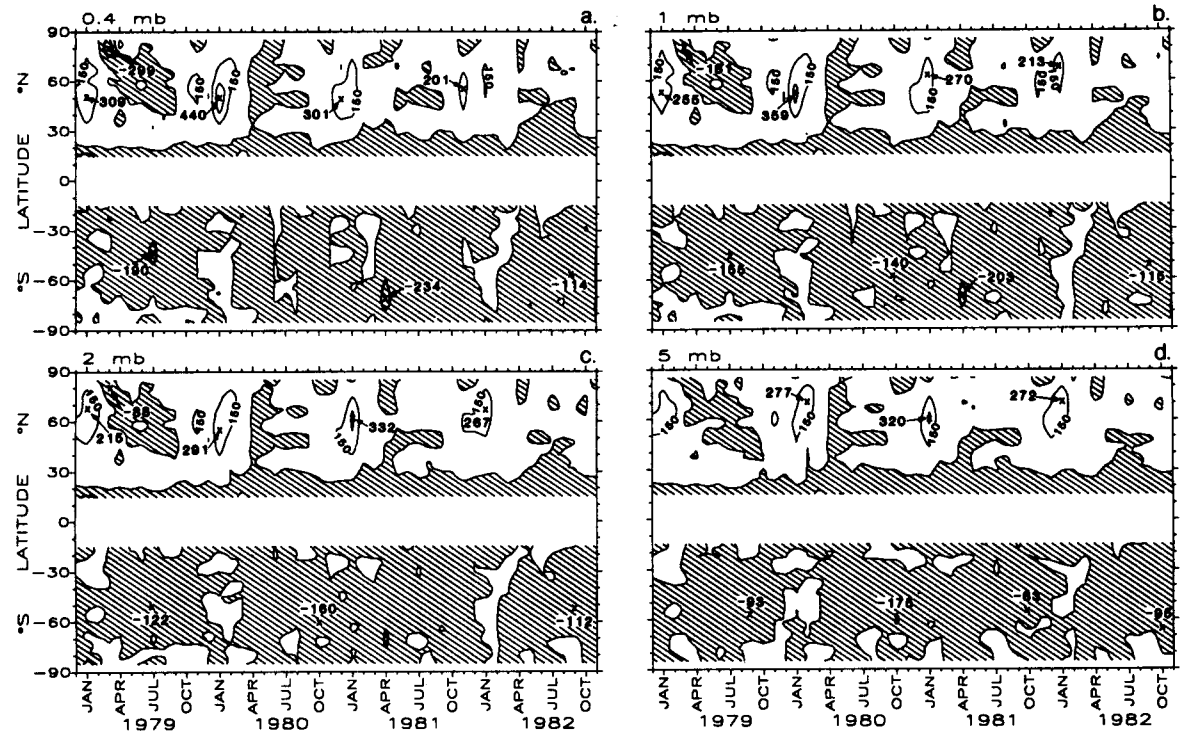

Figure 32. Time-latitude section of northward flux of eastward momentum by the standing eddies at 0.4 mb, 1 mb, 2 mb and 5 mb.

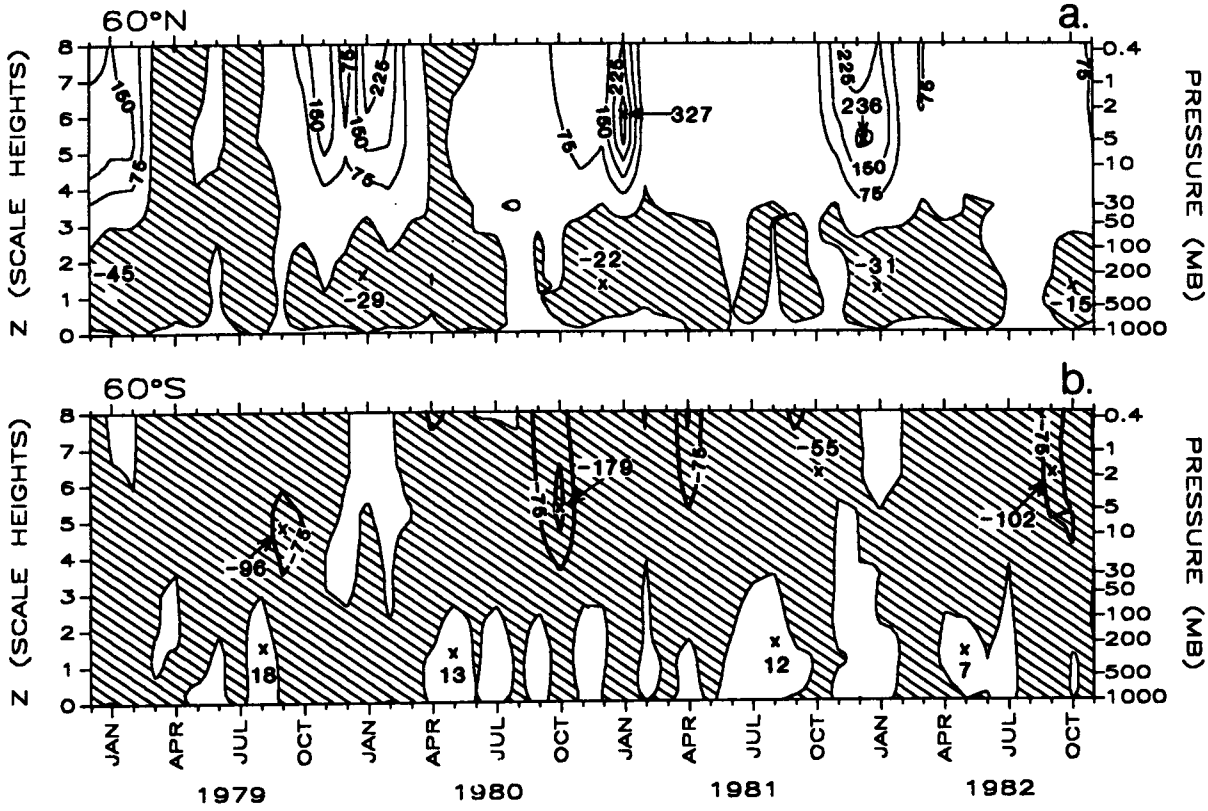

Figure 33. Time-altitude section of northward flux of eastward momentum by the standing eddies, (a) at 60°N, (b) at 60°S.

3.6.2 Due to Transient Eddies

3.6.2.1 Latitude-Altitude Section

Fig. 34 shows the latitude-altitude cross sections of the northward fluxes of westerly momentum due to transient eddies $[\overline{u'v'}]$. Regions of negative values are shaded. The largest value of $[\overline{u'v'}]$ is about 2/3 of the $[\overline{u^*v^*}]$ in the NH, but is almost equal in magnitude in the SH. In the diagrams of $[\overline{u'v'}]$ two maxima of poleward momentum fluxes are seen, one in the upper stratosphere (the maximum value is in the mesosphere), and the other in the troposphere. These two maxima are associated with the stratospheric and tropospheric jets. Some of the main highlights are described below.

(a) In the stratosphere wavenumber one does not dominate the transient eddy momentum fluxes. In the NH both wave 1 and wave 2 play about equal roles in contributing to the total momentum flux. Wave 3 also provides a substantial amount of momentum flux. However, in the SH wave 2 appears to have more influence than any other wavenumber, and wave 1 acts as a secondary contributor. In some cases the contribution of wave 3 is nearly as great as that of wave 1 (Figs. 35-37).

Concerning the seasonal cycle, the momentum flux in the NH begins to build its strength in middle fall, reaches its annual maximum in late winter, declines in early spring and finally drops to a minimum level in summer. A similar annual pattern happens in the SH. A difference is that the largest annual value is about 40% higher in the NH than in the SH (Fig. 34).

(b) In the troposphere, the maximum momentum in the vicinity of the tropospheric jet appears year-round both in the NH and the SH. The largest magnitude occurs in early spring in the NH, but in middle winter in the SH. The seasonal maximum values are about equal in both hemispheres. The tropospheric momentum fluxes originate from waves with wavenumbers higher than 3 both in the NH and SH.

3.6.2.2 Time-Latitude and Altitude Sections

Fig. 38 shows the time-latitude section of $[\overline{u'v'}]$ at 0.4 mb, 1 mb, 2 mb and 5 mb. The time-latitude views of $[\overline{u'v'}]$ at 60°N and 60°S latitudes for the 4 year period are presented in Fig. 39. Examining these figures one can easily find the following:

(a) The magnitude of the annual maximum poleward momentum flux is larger in the NH than in the SH by as much as a factor of 2.

(b) The interannual variation in the seasonal changes of the momentum flux is large in both hemispheres.

(c) Wave 1 no longer dominates the transient momentum flux field as in the standing eddy case. Furthermore, in years 1 and 2 the wave 1 flux is actually less than the wave 2 flux (not shown).

3.7 Eliassen-Palm Flux and Flux Divergences

3.7.1 E-P Flux Vectors

The four-year averaged monthly mean Eliassen-Palm (E-P) flux vectors from the standing and transient eddies are shown in Fig. 40 and Fig. 41 respectively. The vectors reflect the heat and momentum fluxes; namely the poleward heat flux corresponds to upward E-P flux and the northward momentum flux corresponds to the southward E-P flux. The highlights of the annual cycle of the E-P flux vectors in the NH have been summarized in our previous work (Wu et al., 1984). With regard to the interhemispheric differences, the following points are noted (Shiotani and Hirota, 1985):

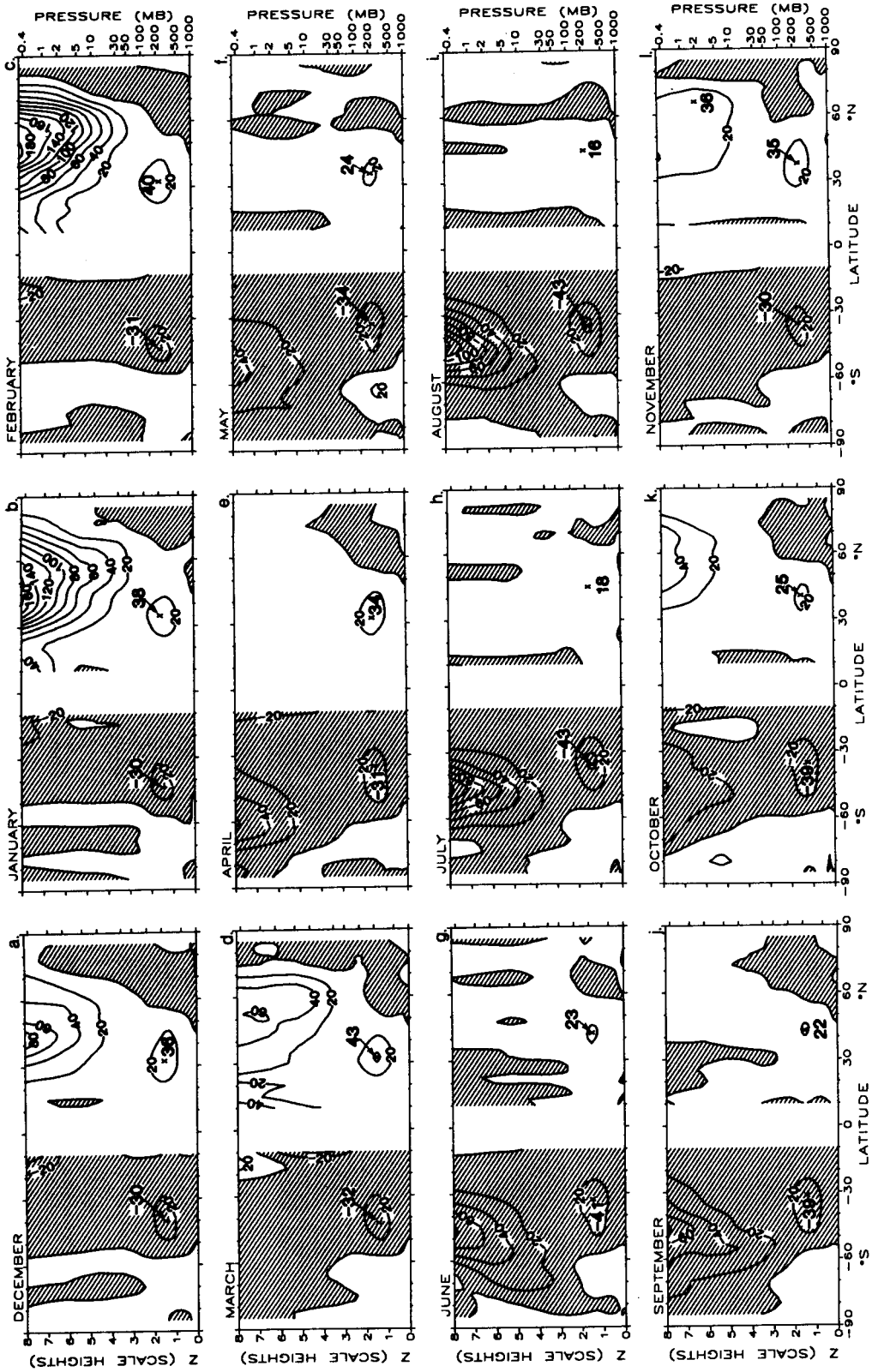

Figure 34. Monthly four year mean northward flux of eastward momentum by the transient eddies $\overline{[u'v']}$ (m^2/sec^2).

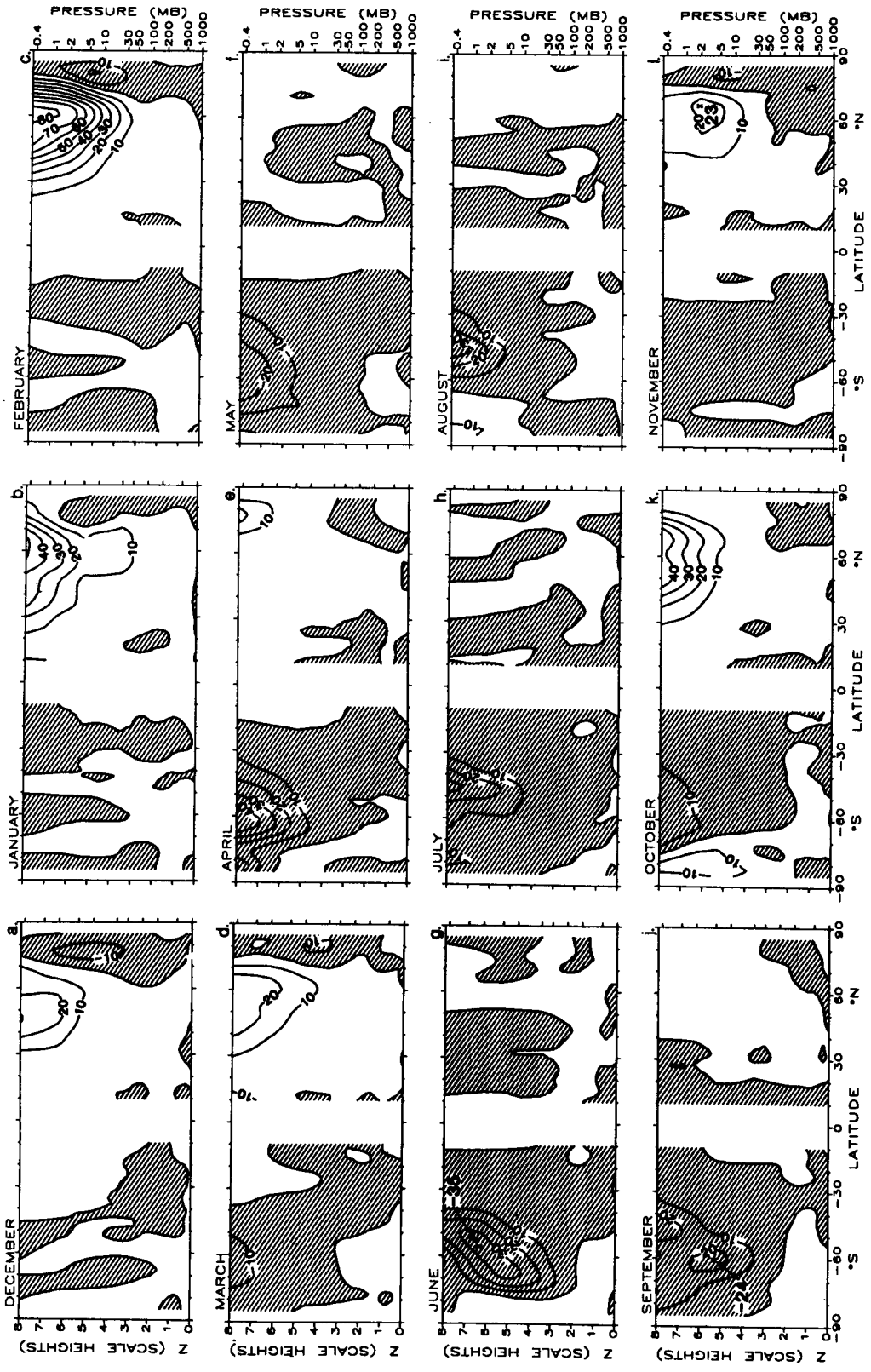

Figure 35. Northward flux of eastward momentum by the transient eddy zonal wavenumber one $[\overline{u'v'}]_{m=1}$ (m^2/sec^2).

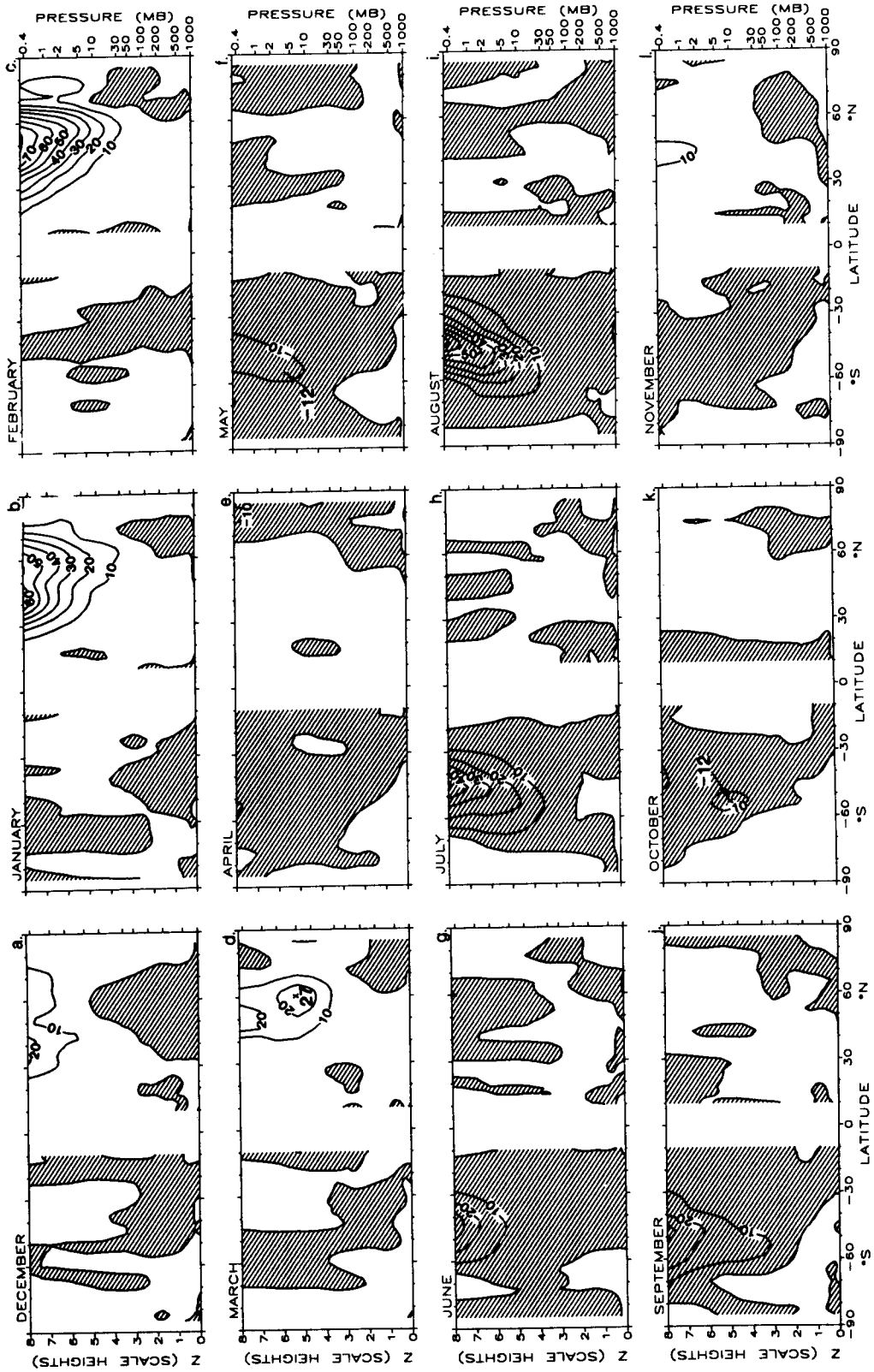

Figure 36. As in Figure 35, but for zonal wavenumber two.

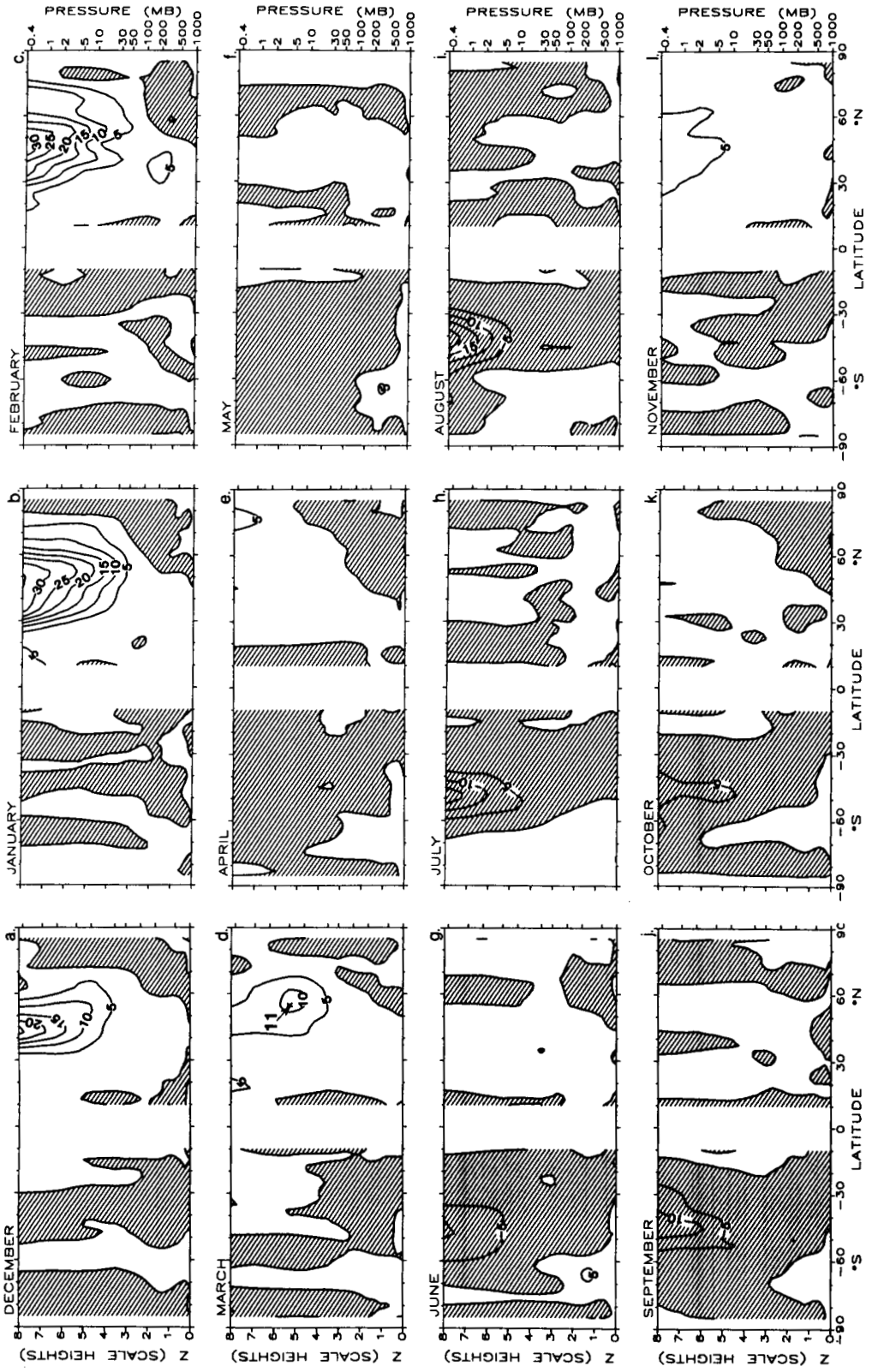

Figure 37. As in Figure 35, but for zonal wavenumber three.

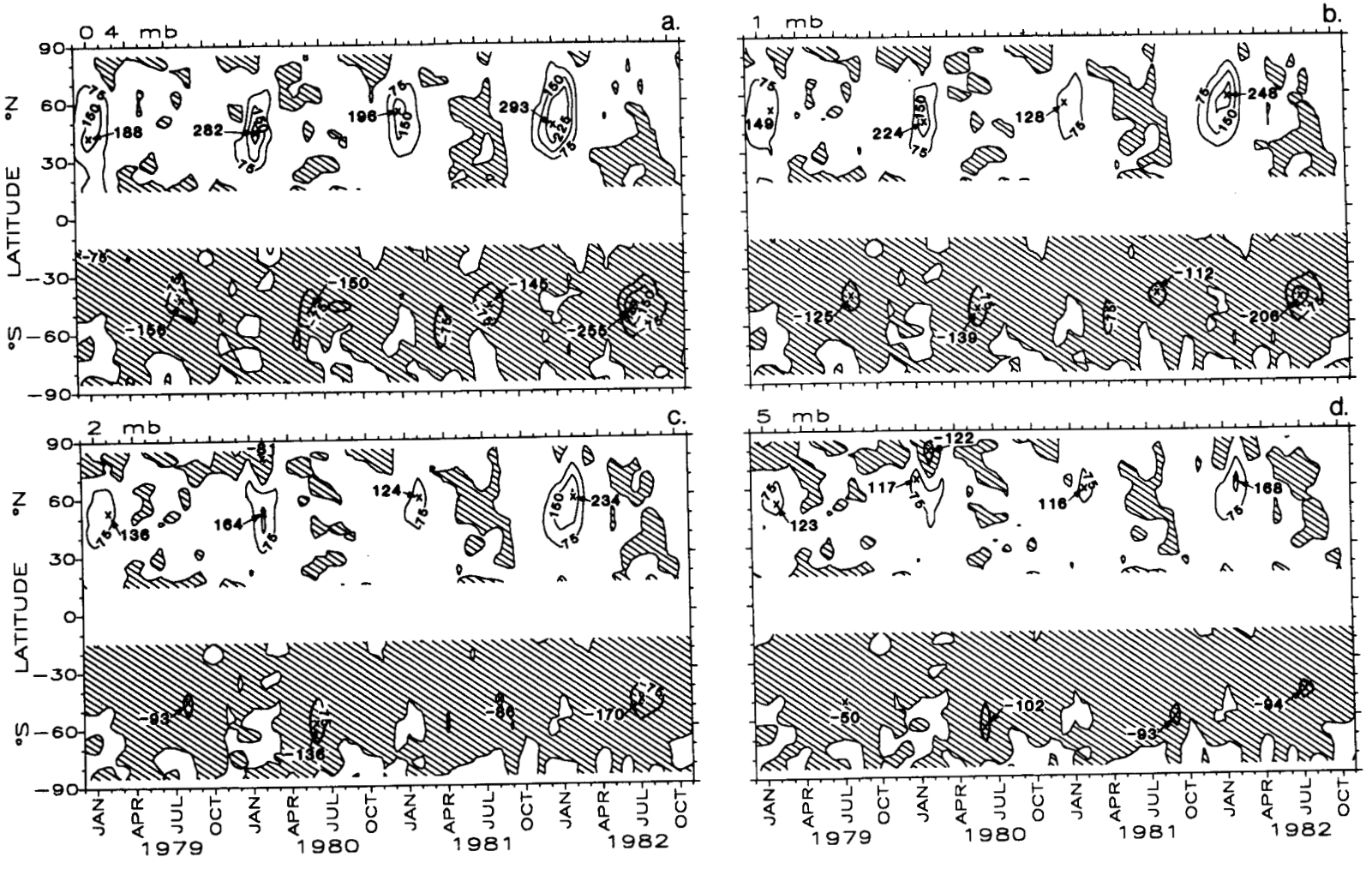

Figure 38. Time-latitude section of northward flux of eastward momentum by the transient eddies at 0.4 mb, 1 mb, 2 mb and 5 mb.

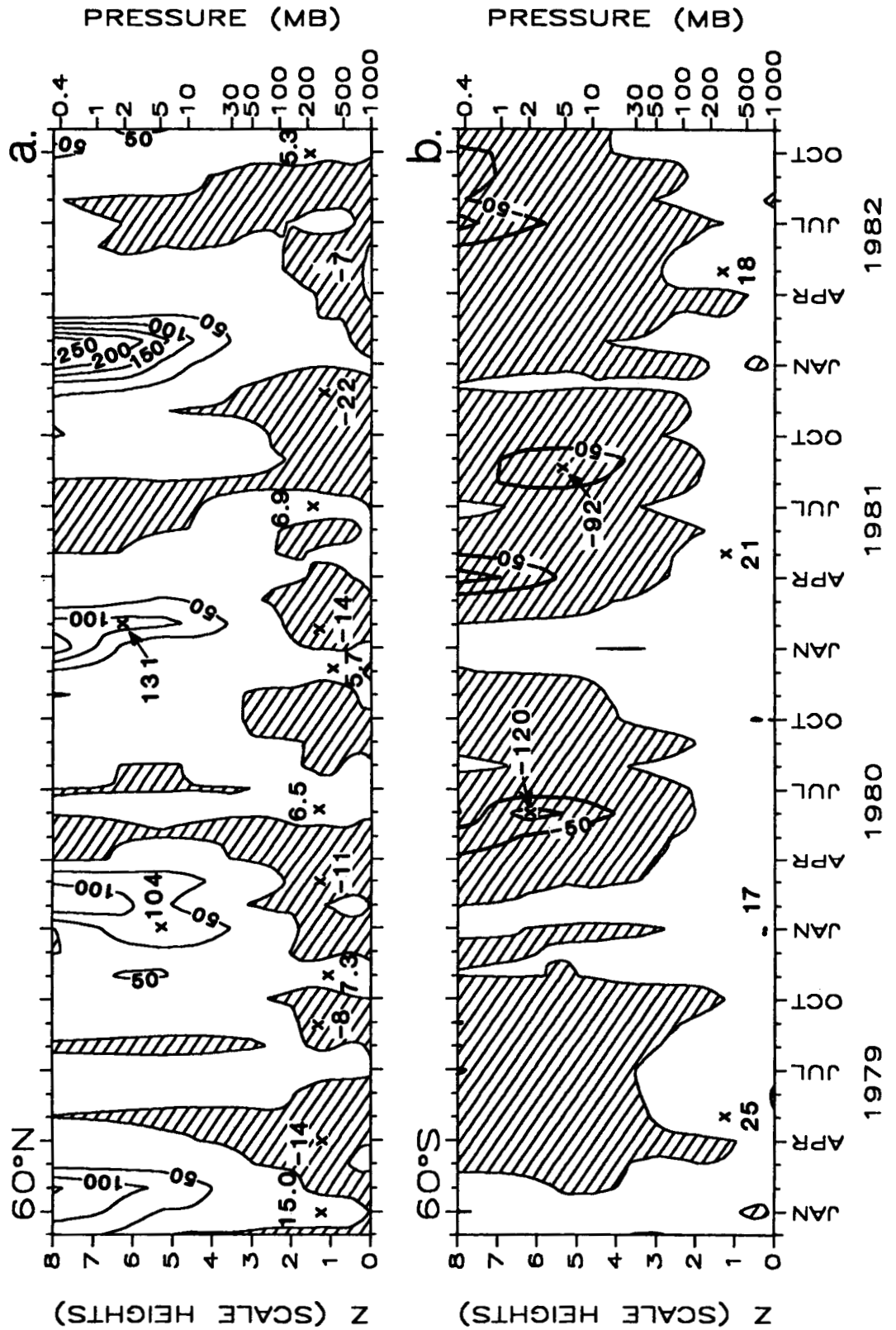

Figure 39. Time-altitude section of northward flux of eastward momentum by the transient eddies, (a) at 60°N, (b) at 60°S.

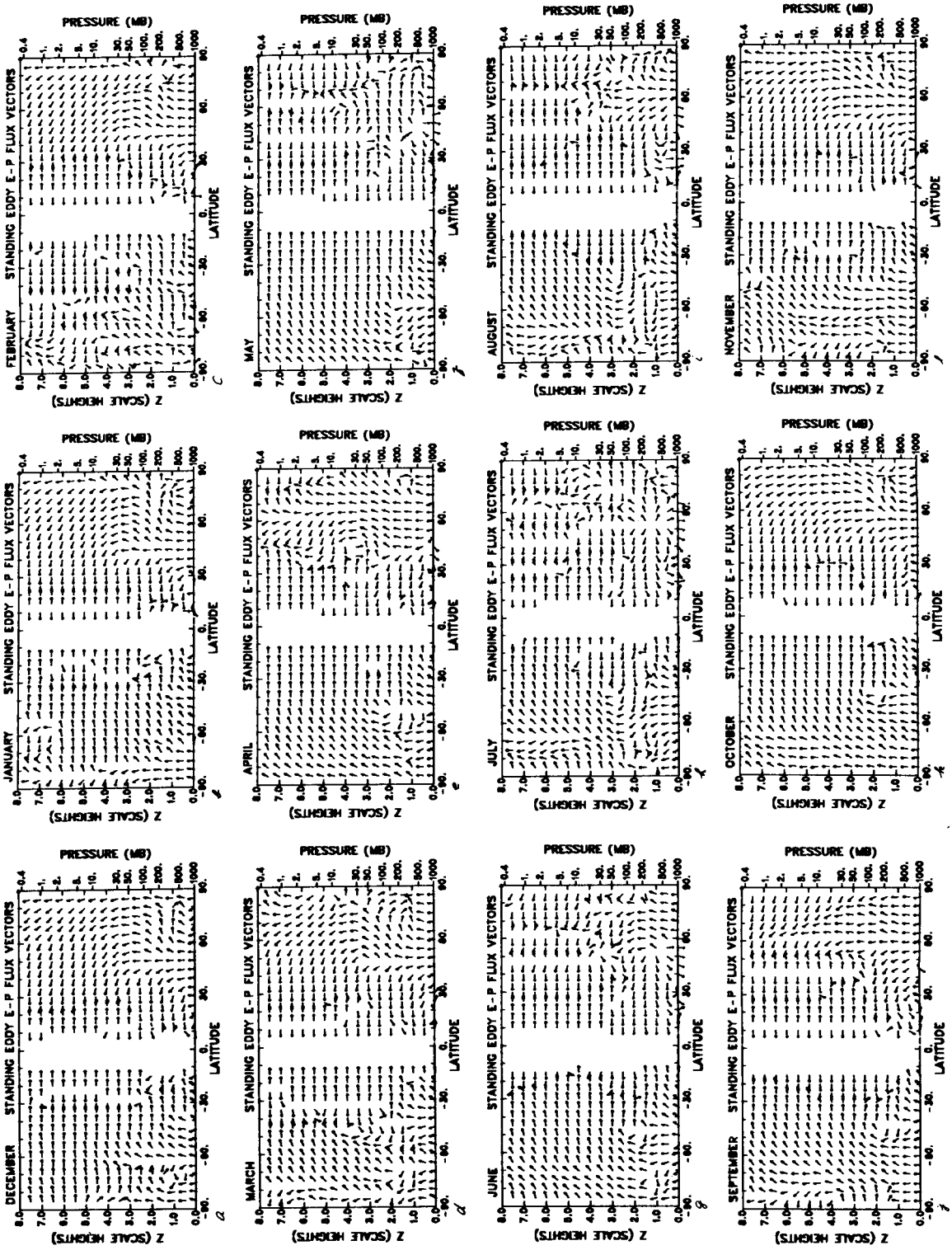

Figure 40. Monthly four year mean Eliassen-Palm flux vectors from the standing eddy fluxes. All of the arrows are the same length. The vertical vector component is magnified by a factor of 100 with respect to the horizontal component.

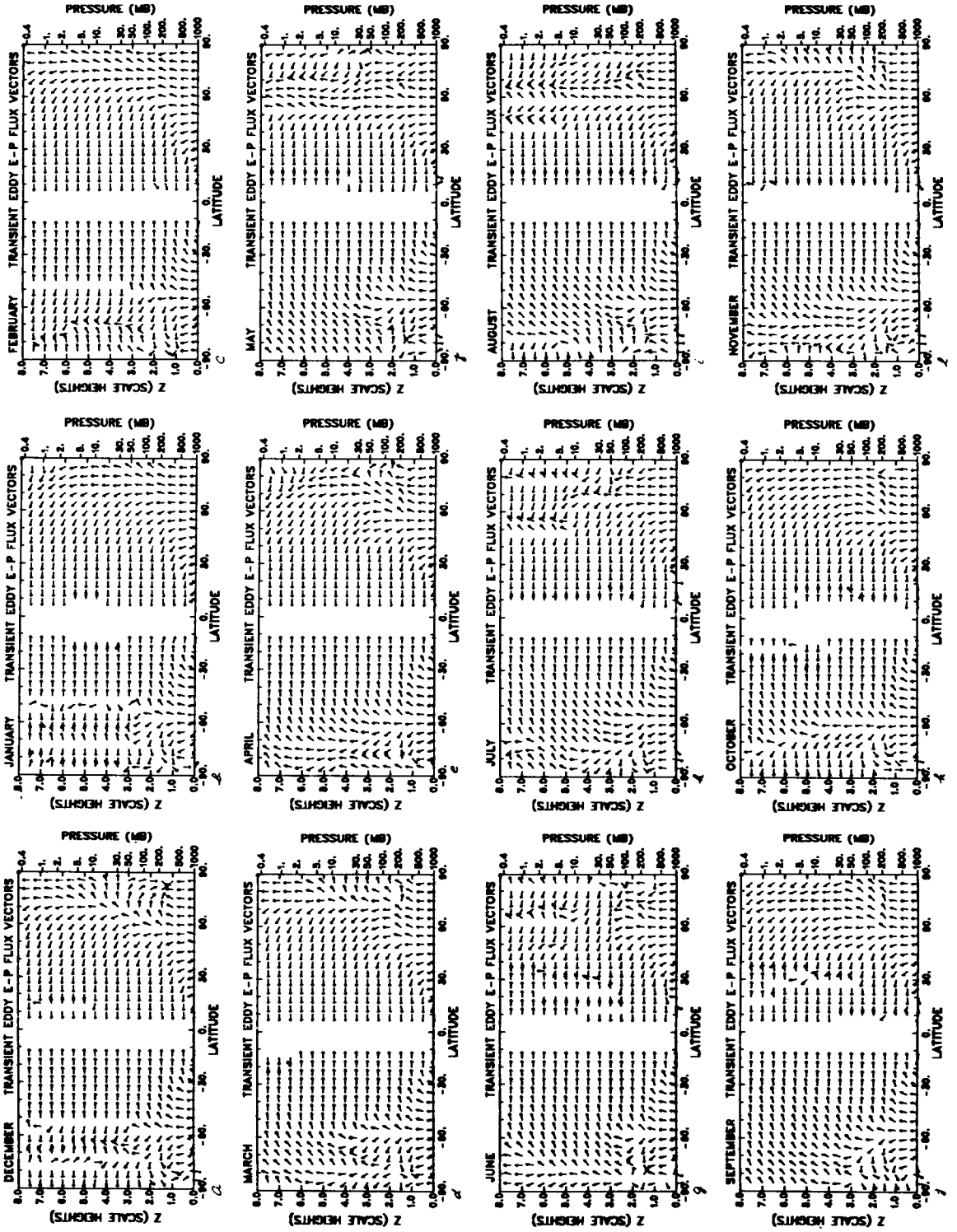

Figure 41. As in Figure 40, but for transient eddy fluxes.

3.7.1.1 From Standing Eddies

During NH winter, the E-P flux vectors are generally pointing upward with an equatorward component south of about 45°N and poleward north of that latitude below about 30 mb. In the middle and upper stratosphere, the vectors are upward and southward. In the NH a bifurcation near the pole is seen in December, January and March at about 200 mb level where some propagation is downward into the polar troposphere and some is upward into the polar stratosphere. There is no clear indication of a similar feature, in the SH counterpart. During spring the upward propagation is more apparent in the SH than in the NH. To a large degree the propagation pattern in SH spring looks like NH winter.

Looking at the wave components (not shown), one finds that the bifurcation in December appears to result from wavenumber 2 and that those occurring in January and March are due to wavenumber one (see Geller et al., 1983).

3.7.1.2 From Transient Eddies

Generally speaking, the E-P flux vectors look similar in both hemispheres in the stratosphere, but some differences are seen in the troposphere. Wavenumber one shows a relatively larger influence. In the NH winter and in the SH spring wavenumber two's effect is comparatively higher (not shown).

3.7.2 E-P Flux Divergences
3.7.2.1 From Standing Eddies

The E-P flux divergence ($\nabla \cdot F$) is a driving force to the zonal winds. The positive value of $\nabla \cdot F$ act as an acceleration force for the zonal westerlies, and the negative value of $\nabla \cdot F$ is a deceleration force for the zonal westerlies. Fig. 42 shows the E-P flux divergence from the standing eddies $(\nabla \cdot F)_s$ for the twelve calendar months. Regions of negative values (i.e. convergence) are shaded. The seasonal changes of the $(\nabla \cdot F)_s$ and some other features in the NH have been described in Wu et al., (1984)^s(see also, Mechoso et al., 1985; Hartman et al., 1984). Some main points on the interhemispheric differences may be noted below.

(a) In the northern polar latitudes (north of about 60°N) and between about 200 mb and 1 mb there is a positive region of $(\nabla \cdot F)_s$. This positive region begins to increase in size and value in October or^{s}November. It continues to grow throughout the whole winter. In January, the positive value reaches highest annual magnitude of about 25 m/sec/day. In February, the magnitude of the maximum drops to about half of January's value, while the size of the positive area remains about the same. Further decrease in size and magnitude is seen in March. In the SH we only see a narrow band of positive value centered at about 70°S during the months of June, July and August. The highest annual positive value is about 2.8 m/sec/day and occurs in September. After October, both area and magnitude decrease steadily.

It should be noted at this point that a recent study of Robinson (1986) has demonstrated that the large values for the E-P flux divergence in the polar stratosphere are spurious and caused by using geostrophic winds. Boville (1986) has also shown that the errors in the quasigeostrophic E-P flux divergence are at least equal to or even larger than the true divergence in the winter stratosphere.

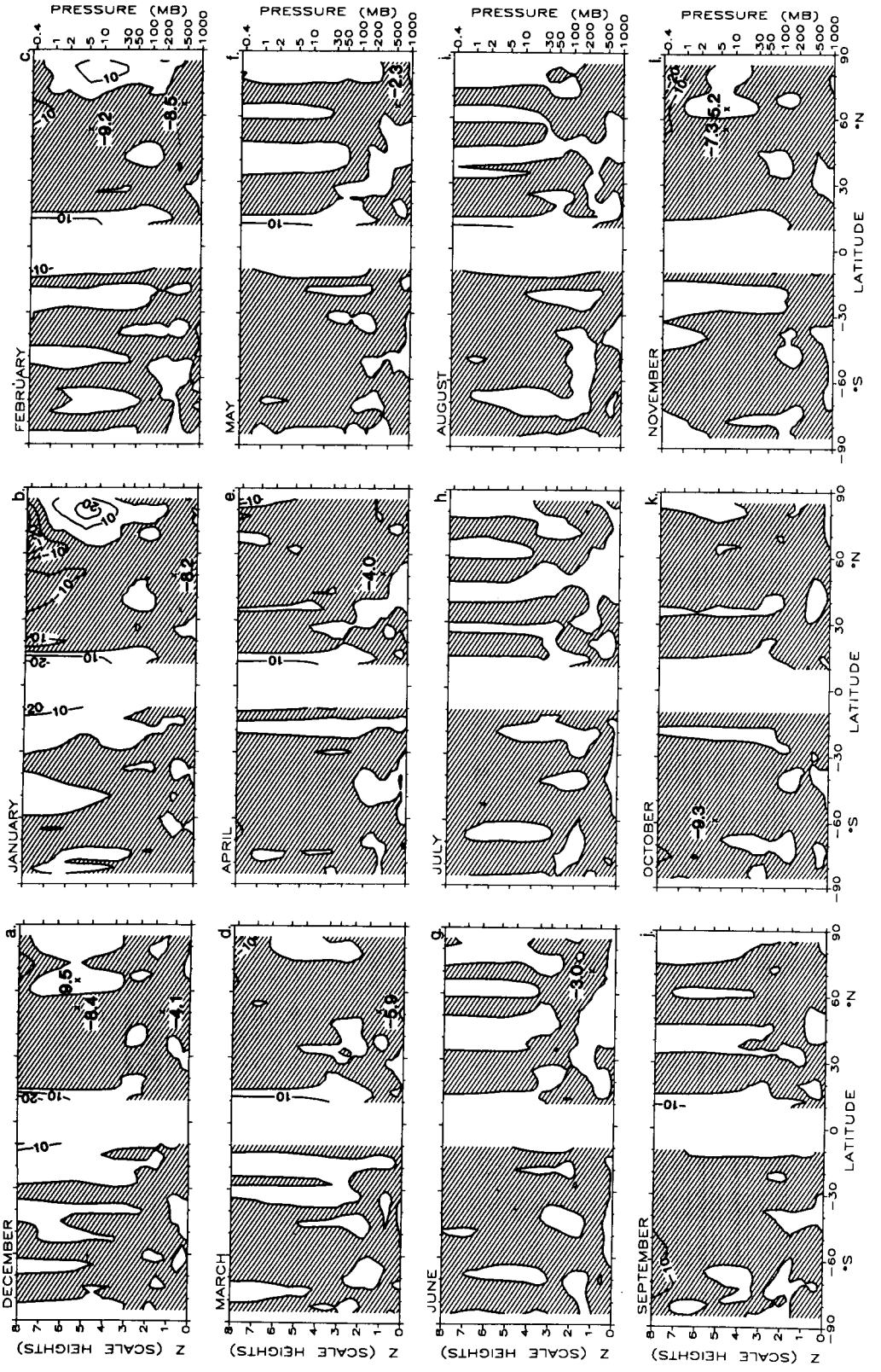

Figure 42. Monthly four year mean Eliassen-Palm flux divergences (10^{-5}m/sec^2) resulting from the standing eddies.

(b) Accompanying the positive area of $(\nabla\cdot F)_s$, there is a negative region situated above about 1 mb and extending from high to low latitudes. In the NH this deceleration force acts upon the westerlies from October through February with the highest values of about -30 m/sec/day occurring in January (Note that in this month the acceleration force or positive $(\nabla\cdot F)_s$ is also the strongest and that the planetary waves have their largest amplitudes). Beginning in March the negative magnitude of $(\nabla\cdot F)_s$ drops sharply. In the SH the zonal westerlies in the corresponding location do not receive much deceleration force due to the planetary waves in June, July and August (SH winter). This is consistent with the fact that the speed of the westerlies is higher in the SH than in the NH winter. Substantial deceleration forces appear in September or October (or early or middle spring in the SH), when the amplitudes of planetary waves in the SH are the highest.

(c) In the stratosphere the strongest influence on the $(\nabla\cdot F)_s$ fields is from the planetary wavenumber one, but in the tropospheric tropics, the waves with wavenumber higher than 3 are more important (Figs. 43-45).

In order to see the year-to-year variations, we present the time-latitude section of $(\nabla\cdot F)_s$ at 5 mb and the time-altitude sections at 80°N and 80°S in Figs. 46-47 for the 4 year period. One can see that the interannual variability is large in both the NH and SH. Note that the dipole structure (positive at high latitudes and negative at middle or lower latitudes) is seen clearly in Fig. 46 in the SH as pointed out by Hartmann et al. (1984), and Shiotani and Hirota (1985).

3.7.2.2 From Transient Eddies

The E-P flux divergences from the transient eddies $(\nabla\cdot F)_t$ are presented in Fig. 48, and their wave decompositions for the first three zonal harmonics are shown in Figs. 49-51. Comparing these figures with those of Figs. 42-45, we find the following:

(a) The absolute value of $(\nabla\cdot F)_t$ is smaller than $(\nabla\cdot F)_s$. The largest negative value is -10 in $(\nabla\cdot F)_t$ vs. -30 in $(\nabla\cdot F)_s$, and the largest positive value is 4.4 vs. 25 in the fields of transient and standing eddy E-P flux divergences, respectively (see Figs. 42b and 48b and c).

(b) The contribution from planetary wavenumber 2 in the $(\nabla\cdot F)_t$ is nearly comparable to that from wavenumber 1.

The interannual variations in $(\nabla\cdot F)_t$ are portrayed in Figs. 52 and 53. Large variations in both hemispheres in the stratosphere can be detected in these diagrams. For example, the maximum divergence at 65°N in the NH changes from 6 to 11, 6 and less than 5 in the four year period (see Fig. 53), while at 5 mb the value varies from 9 to 15, 16 and 3 (see Fig. 52). Note that the values given above are not at the same location. In the troposphere, there is a convergence zone appearing in both hemispheres (Fig. 53). This convergence does not change much from year-to-year as compared with that in the upper stratosphere.

4. Summary and Concluding Remarks

4.1 Summary of Results

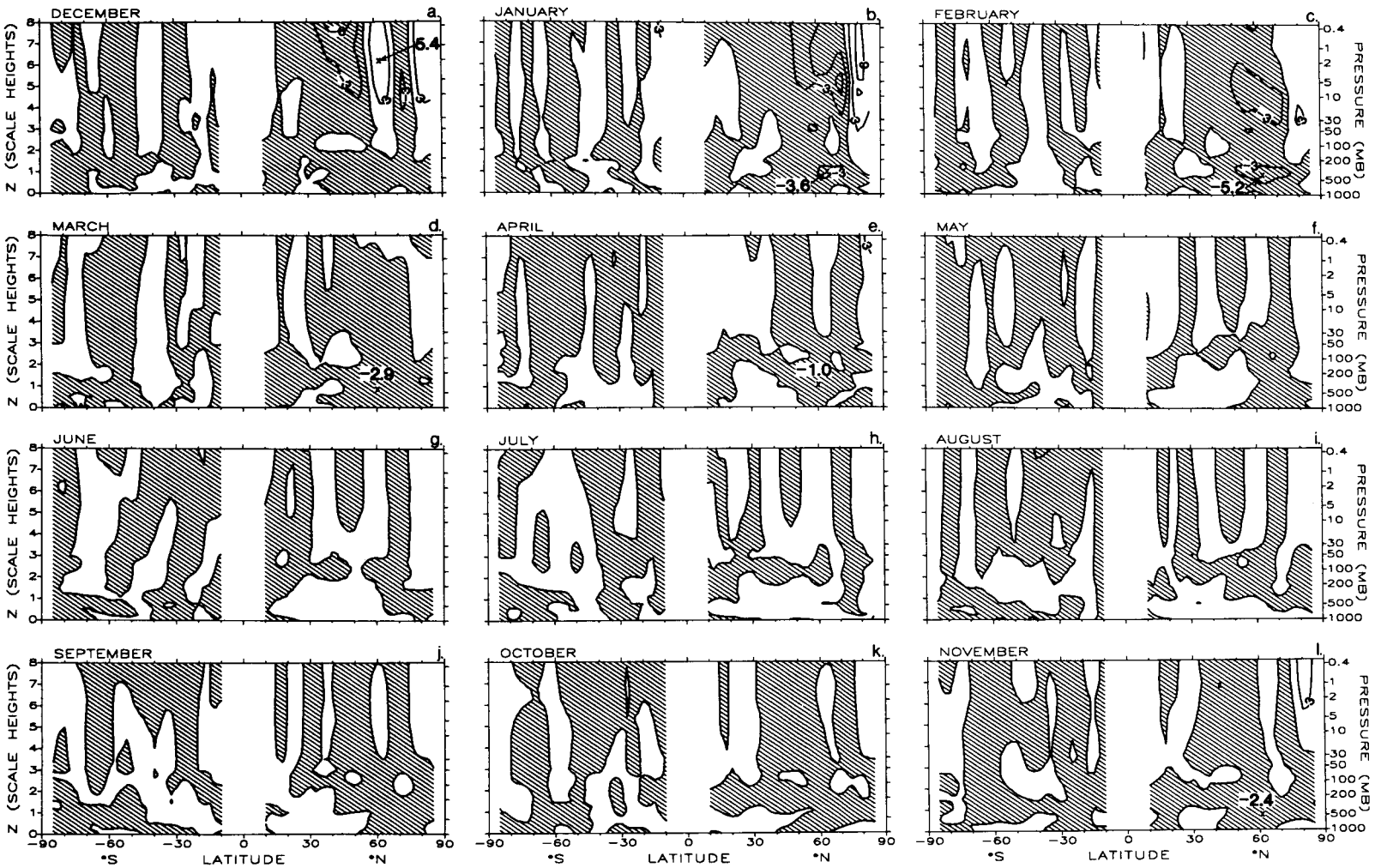

Figure 44. As in Figure 42, but for zonal wavenumber two.

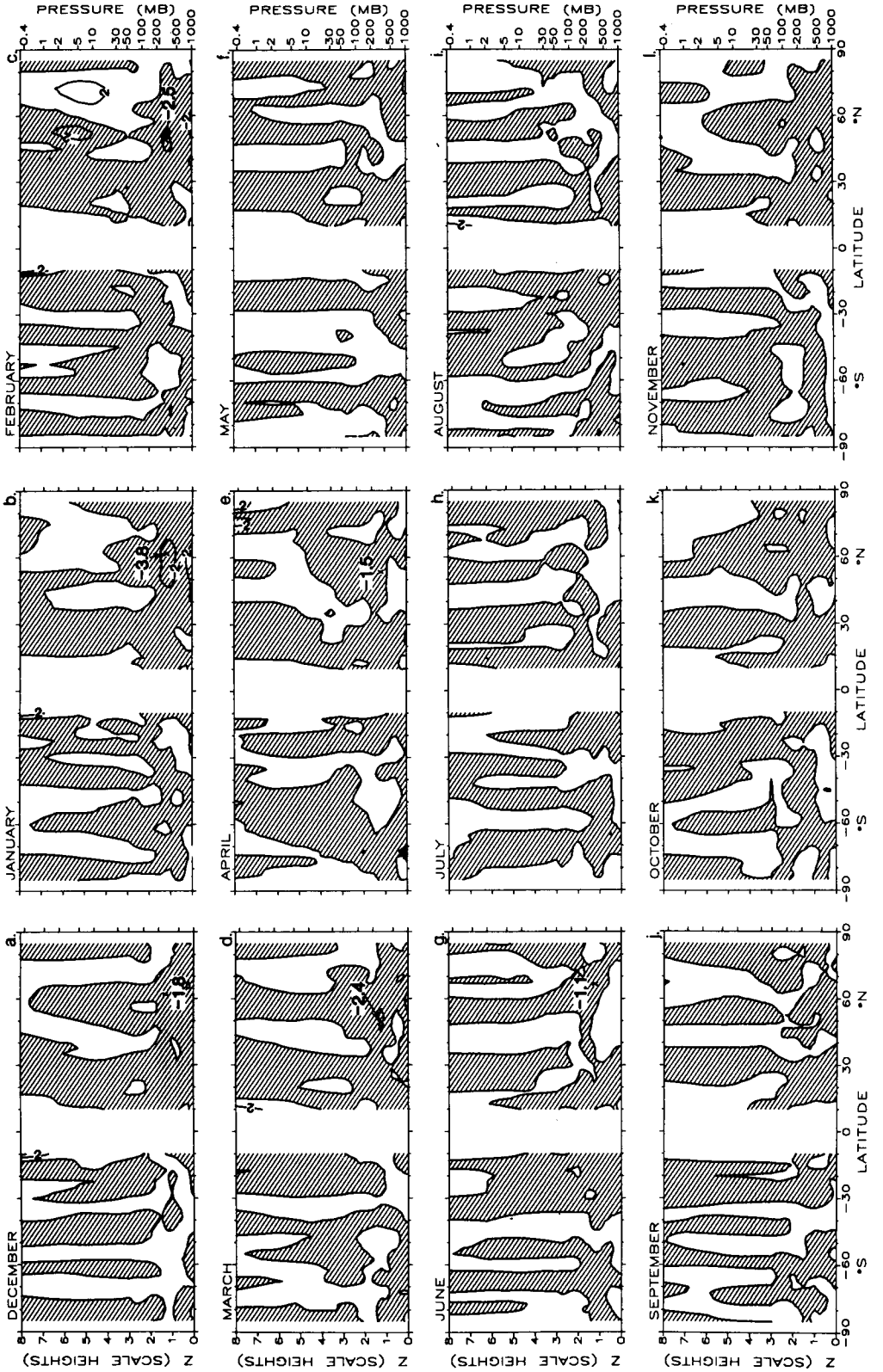

Figure 45. As in Figure 42, but for zonal wavenumber three.

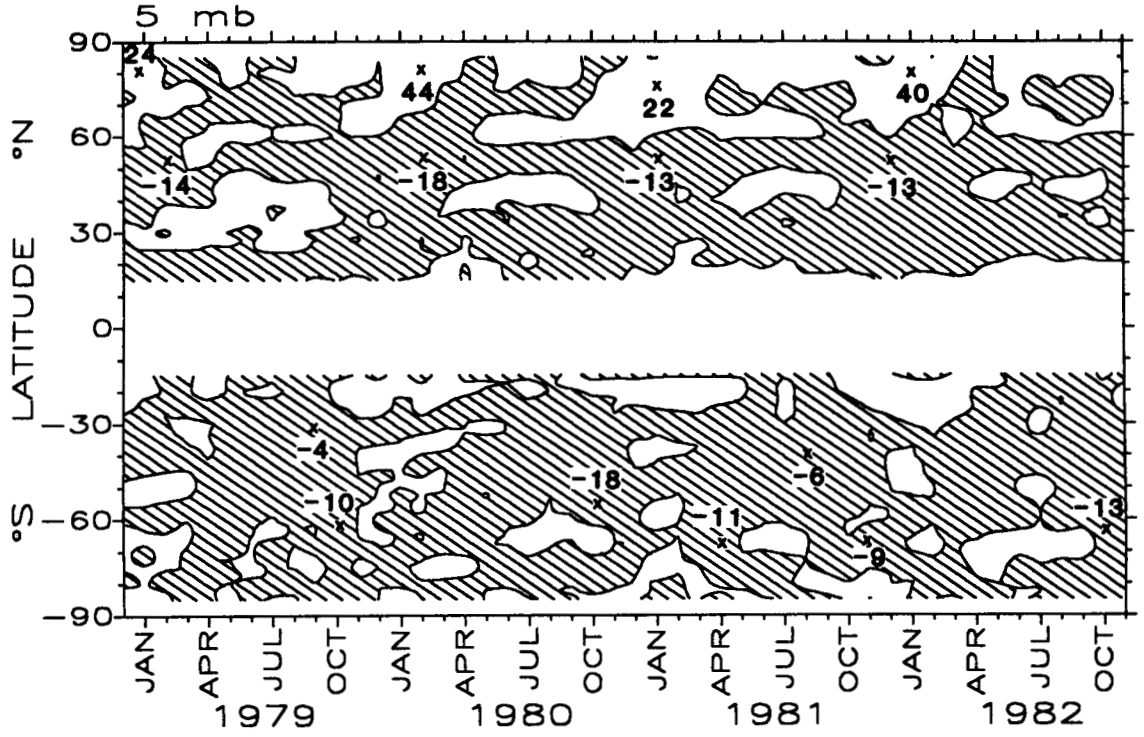

Figure 46. Time-latitude section of Eliassen-Palm flux divergences (10^{-5}m/sec^2) resulting from the standing eddies at 5 mb.

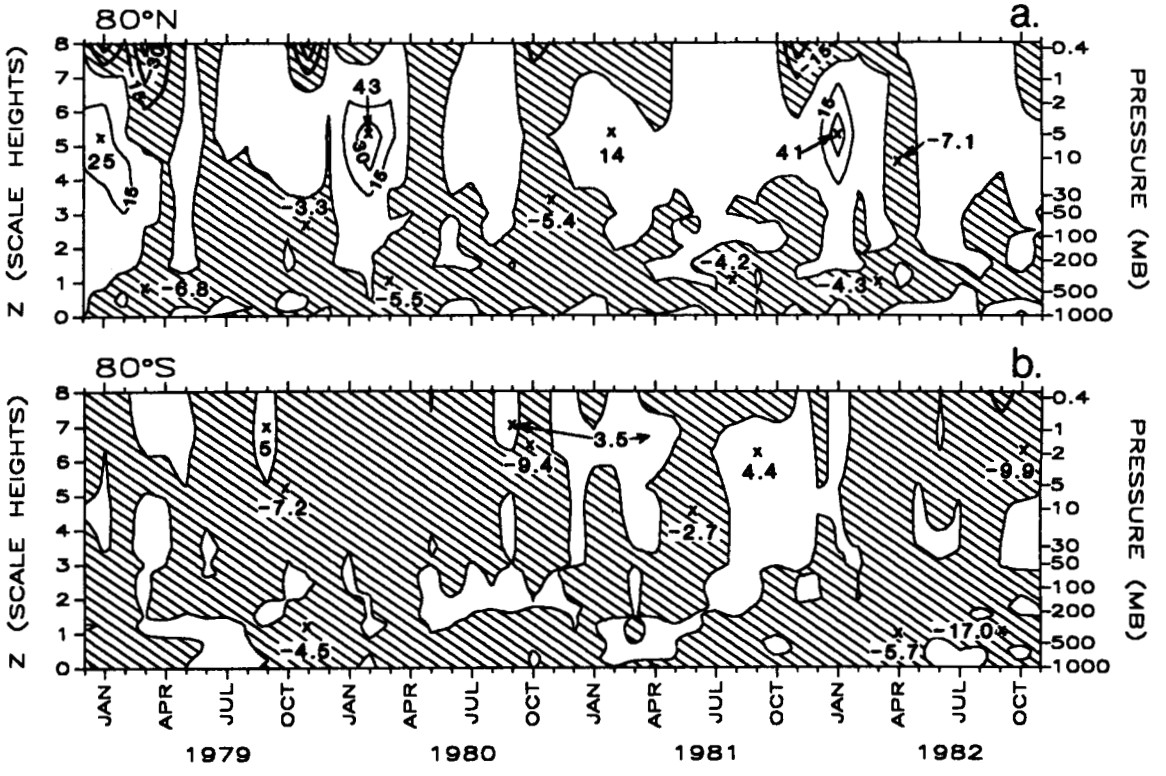

Figure 47. Time-altitude section of Eliassen-Palm flux divergences (10^{-5}m/sec^2) resulting from the standing eddies, (a) at 80°N, (b) at 80°S.

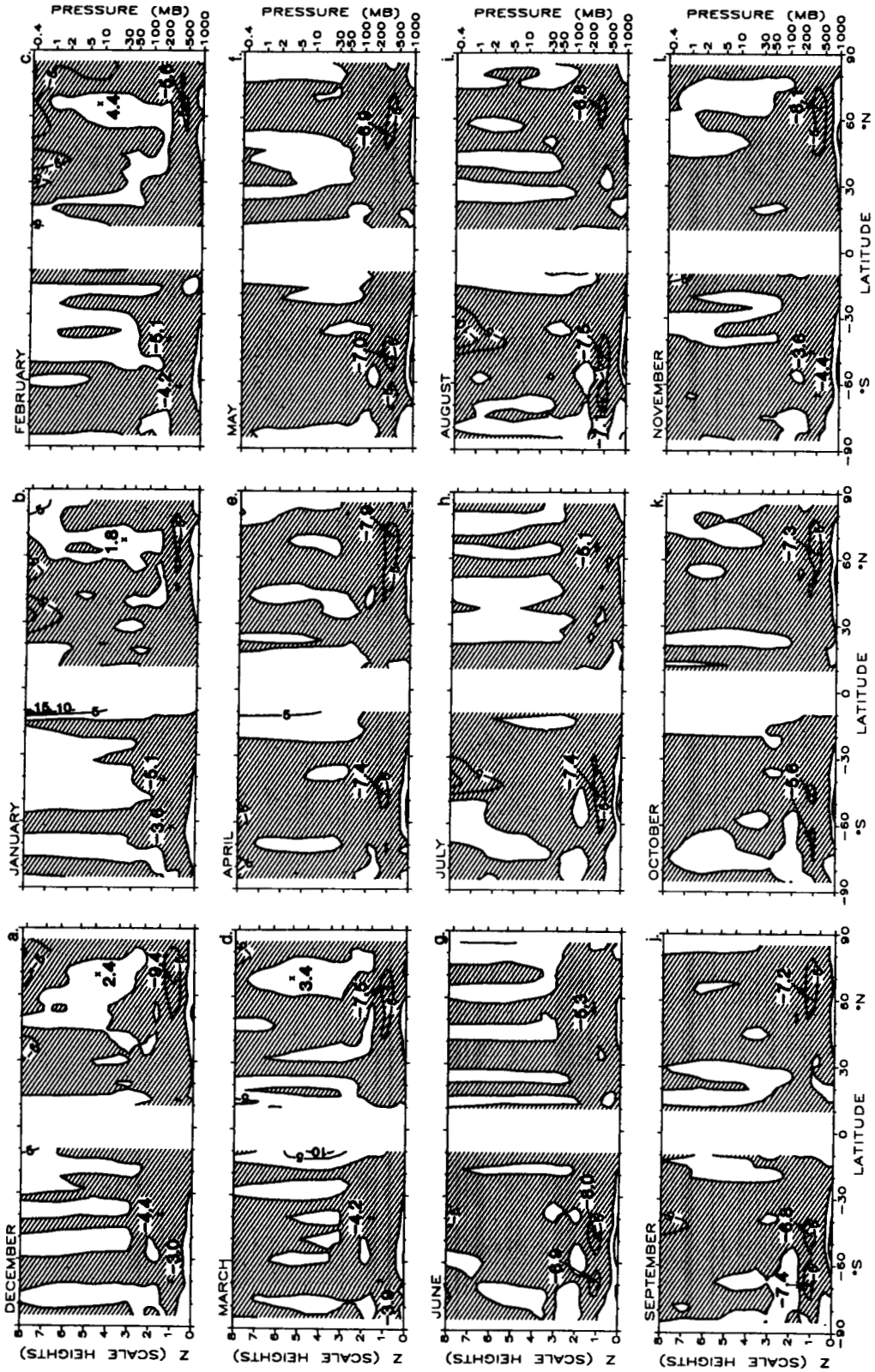

Figure 48. As in Figure 42, but for transient eddy fluxes.

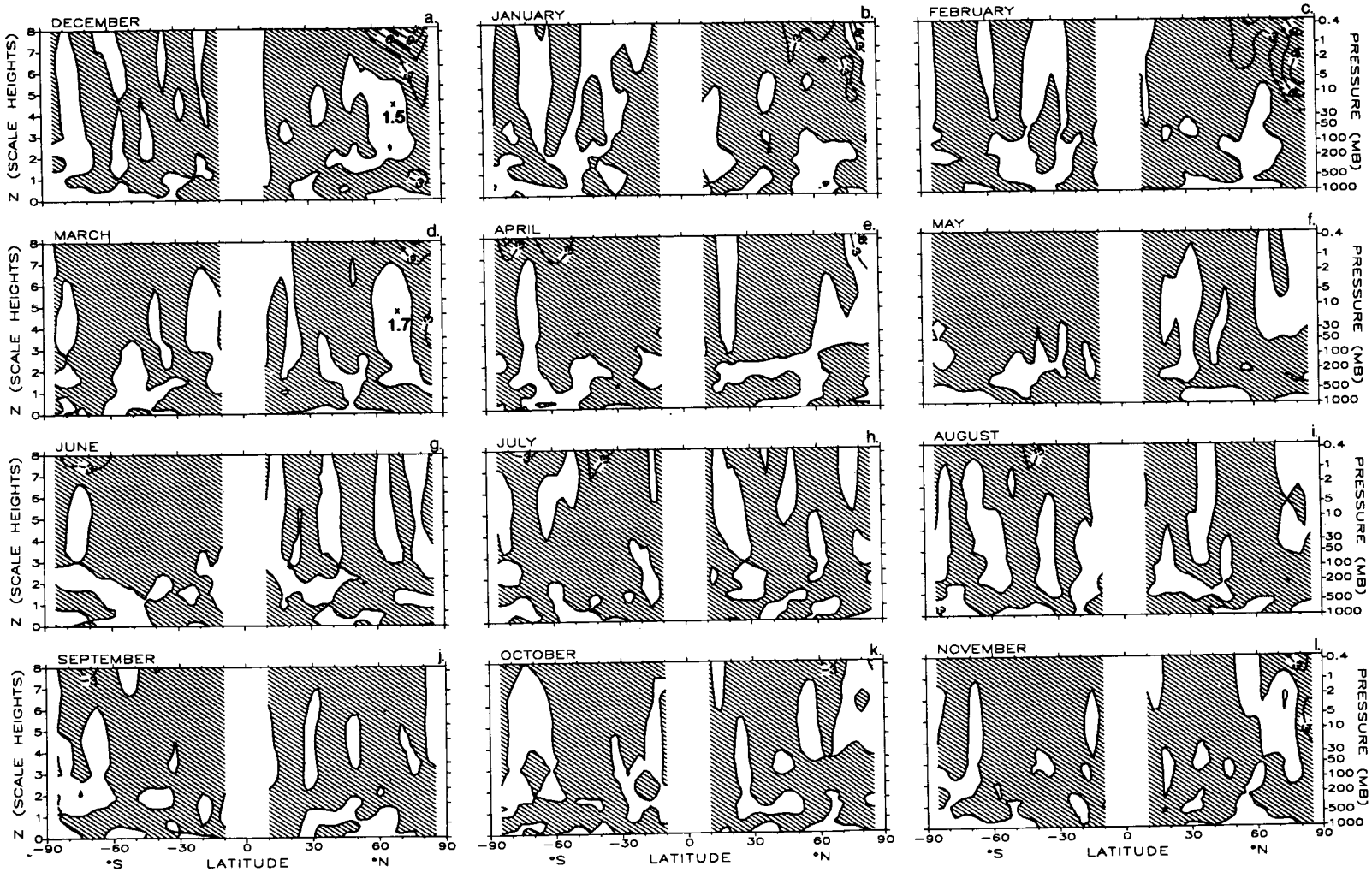

Figure 49. Four-year mean Eliassen-Palm flux divergences (10^{-5} m/sec^2) resulting from the transient eddy zonal wavenumber one.

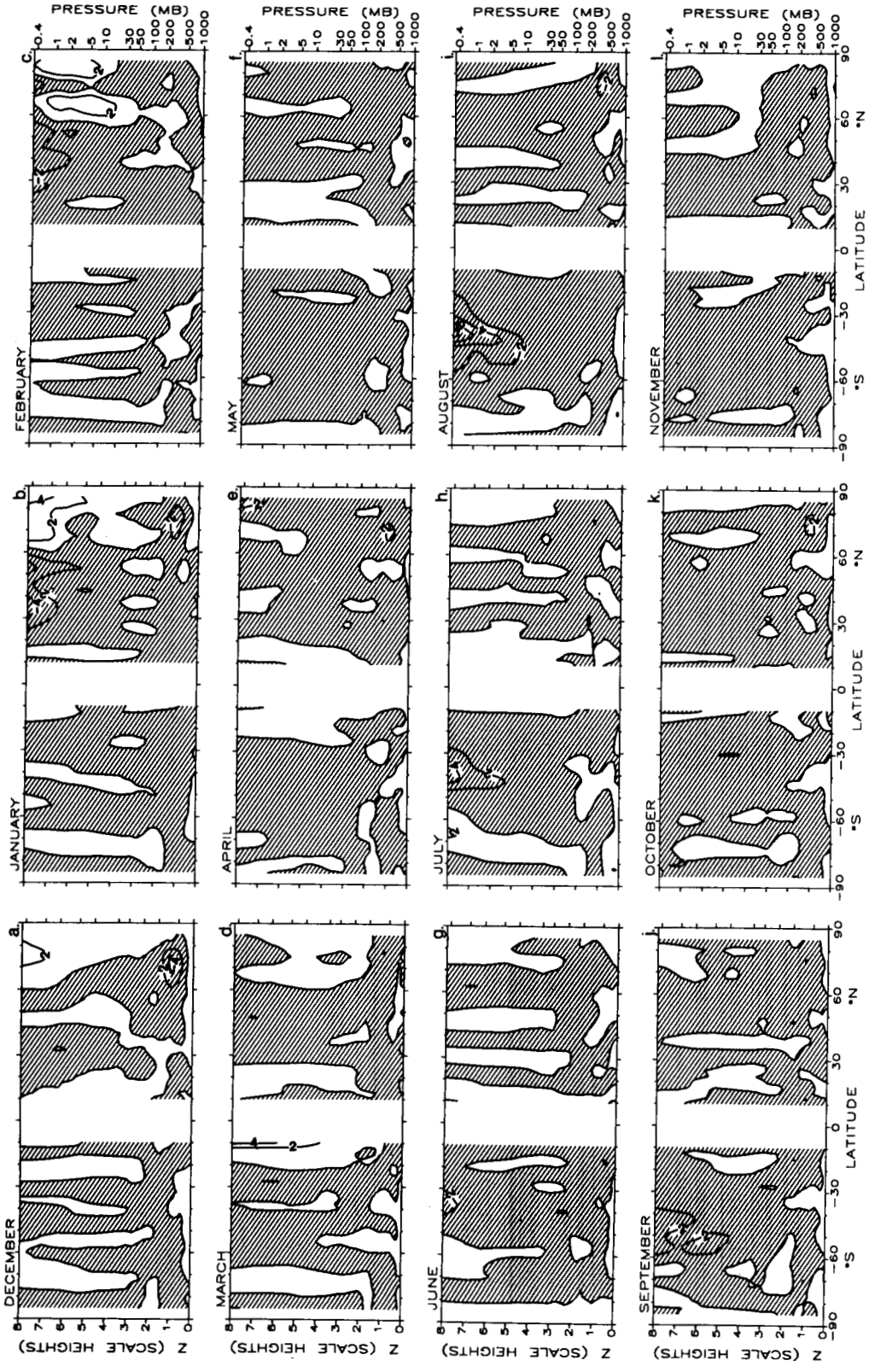

Figue 50. As in Figure 49, but for zonal wavenumber two.

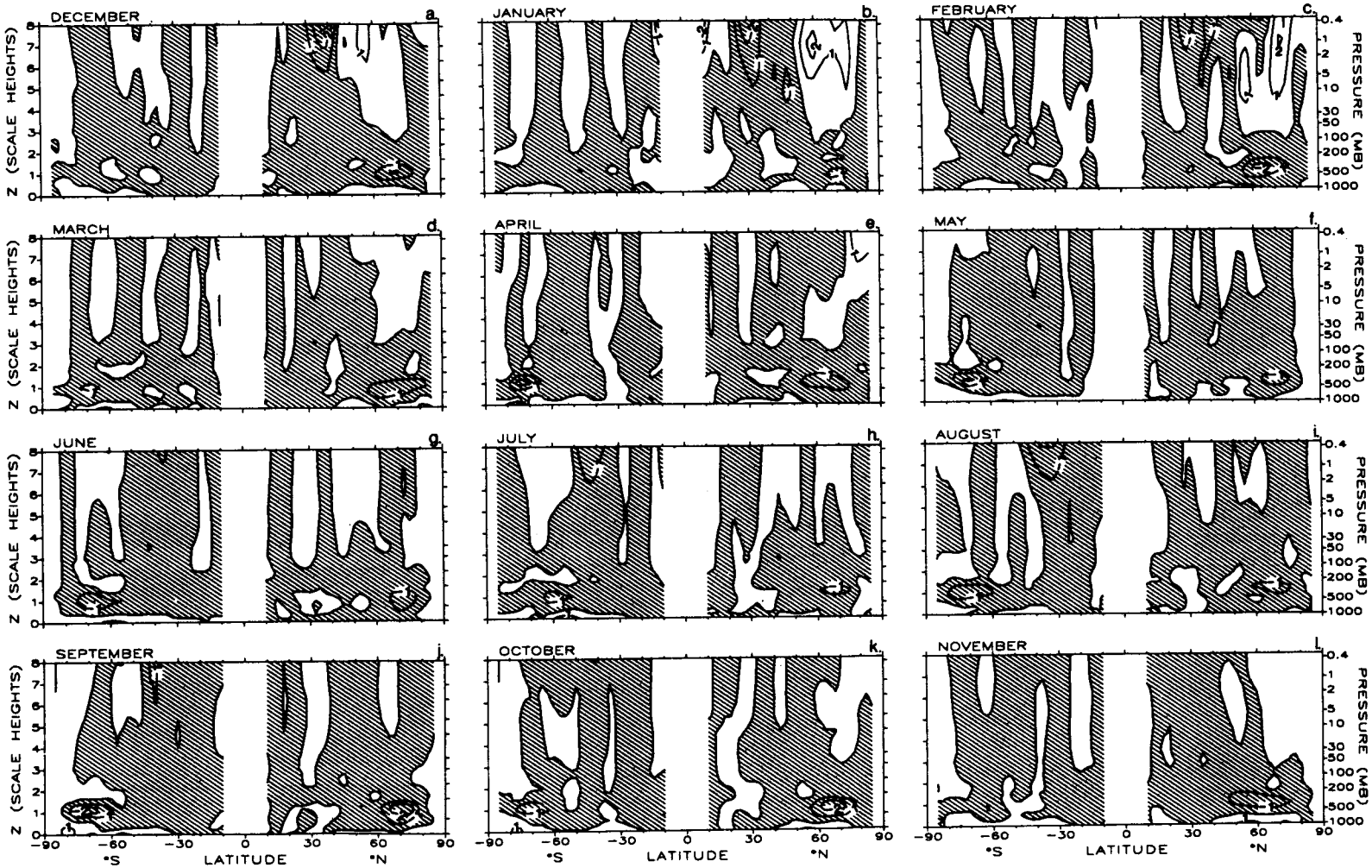

Figure 51. As in Figure 49, but for zonal wavenumber three.

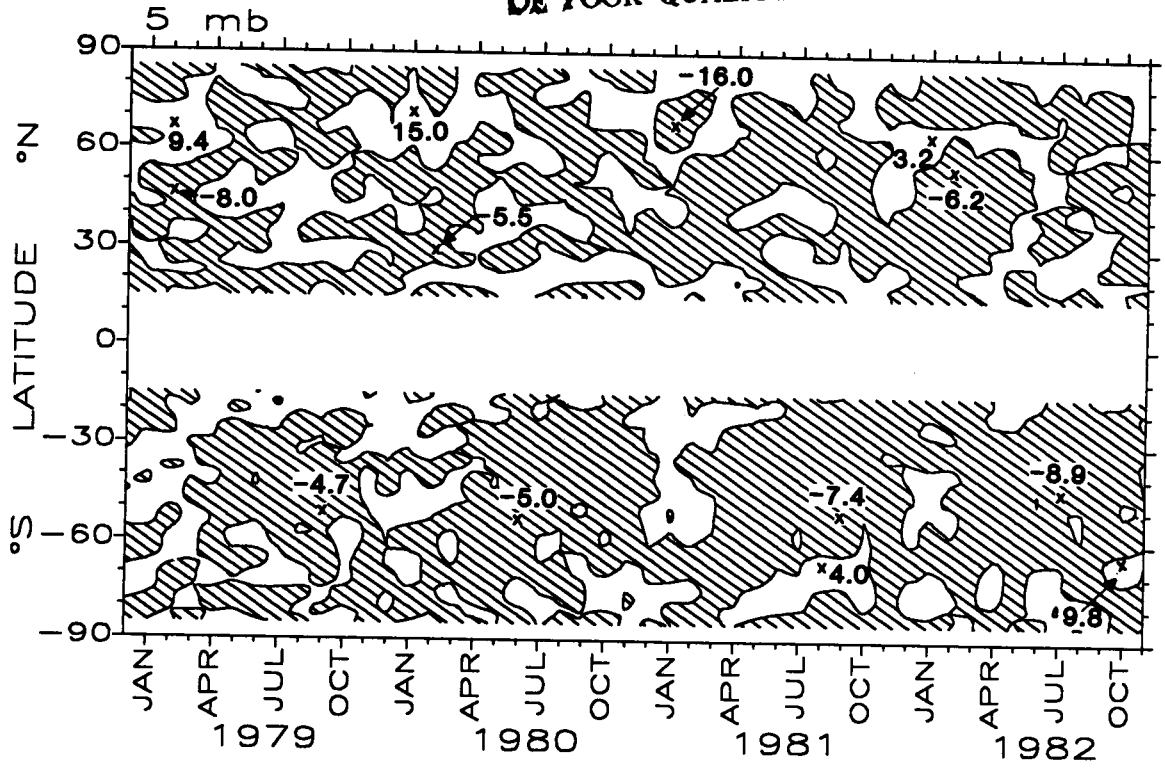

Figure 52. As in Figure 46, but for transient eddies.

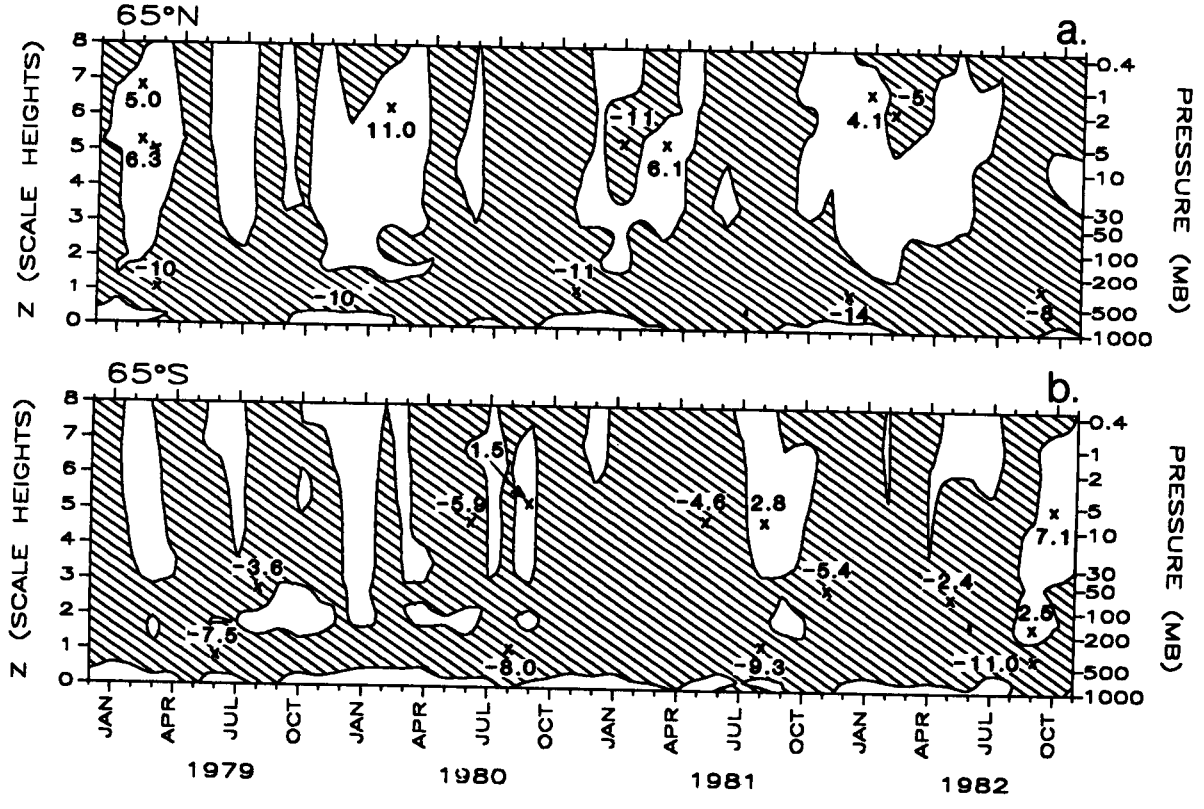

Figure 53. As in Figure 47, but for transient eddies (a) at 65°N, (b) at 65°S.

structure and dynamics of the troposphere and the stratosphere have been analyzed for annual, interhemispheric, and interannual variations. Results are presented in graphical and tabular forms. The major features of interest are summarized below.

(A) Zonal Mean Temperature

(1) The temperatures in the polar upper stratospheric regions are higher in the SH summer than in the NH summer.

(2) The polar winter lower stratosphere temperature is colder in the SH than in the NH.

(3) In the upper stratosphere, the winter South Pole is warmer than in the southern midlatitudes.

(4) The annual variation in monthly mean temperature is larger in the SH than in the NH in the upper stratosphere high latitudes.

(5) Both in the NH and SH, the temperature fields in the polar latitudes fluctuate abruptly during winter and spring, but very little during summer.

(B) Zonally Averaged Zonal Winds

(1) The winter stratospheric westerlies are stronger in the SH than in the NH. The maximum speed of the summer easterlies is also larger in the SH.

(2) The center of the stratospheric westerly jet in the NH is above the stratopause and often splits in late winter, whereas the jet in the SH stratosphere moves poleward and downward during winter and is closed below the stratopause in August.

(3) The maximum speed of the tropospheric jet is higher in the NH than in the SH.

(4) The interannual variation of the location of the stratospheric maximum westerlies is larger in the NH than in the SH.

(5) The stratosphere zonal wind may reverse its direction from westerly to easterly in the NH high latitude during stratospheric warming periods, but a complete reversal in the zonal wind direction during SH warming is never seen owing to a weaker planetary wave strength.

(C) Planetary Waves

(1) The seasonal cycle of the planetary wavenumber 1 is more pronounced and the wave amplitude is larger in the NH than in the SH.

(2) In the NH the largest wavenumber 1 amplitude occurs in middle winter and the wave decays after early spring; in the SH the wavenumber 1 obtains its highest value in early spring and the wave is still active until middle or late spring.

(3) The average maximum amplitude of planetary wavenumber 2 is less than half of wavenumber 1 in both hemispheres. In the NH the location of the wavenumber 2 maximum is at least 10 km lower than that of the wavenumber 1 maximum, whereas in the SH the difference in altitude of the wavenumber 1 and the wavenumber 2 maximum is less than in the NH.

(4) Planetary wavenumber 3 also has seasonal variation in both hemispheres. The seasonal cycle is more pronounced in the NH than in the SH. The largest amplitude occurs in middle winter in both hemispheres in contrast to the wavenumber 1 case in which a time lag of about 2 months is seen in the SH.

(5) The interannual variation of planetary waves is larger in the NH than in the SH.

(D) Heat Fluxes

(a) Due to Standing Eddies

(1) The annual variation of the heat flux due to standing eddies is more pronounced in the NH than in the SH. The maximum poleward flux occurs in winter in the NH but in spring in the SH.

(2) The poleward heat flux is about 3 to 5 times higher in the NH than in the SH depending on whether it is in spring or winter.

(3) The stratosphere standing eddy heat fluxes are determined by the planetary wave structure. The first two harmonics of the waves account for the largest portion of the variance of the eddy heat fluxes.

(4) The contribution from the individual waves to the total standing eddy heat fluxes differs from one hemisphere to the other. In the NH although planetary wavenumber 1 provides a large part of heat flux, wavenumber 2 can also contribute a substantial portion of the total eddy flux in winter, whereas in the SH wavenumber 1 dominates the overall situation. In spring the heat flux in the NH begins to decrease rapidly after March, but in the SH the heat flux remains strong until middle spring. Furthermore, the poleward heat flux in the SH during spring repeats year after year, but no similar flux is seen in the NH spring.

(b) Due to Transient Eddies

(1) In the SH the transient eddy flux is in general greater than the standing eddy flux during southern winter, but smaller during southern spring. In the NH the magnitude of the transient eddy heat fluxes are less than half of that due to the standing eddies from October to March except in February.

(2) In the NH, although the wavenumber 1 flux is relatively larger than the wavenumber 2 flux, wavenumber 1 can not claim a dominant role as it does in the standing eddy flux case. In the SH, the wavenumber 1 flux is in fact less than the wavenumber 2 flux.

(3) The interannual variations in magnitude and time of occurrence of the annual peak flux differ between the two hemispheres.

(E) Momentum Fluxes

(a) Due to Standing Eddies

(1) The seasonal cycle is more pronounced in the NH than in the SH and the magnitude of the maximum poleward momentum flux is also larger in the NH. The maximum flux occurs in middle winter in the NH but in early spring in the SH.

(2) In middle and high latitudes and in the stratosphere, wavenumber 1 in the SH dominates the standing eddy momentum flux field and the effect of wavenumber 2 is almost negligible, but in the NH wavenumber 2 can contribute as much as one third of the total flux.

(3) In the low latitudes and in the troposphere, there is a secondary westerly momentum flux maximum in the NH at about 30°N. This maximum appears almost year-round with the largest annual value occurring in late fall or early spring. No similar feature is seen in the SH.

(4) The year-to-year changes in magnitude and the location of the maximum poleward flux are different in the two hemispheres.

(5) Planetary wavenumber 1 provides the largest portion of the total standing eddy momentum flux both in the NH and in the SH.

(b) Due to Transient Eddies

(1) In the stratosphere wavenumber 1 does not dominate the transient eddy momentum fluxes. In the NH wavenumber 1 and 2 contribute about equal amount to the flux, but in the SH wavenumber 1 acts as a secondary contributer.

(2) A similar annual cycle is seen in each hemisphere with the annual maximum value occurring in late winter.

(3) In the stratosphere the annual largest poleward flux is higher in the NH, but in the troposphere the magnitude is about equal in both hemispheres.

(F) E-P Flux Vectors

(a) From Standing Eddies: During NH winter the E-P flux vectors are generally pointing upward with an equatorward component south of about 45°N and poleward north of that latitude below about 30 mb. In the middle and upper stratosphere, the vectors are upward and southward. A bifurcation near the North Pole at about the 200 mb level is seen in December, January and March, but no clear indication of a similar feature is found in the SH.

(b) From Transient Eddies: Generally speaking, the E-P flux vectors look similar in both hemispheres in the stratosphere, but some differences are seen in the troposphere.

(G) E-P Flux Divergences

(a) From Standing Eddies

(1) In the northern polar latitudes and between about 200 mb and 1 mb there is a positive region of divergence from about November to March with the largest positive value of about 25 m/sec/day in January. In the SH the size of the positive region is greatly reduced in the corresponding season and the highest positive value is only about 2.8 m/sec/day.

(2) There is a negative region of E-P flux divergence accompanying the positive area. In the NH the largest negative value is about -30 m/sec/day occurring in January, but this drops to about -15 m/sec/day in the SH in September.

(3) In the stratosphere the strongest influence on the E-P flux divergences is from planetary wavenumber 1, but in the troposphere the waves with wavenumber higher than 3 are more important.

(b) From Transient Eddies

(1) The absolute value of transient E-P flux divergence is much smaller than the standing eddy E-P flux divergence.

(2) The contribution from the planetary wavenumber 2 to the total transient eddy E-P flux divergences is nearly comparable to that from wavenumber 1.

4.2 Remarks

Despite our effort in compiling the present statistics, much yet remains to be done. Four years of data can only be considered as a short sample. The representativeness of the mean state of the stratosphere is obviously open to question. Currently, we are doubling the data base by including a second 4 year dataset in the compilation. We realize that lengther records are necessary to allow us to properly address the questions of interannual variability, the definition of anomalies, the long-term mean state of the general circulation, and the interhemispheric relationships. Another aspect of the problem affecting the statistics is associated with the quality of

data. The major error sources in the dataset are the uncertainty of the instrumental error, different techniques used in the data collection and processing, missing data treatment and the analysis schemes adopted by different investigators. These biases should be examined in detail. In this report, only limited work is done, such as to remove some obvious bad data and to perform a consistent check in the data set and the results. It should be noted that all the figures presented here were plotted by a computer using NCAR graphics software. By and large, the results look reasonable in comparison with those published by many other investigators, and we believe that the major features are captured.

References

Barnett, J. J., 1974: The mean meridional temperature behavior of the stratosphere from November 1970 to November 1971 derived from measurements by the Selective Chopper Radiometer on Nimbus IV, Quart. J. Roy. Met. Soc., 100, 505-530.

Barnett, J. J. and M. Corney, 1985: Middle atmosphere reference model derived from satellite data, Handbook for MAP, 16, 47-85.

Boville, B. A., 1986: The validity of the geostrophic approximation in the winter stratosphere and troposphere, submitted to J. Atmos. Sci.

Dopplick, T. G., 1971: The energetics of the lower stratosphere including radiative effects, Quart. J. R. Meteorol. Soc., 97, 209-237.

Finger, F. G., H. M. Woolf and C. E. Anderson, 1965: A method for objective analysis of stratospheric constant-pressure charts. Mon. Wea. Rev., 93, 619-638.

Fritz, S. and S. D. Soules, 1970: Large-scale temperature changes in the stratosphere observed from Nimbus III, J. Atmos. Sci., 27, 1091-1097.

Geller, M. A., M.-F. Wu and M. E. Gelman, 1983: Troposphere-stratosphere (surface-55 km) monthly winter circulation statistics for the northern hemisphere four year averages, J. Atmos. Sci., 40, 1334-1352.

Gelman, M. E., and R. M. Nagatani, 1977: Objective analyses of height and temperature at the 5-, 2-, and 0.4-mb levels using meteorological rocketsonde and satellite radiation data. Space Research XVII, COSPAR 117-122.

Gelman, M. E., A. J. Miller, R. N. Nagatani and H. D. Bowman II, 1982: Mean zonal wind temperature structure during the PMP-1 winter periods, Adv. Space Research XXIV COSPAR, 2, 159-162.

Gelman, M. E., A. J. Miller, K. W. Johnson and R. M. Nagatani, 1986: Detection of long term trends in global stratospheric temperature from NMC analyses derived from NOAA satellite data, Adv. Space Research, in press.

Hartmann, D. L., 1976: The structure of the stratosphere in the Southern Hemisphere during late winter 1973 as observed by satellite, J. Atmos. Sci., 33, 1141-1154.

Hartmann, D. L., C. R. Mechoso, and R. S. Harwood, 1984: Observations of wave-mean flow interaction in the Southern Hemisphere, J. Atmos. Sci., 41, 351-362.

Hirota, I., Seasonal variation of planetary waves in the stratosphere observed by the Nimbus 5 SCR, 1976: Quart. J. R. Met. Soc., 102, 757-770, 1976.

Hirota, L. T. Hirooka and M. Shiotani, Upper stratospheric circulation in the two hemispheres observed by satellites, 1983: Quart. J. Roy. Meteor. Soc., 109, 443-454.

Mechoso, C. R., D. L. Hartmann, and J. D. Ferrara, 1985: Climatology and interannual variability of wave, mean-flow interaction in the Southern Hemisphere, J. Atmos. Sci., 42, 2189-2206.

Oort, A. H., 1983: Global atmospheric circulation statistics, 1958-1973, NOAA Prof. Paper 14, 180pp.

Robinson, W. A., 1986: The application of the quasi-geostrophic Eliassen-Palm flux to the analysis of stratospheric data, J. Atmos. Sci., 43, 1017-1023.

Rodgers, C. D., 1984a: Coordinated study of the behavior of the middle atmosphere in winter (PMP-1). Handbook for MAP Volume 12, pp. 154.

Rodgers, C. D., 1984b: Workshops on Comparison of data and derived dynamical quantities during Northern Hemisphere winters, Adv. Space Res., 4, 117-125.

Rosenfield, J. E., M. R. Schoeberl, and M. A. Geller, 1987: A computation of

the stratospheric diabatic circulation using an accurate radiative transfer model, J. Atmos. Sci., 44, 859-876.

Shiotani, M. and I. Hirota, 1985: Planetary wave-mean flow interaction in the stratosphere: A comparison between the Northern and Southern Hemispheres, Quart. J. Roy. Meteor. Soc., 111, 309-334.

Smith, W. L., H. M. Woolf, C. M. Hayden, D. Q. Wark and L. M. McMillian, 1979: TIROS-N operational vertical sounder, Bull. Amer. Meteor. Soc., 60,1177 -1197

Wu, M. F., M. A. Geller, J. G. Olson, and M. E. Gelman, 1984: Troposphere-stratosphere (Surface - 55 km) monthly general circulation statistics for the Northern Hemisphere - four year averages, NASA Tech. Memo. 86182.

APPENDIX A

DATA SOURCES AND QUALITY

Appendix A: Data Sources and Quality

The following is a more detailed description and discussion of the sources and quality of the temperature data that were used in this study.

Global fields of geopotential height and temperature at stratospheric constant pressure levels 70, 50, 30, 10, 5, 2, 1 and 0.4 mb (corresponding to the approximate altitude interval 18 to 55 km) have been produced since 24 September 1978, as part of regular operations at the National Meteorological Center (NMC). The analysis system for the fields is a modified Cressman, both for the 70 to 10 mb (Finger et al., 1965) and for 5 to 0.4mb (Gelman and Nagatani, 1977). Both data sources and analyses have changed since 1978 as new and improved data and analysis methods have become available. Table A1 summarizes the principal changes that are relevant to a study of the upper stratospheric fields (5-0.4 mb) as well as the lower stratospheric fields (70-10 mb). Data were derived from the succession of operational satellite soundings systems: Vertical Temperature Profiler Radiometer (VTPR) on NOAA 5, Stratospheric Sounding Unit (SSU) on TIROS-N and NOAA 6, and the TIROS Operational Vertical Sounder (TOVS) system on NOAA 6 and NOAA 7.

The TOVS system (see Smith et al., 1979) derives stratospheric soundings from nine stratospheric channels on three instruments, SSU, High Resolution Infrared Sounder (HIRS), and the Microwave Sounding Unit (MSU). Since 17 October 1980, TOVS data have been used for the stratospheric fields. The TOVS soundings derived by the National Environmental Satellite Data and Information Services (NESDIS) provide layer mean temperatures between the standard pressure levels. Geopotential heights are derived at stratospheric levels through the hypsometric equation by converting the TOVS layer mean temperatures to geopotential thickness and adding these thicknesses to a lower boundary condition at 1000 mb. Temperatures derived at the pressure levels are linear interpolations in log pressure of the layer mean temperatures.

TABLE A1: Global Daily 1200 GMT Temperature and Height Fields History of Changes.

Period	Dates	Levels (mb)	Hem.	Data and Analysis Procedures
1	24 Sep. 1978-23, Feb. 1979	70-10	N	Rawinsonde data First guess 50% persistence, 50% regression upward
	70-10	S		Radiosonde and VTPR temperatures
	5-0.4	N, S		Regression from VTPR channels 1, 2
	25 Feb. 1979-16 Oct. 1980	70-10	N	Rawinsonde data
2	(2/25/79-1/20/80; TIROS-N)			First guess 50% persistence, 50%
3	(1/21/80-10/16/80; NOAA6)			TOVS beginning 3 Oct. 1979
	70-10	S		Radiosonde and TOVS temperatures
	5-0.4	N, S		Regression from SSU channels 25, 26
	17 Oct 1980-Present	70-10	N	Rawinsonde data
4	(10/17/80-9/1/81; NOAA6)			First guess 100% TOVS beginning 17
5	(9/2/81-9/1/83; NOAA7)			June 1981
6	(9/2/83-6/18/84; NOAA8)			TOVS first guess saved outside NMC
7	(6/19/84-2/26/85; NOAA7)			octagon grid points beginning
8	(3/27/85--; NOAA9)			29 Feb., 1984
	70-10	S		TOVS (no radiosonde)
	5-0.4	N, S		TOVS

Geopotential heights and temperatures derived from TOVS data within plus and minus 6 h of 1200 GMT are used in a simple Cressman-type analysis system (see Gelman and Nagatani, 1977) to produce stratospheric fields. For the lower stratosphere Northern Hemisphere analyses at 70-10 mb, rawinsonde data continue to be the principal data source with satellite soundings providing important but supplementary information. Data from 5 to 0.4 mb, derived from previous satellite systems, from 24 September 1978 to 16 October 1980 were obtained using simple regression equations relating temperature at each level to the radiances (or brightness temperatures) from two of the stratospheric channels on the VTPR, TIROS-N SSU and NOAA 6 SSU, respectively.

As indicated in Table A1, there have been continual changes in both measurement systems and analysis procedures since the initiation of this data set, 24 September 1978. Since part of the purpose in analyzing this data is to look at interannual changes in stratospheric structure, some attention must be given to the long-term stability of this data set. Therefore, there was an effort by NMC to compare data from meteorological rocketsonde observations with satellite data at the locations of the rocket stations from the analyzed fields closest in time. Rocket stations used for this study were Thule (77°N), Churchill (59°N), Primrose (55°N), Shemya (53°N), Wallops (38°N), Point Magu (34°N), White Sands (32°N), Cape Kennedy (28°N), Barking Sands (22°N), Antigua (17°N), Kwajalein (9°N), and Ascension Island (8°S). Since both rocketsonde hardware and data extraction procedures have been standardized for the stations in the Cooperative Meteorological Rocketsonde Network (CMRN) since at least 1978, we assume that this rocketsonde data may be used as a reasonable and consistent standard against which to gauge the long-term stability of the NOAA/NMC temperature maps. The error estimates for rocketsonde temperature data are found to be 1-3 K over the altitude range 35-55 km.

Gelman et al. (1982) have statistically determined the systematic temperature corrections ΔT to be applied to the satellite-derived temperatures by means of comparison with rocketsonde temperatures. The technique is given below. For the first three time periods a best-fit linear regression equation of the form

$$T_s - T_r = a + bL$$

was made to the satellite analysis minus rocket temperature differences, where a is the temperature adjustment at the equator, b is the slope of the adjustment values with latitude, and L is absolute degrees latitude. Both the values for a and b and the quality of the linear regression fit, as indicated by the standard errors for a and b can be seen in Table A2. The temperature adjustments are at most 9°C, and the largest adjustments occur nearest the equator or North and South Pole. The adjustments are recommended for application in the northern as well as in the southern hemisphere, even though the rocketsonde stations used to derive the adjustments are almost exclusively in the northern hemisphere. This is a significant limitation. In our computations the SH data were adjusted in the same manner as the NH.

For periods four to eight, when we changed to the use of the operational TOVS data, adjustments that do not vary with latitude have been derived based on rocketsonde comparisons. Two reasons may be offered for the adjustment not varying with latitude, for the later periods. The use of TOVS data, derived from nine channels of the three instruments, and regression retrieval method

that divides the statistics into 5 latitude bands, diminishes the likelihood that systematic biases vary in a simple way with latitude. Secondly, during the 1980's there was a severe curtailing of the scope and number of launches of rockets from the CMRN. Furthermore, with the closing of the two northern stations of Thule and Churchill, the latitudinal extent was severely curtailed. The suggested adjustments for the 5, 2, 1 and 0.4 mb levels for periods 4 to 8 are shown in Table A3.

All comparisons are shown as analysis minus rocket. Thus the adjustments from Table A2 and A3 should be subtracted from the archival analysis temperatures.

Rodgers (1984a,b) has made a detailed examination on the temperature data collected by various instruments from several satellites. He has identified and discussed the error sources in retrieving the meteorological data via a satellite.

Comparison of the NMC data with other satellite experiments is generally good up to about 2 mb, and the precision of the NMC data increases from about 7K to 5K with the implementation of the SSU on TIROS-N. However, at the 0.4 mb level, there is little radiance information from which temperatures are derived. Thus, our computations above 2 mb should not be taken as being very reliable.

The number of conventional radiosonde stations is larger in the NH than in the SH. Thus, the SH lower boundary values of geopotential height are less well determined than in the NH.

The largest temperature corrections ΔT always occur nearest the Equator and the North Pole. At 80°N and 0.4 mb the temperature has about 1.5°C reduction for period 1 and about 6.7°C increment for period 2. The change in T is generally less for other locations. The accompanying thermal zonal wind corrections are less than 1 m/sec in the polar region. The largest zonal wind modification is in the tropical region where the maximum deviation of the zonal wind speed may reach 4 m/sec (see Gelman et al., 1982).

TABLE A2: Regression Coefficients and Standard Errors for Adjusting Satellite Analysis Temperatures to Rocketsonde Values

Period			5 mb	2 mb	1 mb	0.4 mb	Number of Rockets	
1	24 Sept. 1978	a	-0.1893	0.2985	-0.1615	-1.3647		
	to	Standard error (a)	0.681	0.593	0.9277	0.900	300	
	22 Feb. 1979	b	-0.0334	-0.0574	-0.0185	0.0365		
	Standard error	(b)	0.0173	0.0150	0.0236	0.0231		
2	25 Feb. 1979	a	-4.0515	-4.713	-1.818	6.831		
	to	Standard error (a)	0.275	0.291	0.401	0.395	664	
	20 Jan. 1980	b	0.069	0.0165	-0.0569	-1.702		
	Standard error	(b)	0.00699	0.00740	0.0100	0.010		
3	21 Jan. 1980	a	-5.1422	-6.0425	-0.917	8.829		
	to	Standard error (a)	0.3076	0.398	0.4383	0.442	516	
	16 Oct. 1980	b	0.0843	0.0612	-0.0396	-0.2039		
	Standard error	(b)	0.00740	0.00960	0.0106	0.0110		

TABLE A3: Temperature Differences (^{0}C) and Standard Error of the Average Differences for Satellite Analysis Minus Rocket. Values to be Subtracted for Adjusting Analysis Temperatures.

Period	Dates		5 mb	2 mb	1 mb	0.4 mb	Number of Rocketsondes
4	10/17/80	Diff.	2.2	-3.2	-7.0	0.9	363
	9/1/81	St. error	.4	.5	.5	1.1	
5	9/2/81	Diff.	5.7	-1.1	-8.3	5.4	481
	9/1/83	St. error	.6	.3	.4	.8	
6	9/2/83-	Diff.	-0.5	-4.9	-5.4	-0.7	141
	6/18/84	St. error	.6	.5	.4	1.1	
7	6/19/84	Diff.	1.9	-3.7	-4.0	2.2	80
	2/26/85	St. error	1.3	1.2	1.4	.8	
8	3/27/85-	Diff.	5.7	-3.3	-6.9	8.5	111
		St. error	.4	.4	.5	.6	

Since the temperature corrections were only made with varying latitude, the longitudinal gradient of temperature remains the same. Consequently, there is no effect on the planetary wave structure and the computations of meridional winds at each grid point.

APPENDIX B

TABLES (NORTHERN HEMISPHERE)

APPENDIX C

TABLES (SOUTHERN HEMISPHERE)

NASA
National Aeronautics and Space Administration

Report Documentation Page

1. Report No.	2. Government Accession No.	3. Recipient's Catalog No.
NASA TM-100690		

4. Title and Subtitle

Global Atmospheric Circulation Statistics--
Four Year Averages

5. Report Date

June 1987

6. Performing Organization Code

616

7. Author(s)

M. F. Wu, M. A. Geller, E. R. Nash, and
M. E. Gelman

8. Performing Organization Report No.

87B0437

10. Work Unit No.

9. Performing Organization Name and Address

Goddard Space Flight Center
Greenbelt, Maryland 20771

11. Contract or Grant No.

13. Type of Report and Period Covered

Technical Memorandum

12. Sponsoring Agency Name and Address

National Aeronautics and Space Administration
Washington, D.C. 20546-0001

14. Sponsoring Agency Code

15. Supplementary Notes

E. R. Nash is affiliated with Applied Research Corporation, Landover, Maryland. M. E. Gelman is affiliated with the National Oceanic and Atmospheric Administration, Washington, D.C.

16. Abstract Four year averages of the monthly mean global structure of the general circulation of the atmosphere are presented in the form of latitude-altitude, time-altitude and time-latitude cross sections. The numerical values are given in tables. Basic parameters utilized include daily global maps of temperature and geopotential height for 18 pressure levels between 1000 and 0.4 mb for the period December 1, 1978 through November 30, 1982 that were supplied by NOAA/NMC. Geopotential heights and geostrophic winds are constructed using the hydrostatic and geostrophic formulae. Meridional and vertical velocities are calculated using the thermodynamic and continuity equations. Fields presented in this report are zonally averaged temperature, zonal, meridional and vertical winds, and amplitude of the planetary waves in geopotential height with zonal wave numbers 1-3. The northward fluxes of sensible heat and eastward momentum by the standing and transient eddies along with their wavenumber decomposition and Eliassen-Palm flux propagation vectors and divergences by the standing and transient eddies along with their wavenumber decomposition are also given. Large interhemispheric differences and year-to-year variations are found to originate in the changes in the planetary wave activity.

17. Key Words (Suggested by Author(s))	18. Distribution Statement
Atmospheric circulation statistics General circulation statistics Meteorological analysis	Unclassified - Unlimited Subject Category 47

19. Security Classif. (of this report)	20. Security Classif. (of this page)	21. No. of pages	22. Price
Unclassified	Unclassified		

NASA SCIENTIFIC AND TECHNICAL DOCUMENT AVAILABILITY AUTHORIZATION (DAA)

To be initiated by the responsible NASA Project Officer, Technical Monitor, or other appropriate NASA official for all presentations, reports, papers, and proceedings that contain scientific and technical information. Explanations are on the back of this form and are presented in greater detail in NHB 2200.2, "NASA Scientific and Technical Information Handbook."

☐ Original
☐ Modified

(Facility Use Only)
Control No _____
Date _____

I. DOCUMENT/PROJECT IDENTIFICATION (Information contained on report documentation page should not be repeated except title, date and contract number)

Title: Global Atmospheric Circulation Statistics-Four Year Averages

Author(s): Mao-Fou Wu, Marvin A. Geller, Eric Nash, and Melvyn E. Gelman

Originating NASA Organization: Atmospheric Chemistry and Dynamics Branch (Code 616)

Performing Organization (if different) _____

Contract/Grant/Interagency/Project Number(s) TM 100690

Document Number(s) _____ Document Date: _____

(For presentations or externally published documents, enter appropriate information on the intended publication such as name, place, and date of conference, periodical or journal title, or book title and publisher: _____

These documents must be routed to NASA Headquarters, International Affairs Division for approval. (See Section VII))

II. AVAILABILITY CATEGORY

Check the appropriate category(ies):

Security Classification: ☐ Secret ☐ Secret RD ☐ Confidential ☐ Confidential RD ☒ Unclassified

Export Controlled Document - Documents marked in this block must be routed to NASA Headquarters International Affairs Division for approval.

☐ ITAR ☐ EAR

NASA Restricted Distribution Document

☐ FEDD ☐ Limited Distribution ☐ Special Conditions-See Section III

Document disclosing an invention

☐ Documents marked in this block must be withheld from release until six months have elapsed after submission of this form, unless a different release date is established by the appropriate counsel. (See Section IX).

Publicly Available Document

☒ Publicly available documents must be unclassified and may not be export-controlled or restricted distribution documents.

☐ Copyrighted ☐ Not copyrighted

IN-47
113619
74P.

III. SPECIAL CONDITIONS

Check one or more of the applicable boxes in each of (a) and (b) as the basis for special restricted distribution if the "Special Conditions" box under NASA Restricted Distribution Document in Section II is checked. Guidelines are provided on reverse side of form.

a. This document contains:

☐ Foreign government information ☐ Commercial product test or evaluation results ☐ Preliminary information ☐ Information subject to special contract provision

☐ Other - Specify _____

b. Check one of the following limitations as appropriate:

☐ U.S. Government agencies and U.S. Government agency contractors only ☐ NASA contractors and U.S. Government agencies only ☐ U.S. Government agencies only

☐ NASA personnel and NASA contractors only ☐ NASA personnel only ☐ Available only with approval of issuing office: _____

IV. BLANKET RELEASE (OPTIONAL)

All documents issued under the following contract/grant/project number _____ may be processed as checked in Sections II and III.

The blanket release authorization granted _____ (Date) is:

☐ Rescinded - Future documents must have individual availability authorizations. ☐ Modified - Limitations for all documents processed in the STI system under the blanket release should be changed to conform to blocks as checked in Section II.

V. PROJECT OFFICER/TECHNICAL MONITOR

Marvin A. Geller	610		7/13/87
Typed Name of Project Officer/Technical Monitor	Office Code	Signature	Date

VI. PROGRAM OFFICE REVIEW ☐ Approved ☐ Not Approved

Dixon Butler	EEU		7/14/87
Typed Name of Program Office Representative	Program Office and Code	Signature	Date

VII. INTERNATIONAL AFFAIRS DIVISION REVIEW

☒ Open, domestic conference presentation approved. ☐ Export controlled limitation is not applicable.

☐ Foreign publication/presentation approved. ☐ The following Export controlled limitation (ITAR/EAR) is assigned to this document: _____

☐ Export controlled limitation is approved.

Richard J H Becker	Director of Int'l Affairs		8/4/87
International Affairs Div. Representative	Title		Date

VIII. EXPIRATION OF REVIEW TIME

The document is being released in accordance with the availability category and limitation checked in Section II since no objection was received from the Program Office within 20 days of submission, as specified by NHB 2200.2, and approval by the International Affairs Division is not required.

Name & Title _____ Office Code _____ Date _____

Note: This release procedure cannot be used with documents designated as Export Controlled Documents, conference presentations or foreign publications.

IX. DOCUMENTS DISCLOSING AN INVENTION

a. This document may be released on _____ (Date) Installation Patent or Intellectual Property Counsel _____ Date _____

b. The document was processed on _____ (Date) in accordance with Sections II and III as applicable. NASA STI Facility _____ Date _____

X. DISPOSITION

Completed forms should be forwarded to the NASA Scientific and Technical Information Facility, P.O. Box 8757, B.W.I. Airport, Maryland 21240, with either (check box):

☐ Printed or reproducible copy of document enclosed

☐ Abstract or Report Documentation Page enclosed. The issuing or sponsoring NASA installation should provide a copy of the document, when complete, to the NASA Scientific and Technical Information Facility at the above listed address